
The impact of Interleukin-6 and alpha2-Macroglobulin on the coagulation system

Dissertation

Zur Erlangung des Grades
Doktor der Naturwissenschaften

Am Fachbereich Biologie
Der Johannes Gutenberg-Universität Mainz

Tanja Knopp

geb. am 28.06.1990 in Völklingen

Mainz, August 2022

Dekan

1. Berichterstatter:

2. Berichterstatter:

Tag der mündlichen Prüfung: 15.12.2022

INDEX

INDEX	I
ABBREVIATIONS	IV
1. INTRODUCTION	1
1.1. The coagulation system	1
1.2. The interaction of inflammation and coagulation	3
1.2.1. The impact of Interleukin-6 on coagulation and inflammation	3
1.3. The antiproteinase alpha-2-macrogobulin in the context of hemostasis	7
1.4. Our mouse model of IL-6 overexpression in myeloid cells (LysM-IL-6^{OE} mice)	10
1.5. Objective of my thesis	13
2. MATERIAL AND METHODS	15
2.1. Chemicals and equipment	15
2.2. Buffer	17
Lysis buffer	17
Tris/acetate/EDTA (TAE) buffer	17
Git buffer	17
RIPA buffer	18
Sample buffer (6x)	18
Separating gel buffer	18
Stacking gel buffer	18
Transfer buffer	19
Blocking buffer I	19
1x Ammonium/chloride/potassium (ACK) buffer	19
2.3. Mouse Experiments	20
2.3.1. LysM-IL-6 ^{OE} Mice	20
2.3.2. Subtotal vena cava stenosis model	20
2.3.3. High-frequency ultrasound	22
2.3.4. Tail bleeding assay	23
2.3.5. Adenoviral construct and treatment	23
2.3.6. Bone marrow transplantation	24
2.3.7. Euthanasia of mice	25
2.3.8. Organ isolation und preparation	26
2.3.8.1. Mouse blood isolation	26
2.3.8.2. Spleen	26
2.4. Molecular Biology	26

2.4.1.	DNA isolation.....	26
2.4.2.	Quantitative real-time PCR	27
2.4.3.	Polymerase Chain Reaction (PCR).....	28
2.4.4.	Agarose gel electrophoresis	29
2.4.5.	RNA isolation and measurement	30
2.5.	Cell Biology.....	30
2.5.1.	Blood count	30
2.5.2.	Hepatocyte isolation	30
2.5.3.	Flow cytometry analysis.....	31
2.6.	Biochemistry.....	32
2.6.1.	Protein isolation.....	32
2.6.2.	Sodium dodecyl sulfate-polyacrylamide gel electrophoresis (SDS-PAGE) 33	
2.6.3.	Western blot analyses	34
2.6.4.	Enzyme-linked immunosorbent assay (ELISA)	35
2.7.	Coagulation Biology.....	35
2.7.1.	Erythrocytes sedimentation rate	35
2.7.2.	Thrombin-triggered clotting time	35
2.7.3.	Analysis of coagulation parameters	36
2.7.4.	Thrombin Generation Assay	36
2.8.	Histology.....	37
2.8.1.	Peripheral blood smear.....	37
2.8.2.	Pappenheim staining	37
2.8.3.	Hematoxylin and eosin (H&E) staining.....	38
2.8.4.	Immunofluorescence staining	38
2.9.	Human patient blood sample.....	38
2.10.	Statistical analysis	39
3.	RESULTS.....	40
3.1.1.	The influence of IL-6 on the coagulation system in mice.....	40
3.1.1.	No thrombus formation after subtotal vena cava ligation in LysM-IL-6 ^{OE} mice 40	
3.1.2.	Hematological analysis of blood and coagulation parameters in LysM-IL-6 ^{OE} mice	41
3.1.3.	Myeloid IL-6 overexpression leads to delayed thrombin generation ...	45
3.1.4.	Coagulation factors and acute phase proteins in LysM-IL-6 ^{OE} mice compared to control mice.....	47
3.1.5.	Myeloid IL-6 overexpression results in erythrocyte aggregation.....	49
3.2.	Myeloid cell-derived IL-6 leads to gut inflammation in LysM-IL-6^{OE} mice compared to control mice	54

3.3.	IBD patients with elevated IL-6 levels shows a delayed Thrombin converting time and formation of erythrocyte aggregates in blood.....	56
3.4.	Bone marrow transplant experiments reveal an IL-6 dose-dependent effect on the coagulation system.....	59
3.5.	Antagonization of A2m with small hairpin-A2m specific adeno-associated virus in LysM-IL-6 ^{OE} mice.....	63
3.5.1.	Establishing the small hairpin-A2m specific adeno-associated virus in our LysM-IL-6 ^{OE} mouse model	63
3.5.2.	Inflammatory analysis after treatment with small hairpin-A2m specific adeno-associated virus in LysM-IL-6 ^{OE} mice	65
3.5.3.	Analyzing the impact of A2m on the coagulation in mice	67
4.	DISCUSSION	73
4.1.	The role of IL-6 during coagulation	73
4.2.	The complex interplay of IL-6 and coagulation in human diseases....	79
4.3.	Conclusion.....	82
5.	SUMMARY	84
6.	Zusammenfassung	86
7.	REFERENCES	89
8.	LISTS	101
8.1.	Tables	101
8.2.	Figures	101
9.	ACKNOWLEDGEMENTS	103
10.	VERSICHERUNG	105
11.	CURRICULUM VITAE	106
12.	PUBLIKATIONEN UND VORTRÄGE	108

ABBREVIATIONS

% (v/v)	Volume percent
°C	Degree Celsius
µm	Micrometer
A2M	Alpha-2-macroglobulin
AAV	Adeno-associated virus
ALAT	Alanine aminotransferase
<i>Alb</i>	<i>Albumin</i>
APC	Activated protein C
APC	Allophycocyanin
APC/Cy7	Allophycocyanin/ Cyanine dye 7
APS	Ammonium persulfate
aPTT	Activated Partial Thromboplastin Time
ASAT	Aspartate aminotransferase
BM	Bone marrow
bp	Base pairs
BSA	Bovine serum albumin
CaCl ₂	Calcium chloride
CAT	Calibrated automated thrombinography
CD	Cluster of differentiation
cre	Cre recombinase
CRP	C-reactive protein
ddH ₂ O	Double-distilled water
DNA	Deoxyribonucleic acid
eGFP	Enhanced green fluorescent protein
ELISA	Enzyme-linked immunosorbent assay
ES	Embryonic stem
ESR	Erythrocytes sedimentation rate
ETP	Endogenous thrombin potential
FACS	Fluorescence-activated cell sorting
FCS	Fetal Calf Serum
FITC	Fluorescein isothiocyanate
FIX	Factor IX
FIXa	Activated Factor IXa
FVIII	Factor VIII
FVIIIa	Activated Factor VIIIa
fwd	Forward
FX	Factor X
FXa	Activated Factor X
FXI	Factor X _a
FXIa	Activated Factor X _a
FXII	Factor XII _a

FXIIa	Activated Factor XIIa
FXIII	Factor XIII
FXIIIa	Activated Factor XIIIa
<i>Fαchain</i>	<i>Fibrinogen α chain</i>
<i>Fβchain</i>	<i>Fibrinogen β chain</i>
<i>Fγchain</i>	<i>Fibrinogen γ chain</i>
g	Standard acceleration due to gravity
H&E	Hematoxylin and eosin
HCL	Hydrochloric acid
HGB	Hemoglobin
IBD	Inflammatory bowel disease
II	Prothrombin
Ila	Thrombin
IL	Interleukin
INR	International Normalized Ratio
IVC	Inferior vena cava
LRP-1	Lipoprotein receptor-related protein-1
LYM	Lymphocytes
LysM ⁺	Lysozyme M ⁺
M	Molar
MCH	Mean corpuscular hemoglobin
mg	Milligram
MgCl	Magnesium chloride
min	Minute/s
ml	Milliliter
mm	Millimeter
mM	Millimolar
MON	Monocytes
MPV	Mean platelet volume
NaCl	Sodium chloride
NaF	Sodium fluoride
NEU	Neutrophils
ng	Nanogram
nm	Nanometer
nM	Nanomolar
OD	Optical density
PB	Pacific blue dye
PBS	Phosphate buffered saline
PCR	Polymerase Chain Reaction
PDWs	Platelet distribution width
PE	Phycoerythrin
PE/Cy7	Phycoerythrin/Cyanine dye 7
PerCp	Peridinin-Chlorophyll-protein
PFA	Roti histo Fix, 4%

PLT	Platelet count
PPP	Platelet-poor plasma
PRP	Platelet rich-plasma
PVDF	Polyvinylidene difluoride
PW-Doppler	Pulse-wave Doppler
qPCR	Quantitative real-time PCR
RBC	Red blood cell
RDWs	Red cell distribution width
rev	Reverse
RNA	Ribonucleic acid
RT	Reverse transcription
SDS	Sodium dodecyl sulfate
SDS	Sodium dodecyl sulfate
SDS-Page	Sodium dodecyl sulfate-polyacrylamide gel electrophoresis
sec	Second/s
SEM	Standard error of the mean
Stat3	Signal transducer and activator of transcription 3
TAE buffer	Tris/acetate/EDTA buffer
TF	Tissue factor
TG	Transgene
tPA	Plasminogen activator
TRIS	Tris(hydroxymethyl)aminomethane
TRIS-HCL	Tris(hydroxymethyl)aminomethane hydrochloric acid
uPA	Urokinase
UV	Ultraviolet
V	Volt
VWF	Von Willebrand Factor
WBC	White blood cells
WT	Wildtype

1. INTRODUCTION

1.1. The coagulation system

The coagulation system is a complex and tightly regulated system that can either promote or inhibit clot formation [1]. The balance of equilibrium is essential: Ineffective clotting, as in hemophilia, carries the risk of bleeding [1-4]. However, overactive coagulation can block blood vessels and induces tissue damage, as in atherosclerotic plaque rupture and stroke [3]. Under normal conditions, inhibiting factors keep the coagulation cascade in balance so that blood can continue to flow. This condition is known as hemostasis [3, 5]. Two different ways of activating coagulation have been described (Figure 1).

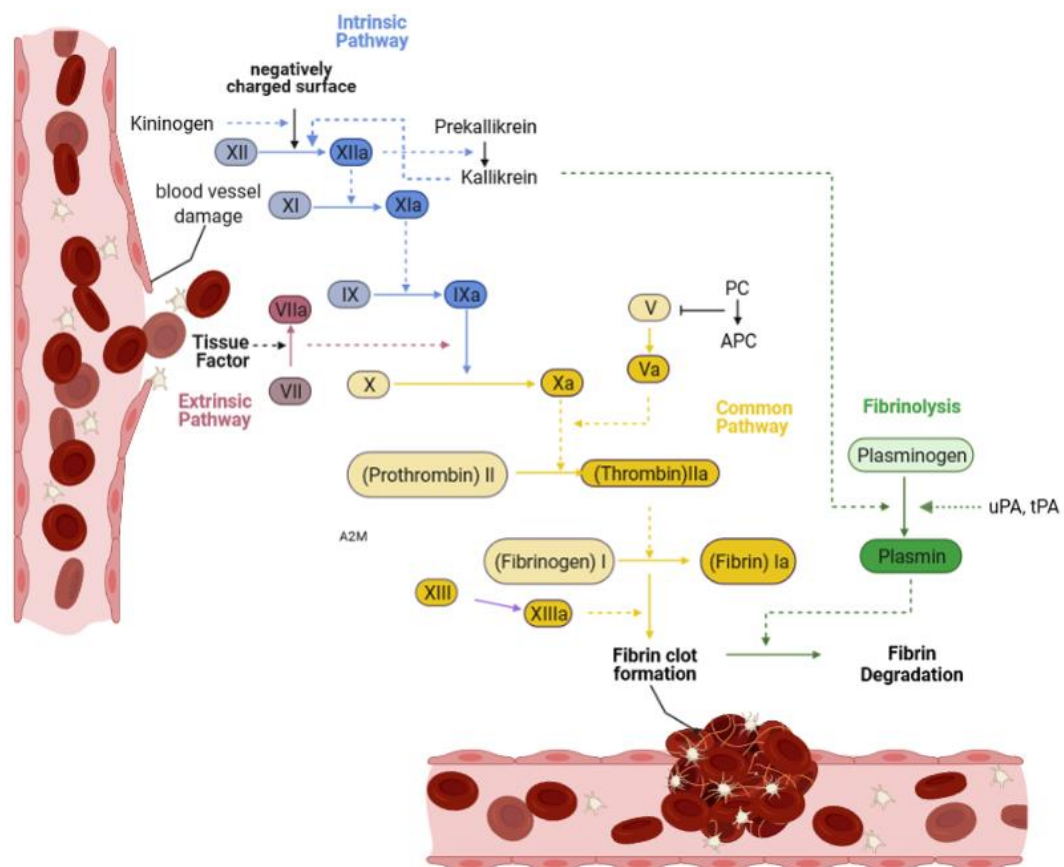


Figure 1 Schematic overview of the coagulation cascade. Solid arrows indicate the conversion to an active protease, while dotted line arrows indicate the activity of the activating upstream protease. Adapted from "Coagulation Cascade", by BioRender.com (2022). Retrieved from <https://app.biorender.com/biorender-templates>.

The intrinsic (contact) pathway (blue pathway Figure 1) is activated by the contact of Factor XII (FXII) with a negatively charged cell surface and with prekallikrein and kininogen [1, 2]. It leads to cleavage and activation of the coagulation factor XIIa (FXIIa), which activates the coagulation factor XIa (FXIa) [1, 6, 7]. The FXIa cleaves and activates coagulation factor IXa (FIXa) [6, 8]. FIXa forms a complex with coagulation factor VIIIa (FVIIIa) and phospholipids, which then activates Xa (FXa) [1, 6]. The activated factor Xa cleaves prothrombin (II), whereby thrombin (IIa) is produced. Thrombin, in turn, cleaves fibrinogen to produce fibrin monomers. The monomers are cross-linked to form fibrin clots by coagulation factor XIIIa (FXIIIa) [2, 3, 6-8]. Even small amounts of thrombin are sufficient to activate the positive coagulation feedback loop. In this case, platelets and coagulation factors V, VIII and XI are activated by thrombin [9]. The additional FIXa binds with FVIIIa on platelets to form the FIXa:FVIIIa complex. This increases the efficiency in activating FX, which leads to a burst of thrombin formation. To prevent uncontrolled thrombin formation, thrombin activates protein C (APC), which binds to thrombomodulin and inhibits the cleavage of FVa and FVIIIa as well as the cleavage of prothrombin [10, 11]. The interaction between the positive and negative feedback loop enables precise control of the coagulation. Vascular injuries initiate the extrinsic coagulation pathway [12] (red pathway Figure 1). Tissue factor (TF) is continuously expressed on the surface of subendothelial tissues [12-14]. Due to injury, subendothelial TF is exposed and activates FVII. FXa, is activated by FVIIa and binds the FXa:FVa complex again, which leads to prothrombin cleavage [2, 12, 15]. Events downstream of the activation of coagulation factor Xa are the same in the intrinsic and extrinsic pathways and is called the common pathway (yellow pathway Figure 1) [15].

The fibrin clot is cleaved once the damaged tissue is repaired [16]. This process is called fibrinolysis (green pathway Figure 1) [16-18]. Plasminogen is activated either by urokinase (uPA) or plasminogen activator (tPA) to plasmin [17, 19]. Fibrin is the main substrate of plasmin. tPA and plasminogen bind on the fibrin surface leading to a better colocalization and

enhanced plasmin generation [3, 16]. Activated plasmin cleaves the cross-linked fibrin to break up the clot.

1.2. *The interaction of inflammation and coagulation*

There is a complicated interplay between inflammatory processes and the coagulation system [11]. It is not uncommon to find an imbalance between coagulation and fibrinolysis activity induced by inflammation leading to hypercoagulation [20]. In the worst case, this may result in thrombotic events such as myocardial infarction, stroke, or disseminated intravascular coagulation (DIC) [21-24]. The process of inflammation is driven by different mediators like cytokines, such as Tumor necrosis factor (TNF α), lipoproteins and bacterial endotoxins [25]. In the clinical situation, plasma levels of various inflammatory markers (e.g high-sensitivity C-reactive protein, serum amyloid A) are increasingly used since an association between increased plasma levels and cardiovascular risk has been shown [24, 26, 27]. Since pro-inflammatory cytokines can affect all coagulation pathways, the intricate relationship between the presence of cytokines, inflammation, and hypercoagulation is of most interest [26]. Generally, inflammation can affect all hemostasis: activation of platelets, activation of coagulation and downregulation of anticoagulants and inhibition of fibrinolysis.

1.2.1. *The impact of Interleukin-6 on coagulation and inflammation*

Cytokines associated with inflammatory processes are Interleukin (IL)-6, IL-1 β , TNF α , interferon- γ and transforming growth factor- β [28, 29]. Different types of cells can produce them, but macrophages and monocytes are primary sources [30]. IL-6 is one of the most important drivers of inflammation and stimulates many acute-phase proteins [30-32]. IL-6 is produced at the site of inflammation and plays a crucial role in both acute and chronic inflammation. It is a 26 kDa protein [33] and produced by many

cell types, including activated monocytes and macrophages, endothelial cells, adipocytes, T-helper cells, and B-cells [34, 35].

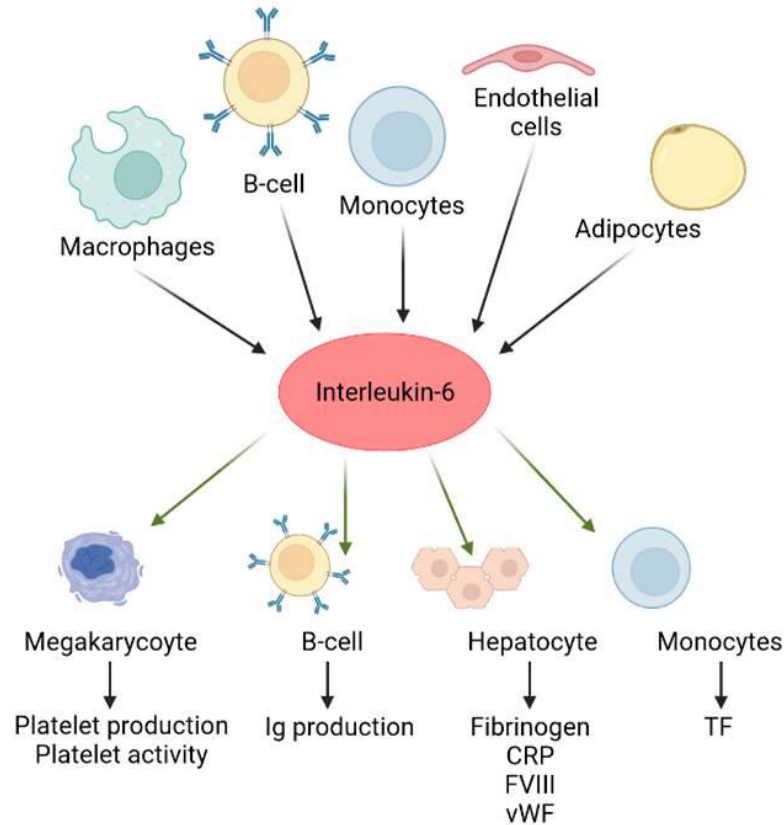


Figure 2 Overview of some of the IL-6 producer and effects of IL-6 [34]. Created with BioRender.com.

IL-6 production has been associated with both pro- and anti-inflammatory effects [36]. Along with IL-1 and $\text{TNF}\alpha$, IL-6 is considered to be one of the most important cytokines during infection and plays an important role in host defense [37]. IL-6 has protective effects during infection, but these activities are critical for maintaining chronic inflammation [38]. This has been shown in models of experimental autoimmune encephalomyelitis, multigenic Castleman's disease, lupus, and plasmacytomas [39-41]. For example, IL-6 signaling plays an essential role in leukocyte recruitment and apoptosis, maintenance of T-cell effector function, and inflammatory activation of tissue in allergy, infection, neuroinflammation, cardiovascular disease, and inflammation-induced cancer [41, 42]. A permanently elevated IL-6 concentration has pathological effects and is one of the main triggers for the dysfunctional chronic inflammatory environment in rheumatoid arthritis [43].

The levels of IL-6 and soluble IL-6 receptor in synovial fluid correlate significantly with the severity of joint destruction [43-45]. In addition, increased IL-6 production has been noted in inflammatory conditions such as inflammatory bowel disease (IBD) like Crohn's disease and ulcerative colitis [46, 47].

Two different IL-6-receptors are involved in IL-6 signaling (Figure 3). On the one hand, IL-6 can bind to the membrane bound receptor complex composed of the IL-6 receptor α (IL-6R α) and the gp130 subunit [48, 49]. This IL-6R is only expressed on certain cell types, for example, hepatocytes and B-cells [50], while endothelial cells and hematopoietic cells do not express the receptor (Figure 3) [51, 52]. On the other hand, IL-6 can bind to the soluble IL-6 receptor α (sIL-6R α) [53]. This soluble form is generated by proteolytic cleavage of membrane-bound IL-6R α [32, 53, 54]. IL-6 together with sIL-6R α forms the sIL-6R α -IL-6 complex that binds the gp130 subunit (Figure 3). All cells expressing the gp130 subunit are thus able to bind the sIL-6R α -IL-6 complex, which activates IL-6 trans-signaling [54]. In principle, the sIL-6R α -IL-6 complex can activate all cells that express gp130 [54-57], but different cell types react differently to this activation.

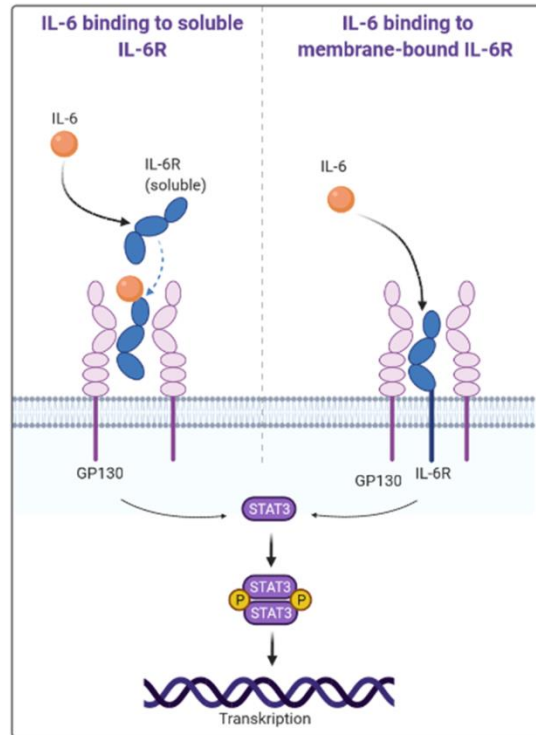


Figure 3 Schematic overview of the IL-6 signaling pathway. IL-6 can bind to soluble IL-6R or membrane-bound IL-6R. Both options lead to the formation of a complex with gp130. IL-6 signals are transduced intracellularly via the JAK/STAT pathway [54]. Created with BioRender.com.

Inflammation is considered as risk factors for venous thromboembolism (VTE) development and elevated IL-6 levels might contribute [58]. Acute inflammation, sepsis, or systemic infection with severe acute respiratory syndrome coronavirus 2 (SARS-CoV-2) are clinical VTE risk factors that can modulate thrombosis through inflammatory mediators [59-63]. Hence, these patients have to be screened thoroughly for VTE development [64-67]. In contrast, diseases like inflammatory bowel disease (IBD), where IL-6 is also of central relevance, are associated with bleeding complications like gastrointestinal bleeding [68]. But IBD is also associated with doubled risk of thrombosis [69, 70]. Up to now, the role of IL-6, which has diverse effects on coagulation, is incompletely understood and will be discussed in the following section of my thesis.

Amrani and colleagues were able to show that IL-6 can regulate the transcription of fibrinogen [71]. Fibrinogen consists of three polypeptides (α , β , and γ) encoded by separate genes. There are promoter regions in α - and γ -Fibrinogen that can be activated by IL-6 [72, 73]. However, it has also been shown that other cytokines involved in inflammation (IL-1 β , IL-4, IL-10, IL-13)

may inhibit the activating effect of IL-6. For example, IL-1 β blocks STAT-3 binding in rats [73]. Here the complex influence of cytokines on hemostasis becomes clear. Increased fibrinogen levels are not only a risk factor for thrombotic events, but are also known as a risk factor for cardiovascular and coronary heart disease [74-76]. In their work, Osterud & Rapaport were able to show that elevated IL-6 levels do not only increase TF expression but also enhance TF surface presentation on monocytes. [77, 78]. Increased TF concentration increases thrombin generation, as TF activates FX by TF-FVIIa complex. Nevertheless, IL-6 may also have an indirect effect here, as it stimulates the inflammation and expression of acute-phase proteins, which in turn may increase the procoagulant activity of TF [79]. As with fibrinogen, other cytokines may counteract the activating effect of IL-6. Also, FVIII can be stimulated by IL-6, which leads to an up-regulation of FVIII. IL-6 has been shown to induce megakaryocytic maturation and increase platelet count *in vitro* and *in vivo* [80-83]. Furthermore, platelets are able to produce IL-6R α [83, 84]. Peng and colleagues could show that animals treated with IL-6 react faster to thrombin stimulation [83, 84].

In summary, the current literature suggests that IL-6 has a prothrombotic influence on the coagulation system.

1.3. The antiproteinase alpha-2-macroglobulin in the context of hemostasis

Alpha-2-macroglobulin (human A2M) is a proteinase inhibitor, which can inhibit a multitude of proteases and non-proteases [85-90]. These include growth factors, TNF- α , incorrectly folded proteins and cytokines [91-93]. The reason for that is the A2M bait region which consists of many protease cleavage sites [94]. A2M is evolutionary highly conserved because of its role in innate immunity [95-97] and is well known as an acute-phase protein. Isaac and colleagues could show that depending on the stimuli, A2M is significantly increasing during inflammation in mice [89]. IL-6 can influence the A2M expression in the liver: IL-6 binds the IL-6R α or sIL-6R α receptor and activates the Janus kinase (Jak) pathway and transcription's signal

transducer and activator of transcription 3 (Stat3). Stat3 can bind the A2M gene promoter, which results in increased transcription of A2M [98-100].

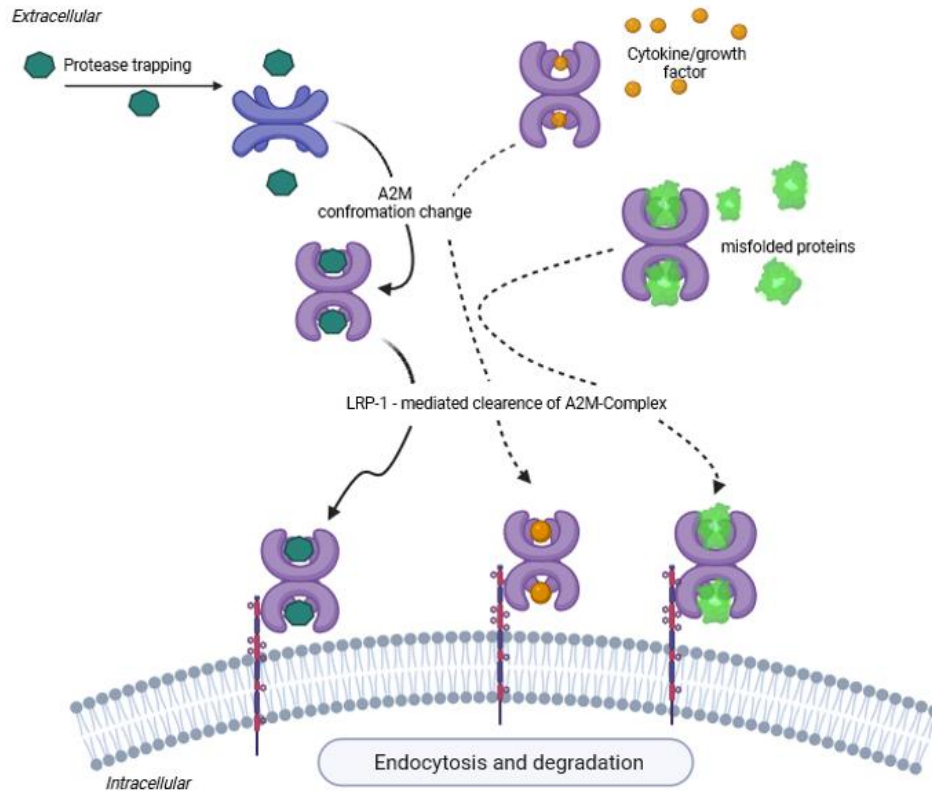


Figure 4 Biological function of A2M adapted from [101]. Tetrameric A2M changes its conformation by covalent binding to proteases (shown in purple), which leads to the exposure of the binding site on A2M for LRP1. Binding to LRP-1 induces the clearance of the A2M complex. Besides that, A2M can bind noncovalent ligands like cytokines, growth factors and misfolded proteins. Created with BioRender.com.

Hepatocytes mainly produce A2M, and also macrophages and fibroblasts are capable to produce it [88, 102, 103]. In humans, two 180kDa large subunits form by covalent disulfide bonds dimers, and two dimers then build by non-covalently binding a 720 kDa homotetramer (Figure 4) [101, 104-106]. The bait region of A2M is located close to the reactive thioester binding site [104, 106]. If a proteinase binds via the thioester binding, a change in conformation occurs (Figure 4) [104, 106]. This leads to the release of the binding sites for low-density lipoprotein receptor-related protein-1 (LRP-1), which is responsible for the clearance of the A2M protease-complex [107, 108]. There is also the possibility that A2M exists as a dimer structure [101]. Hypochlorite induces the dissociation of tetrameric A2M [101]. This results in reduced chaperone activity [101]. However, cytokines and misfolded proteins

can still bind. As a result of the dissociation, the binding sites for LRP-1 are exposed, facilitating degradation in a protease-independent manner (Figure 4) [101].

A2M is associated with coagulation and fibrinolysis (Figure 5) [109]. It has an anticoagulant effect mainly due to thrombin inhibition, while it also displays antifibrinolytic properties by inhibiting plasmin [110-112].

In vivo, A2M is the main inhibitor of free FXa [112, 113]. Via radioactive labeling it was discovered, that A2M binds up to 90% of free FXa in mice within two minutes [114]. A2M can bind to APC (Activated Protein C) and inhibit their effector function [115]. Martos and colleagues showed a correlation between APC-A2M complex plasma levels and venous thromboembolism [116]: The risk of venous thrombosis increased with lower plasma concentrations of the APC-A2M complex [116]. The A2M-dependent APC inhibition depend on Ca^{2+} , Mn^{2+} and Mg^{2+} [110]. The important role of the interaction of A2M and thrombin has been described by diverse groups [85, 117-119]. If A2M binds thrombin, the ability of thrombin to cleave fibrinogen, which is necessary for clot formation is inhibited. The thrombin activity towards smaller binding partners is less influenced, because they still can reach the binding site of thrombin [85, 117, 120, 121]. Thrombin binds to A2M by covalent bonds due to the lysine groups in the proteinase, which reacts with the thioester bonds of the A2M subunits [117, 120]. Mosher already described in 1976 that A2M can activate FXIII in the presence of another protein [122]. This can be attributed to the crystal structure of the receptor-binding domain of A2M. This crystal structure demonstrates that it is approximately 100-residue of the C-terminal domain of FXIII very similar [106]. Shing was able to show that A2M can be a direct ligand for one of the two FXIII subunits [123]. However, the exact function and the relationship between A2M and FXIII are not fully understood [123]. It is known that A2M inhibits fibrinolysis [87, 124, 125]. In addition to the direct inhibition of plasmin, A2M also inhibits tissue plasminogen activator (t-PA), urokinase and kallikrein, which also indirectly impact on fibrinolysis [87, 124, 125].

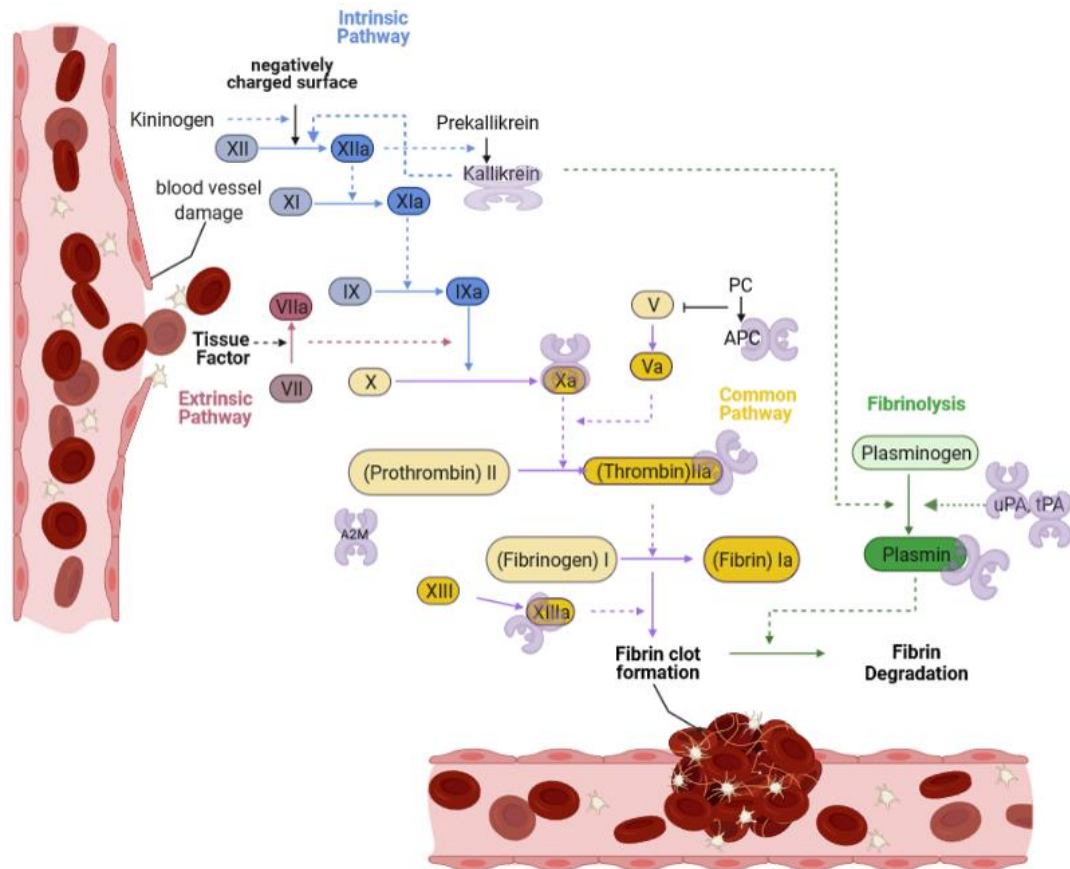


Figure 5 Influence of A2M on coagulation and fibrinolysis cascades. Solid arrows indicate the conversion to an active protease, while dotted line arrows indicate the activity of the activating upstream protease. Free coagulant factors FXa, thrombin and activated protein C (APC) are inhibited by A2M. FXIII subunit B was reported to be inhibited by A2M. A2M can influence fibrinolysis by direct plasmin inhibition and also through inhibition of tissue-plasminogen inhibitor (tPA) and urokinase (uPA) [109]. Adapted from “Coagulation Cascade”, by BioRender.com (2022). Retrieved from <https://app.biorender.com/biorender-templates>.

1.4. *Our mouse model of IL-6 overexpression in myeloid cells (LysM-IL-6^{OE} mice)*

In the following work, I used a new mouse, which allows a conditional IL-6 overexpression combined with an enhanced green fluorescent protein (eGFP), which has been previously described by my former colleague Rebecca Jung (Schueler *et al.* [126]). IL-6 overexpressing mice were generated by gene targeting embryonic stem (ES) cells [127]. A targeting vector has been designed by inserting the cDNA coding for IL-6, followed by an internal ribosome entry site (IRES) and the cDNA coding for an enhanced green fluorescent protein (eGFP) (Figure 6A). The mouse was generated in

the same way as the K14-IL-17A^{ind/+} mouse before [128]. Following homologous recombination into C57BL/6-V6.5 ES cells, the IL-6^{OE} mice have been generated by injection of the cells into fertilized embryos. Crossing homozygous IL-6^{OE/OE} female mice to LysMCre⁺ male mice results in LysM-IL-6^{OE} mice overexpressing IL-6 in LysM⁺ cells heterozygously and Cre^{negative} littermate controls (IL-6^{OE}). Myeloid IL-6 overexpression was confirmed by flow cytometry of splenocytes (Figure 6B and C). Only myeloid cells showed the coupled eGFP signal in addition to the IL-6 product (Figure 6B and C). Furthermore, IL-6 stimulated B-cells to produce IL-6 (Figure 6B and C). Myeloid IL-6 overexpression led to an increased level of circulating plasmatic IL-6 in LysM-IL-6^{OE} mice compared to not detectable IL-6 levels in control mice (Figure 6D). The elevated IL-6 levels in the LysM-IL-6^{OE} mice were lower than what is seen in acute sepsis [129]. Rebecca Jung was able to show that IL-6-mediated inflammation influenced survival [126]. At 10 weeks of age, the mice showed an increased mortality (Figure 6C) [126].

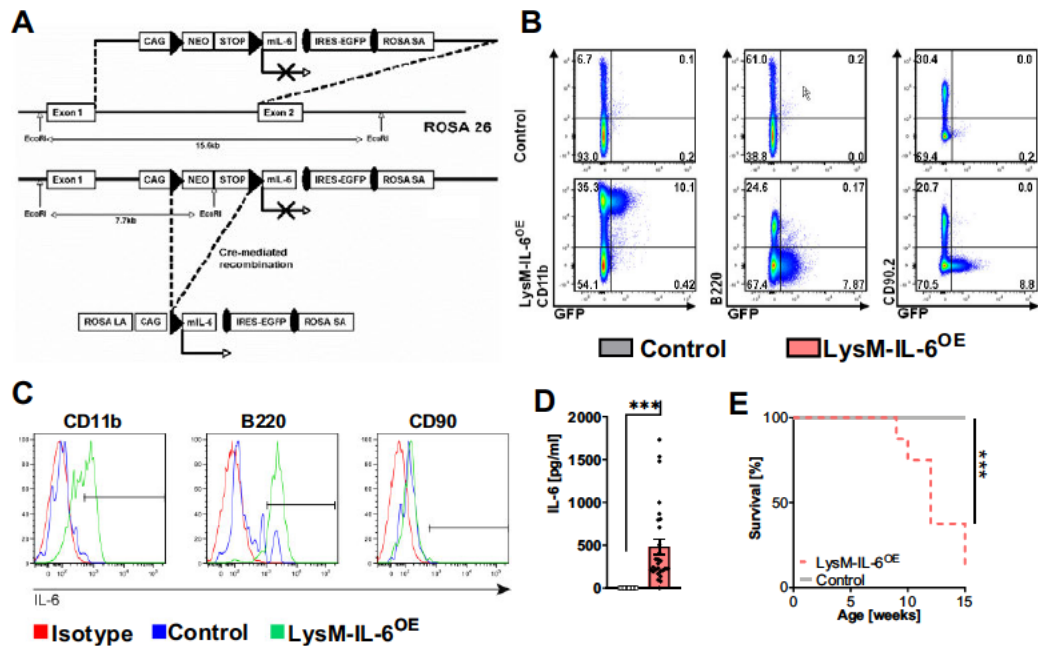


Figure 6 IL-6 overexpression in myeloid cells leads to a reduced life expectancy. A. Generation of the IL-6^{OE} allele by using homologous recombination in embryonic stem cells (C57BL/6-V6.5). Upon Cre-mediated recombination, a lox-P-flanked transcriptional STOP cassette was excised 5' of an IL-6 cDNA insert and an IRES-eGFP element, allowing the expression of IL-6 and eGFP at the same time under the control of the chicken β -actin (CAG) promoter. B. Flow cytometric analysis of splenocytes from LysM-IL-6^{OE} mice and control mice. Cells were stained for CD11b, B220 and CD90.2 and gated versus GFP signal, respectively. Representative plots of n = 4 mice are shown. C. Flow cytometry analysis of splenocytes from LysM-IL-6^{OE} mice and control mice. Cells were stained for CD11b, B220 and CD90.2 and gated versus IL-6 signal, respectively. Representative plots of n = 4 mice are shown. C. Plasmatic IL-6 levels in 10 weeks old LysM-IL-6^{OE} compared to control mice (n.d. = not detectable). N = 19–28, Mann-Whitney t-test. D: Kaplan-Meier survival curve of LysM-IL-6^{OE} and control mice. N = 8 16, Log-rank (Mantel-Cox) test. Figure modified along [117]

1.5. Objective of my thesis

The cytokine IL-6 is of prime importance for switching between the innate and adaptive immune systems [25]. Furthermore, IL-6 appears to influence hemostasis in different ways [73, 130, 131]. Up to now, the exact impact of IL-6 on the coagulation cascade is not well understood. The aim of my thesis is to investigate the influence of IL-6 in hemostasis with a particular focus on coagulation.

In the first part, I investigated the impact of IL-6 on the coagulation system. I analyzed a mouse strain allowing a Cre-mediated IL-6 expression in myeloid cells to study the risk of developing venous thrombosis. Based on the literature, I expected an increased rate of venous thrombosis. Nevertheless, I was confronted with an increased bleeding tendency and reduced venous thrombus formation in the IL-6 overexpression mice. Hence, I wanted to perform a hematological analysis of the blood and the coagulation factors compared to age-matched littermate controls in order to better understand why this bleeding tendency occurred. Furthermore, I wanted to investigate how the acute phase protein A2M was possibly influencing this biological setting since it is already known that IL-6 can trigger A2m expression and participate in coagulation regulation. Since the effect of IL-6 may not only depend on myeloid cell-derived IL-6 I wanted to understand whether the coagulation phenotype that the mice show can be reconstituted by transferring bone marrow cells into control mice. In addition, as part of these experiments, it should also be examined whether the IL-6 effect was dose-dependent and whether even small amounts of donor bone marrow were sufficient to depict the clinical picture.

The results I observed in our mouse model may also be of interest in human diseases, because IL-6 also plays an essential role in the development of IBD [66]. In a “bench-to-bedside” approach, I investigated the impact of elevated IL-6 levels in the acute phase of the disease on clotting and thrombin formation in acute phase IBD patients.

In the last part of my thesis, I aimed to analyze if the increased bleeding tendency in LysM-IL-6^{OE} mice was directly associated with the A2M driven thrombin inhibition.

In total, I performed my thesis to understand the impact of myeloid cell-derived IL-6 on the coagulation cascade and to clarify why mice with increased myeloid IL-6 formation had a reduced thrombus formation.

2. MATERIAL AND METHODS

2.1. Chemicals and equipment

Table 1: List of chemicals

Chemical	Supplier	Country
2-mercaptoethanol	Fluka Chemie GmbH	Buchs, Switzerland
Acetic acid	Sigma-Aldrich	St. Louis, MO, USA
Acrylamide/Bis (40% Lösung)	Bio-Rad	Hercules, CA, USA
Agarose Basic BC	AppliChem	Darmstadt, Germany
Braunol®	B. Braun	Melsungen, Germany
BD FACS Lysing Solution	Becton Dickson GmbH	Franklin Lakes, NJ, USA
Bepanthen® (Eye Cream)	Bayer AG	Leverkusen, Germany
Bovine Serine Albumin	Carl Roth	Karlsruhe, Germany
Calciumchlorid (CaCl ₂)	Carl Roth	Karlsruhe, Germany
Dulbecco's phosphate buffered saline without CaCl ₂ and MgCl ₂ (PBS)	Gibco® life technologies™ or Sigma-Aldrich	Carlsbad, CA, USA St. Louis, MO, USA
ECL Plus WB Detection Systems	GE Healthcare	Chicago, IL, USA
Ethanol	AppliChem GmbH	Darmstadt, Germany
Ethylenediaminetetraacetic acid (EDTA)	Fluka Chemie GmbH	Buchs, Switzerland
Fentanyl y-Janssen 0,5 mg	Janssen-Cilag GmbH	Neuss, Germany
Flumazenil-hameln 0,1 mg/ml	Hameln pharma plus	Hameln, Germany
Fetal Calf Serum (FCS)	Boehringer	Mannheim, Germany
Glycerol	Carl Roth	Karlsruhe, Germany
High Capacity RNA to DNA	Applied Biosystems	Foster City, CA, USA
HEPES	Gibco® life technologies™	Carlsbad, CA, USA
Hydrochloric acid (HCl)	Merck	Darmstadt, Germany
Isoflurane: Forene®	Abbott	Chicago, IL, USA
Isopropyl alcohol	Heidinger	Stuttgart, Germany
Liberase™ TM	Roche	Basel, Switzerland
Magnesium chloride (MgCl)	Roche	Basel, Switzerland
Microscopy Entellan®	Merck®	Darmstadt, Germany
Midazolam-hameln	Hameln pharma plus	Hameln, Germany
Precision Plus Dualcolor Protein Standards	Bio-Rad	Hercules, CA, USA
Proteinase K	Roche	Basel, Switzerland
QuantiTect Probe RT-PCR Kit	Qiagen	Hilden, Germany
RPMI Media 1640	Gibco® life technologies™	Carlsbad, CA, USA
Roti histo Fix, 4% (PFA)	Carl Roth	Karlsruhe, Germany
Sodium chloride (NaCl)	Carl Roth	Karlsruhe, Germany

Sodium deoxycholate	Carl Roth	Karlsruhe, Germany
Sodium dodecyl sulfate (SDS)	Serva Electrophoresis	Heidelberg, Germany
Sodium fluoride (NaF)	Carl Roth	Karlsruhe, Germany
Sodium pyruvate	Gibco® life technologies™	Carlsbad, CA, USA
TaqMan® Gene Expression Assay	Applied Biosystems™	Foster City, CA, USA
Thromboin	Sigma-Aldrich	St. Louis, MO, USA
Tris(hydroxymethyl)aminomethane (TRIS)	Carl Roth	Karlsruhe, Germany
Temgesic 0,3 mg/ml	Reckitt Benckiser	Slough, United Kingdom
Tris(hydroxymethyl)aminomethane hydrochloric acid (TRIS-HCl)	Carl Roth	Karlsruhe, Germany
TRIzol™	Thermo Fischer Scientific	Waltham, MA, USA
Trypan blue	Gibco® life technologies™	Carlsbad, CA, USA
Tween® 20	Appllichem	Darmstadt, Germany

Table 2: List of Instruments and equipment

Name	Supplier
Aspiration system: Vacusafe	Integra Bioscience, Biebertal, Germany
Attune NxT Flow Cytometer	Thermo Fisher Scientific Inc, MA, USA
Centrifuges: 5417R Heraeus or Megafuge 16R	Thermo Scientific, Langenselbold, Germany
Dumont #5/45 Forceps	FST Fine Science Tools GmbH, Heidelberg, Germany
Eppendorf Thermomixer comfort	Eppendorf, Hamburg, Germany
Extra Fine Graefe Forceps	FST Fine Science Tools GmbH, Heidelberg, Germany
Extra Narrow Scissors	FST Fine Science Tools GmbH, Heidelberg, Germany
Gel Doc XR	Bio-Rad, Hercules, CA, USA
Graefe Forceps	FST Fine Science Tools GmbH, Heidelberg, Germany
Halsted-Mosquito Hemostats	FST Fine Science Tools GmbH, Heidelberg, Germany
Heating Block, MB-102	BIOER, Hangzhou, China
Leica M50 Mikroskop	Leica Microsysteme, Wetzlar, Germany
Leica Sp8 (Confocal)	Leica Microsysteme, Wetzlar, Germany
MAGPIX® Luminex's xMAP®	Luminex, MV 's-Hertogenbosch,

	Netherlands
Sterile workbench: Hera Safe	Thermo Scientific, Langenselbold, Germany
T3000 Thermocycler	Biometra, Göttingen, Germany
Tecan Spark®	Tecan, Männedorf, Switzerland
TGeneTouch Thermal Cycler	BIOER, Hangzhou, China
Thermocycler:	Bioer Technology, Hangzhou, China
TMyCycler™ Thermal cycler	Bio-Rad, Hercules, CA, USA
Ultrasound device: Vevo 770 or 3100 System	Visual Sonics, Toronto, Canada

2.2. Buffer

Lysis buffer

TRIS	50 mM
EDTA	25 mM
NaCl	300 mM
SDS	0.2% (v/v)
Proteinase K	0.2 mg/ml

pH adjusted to 7.8.

Tris/acetate/EDTA (TAE) buffer

TRIS	40 mM
Acetic acid	18 mM
NaCl	100 mM
EDTA	10 mM

Git buffer

Guanidiniumthiocyanat	4 M
Na-Citrat pH=7,0	25 mM
N-Lauroylsarcosin	0.5 %
B-Mecaptoehtanol	0.1 mol/l

RIPA buffer

Triton X-100,	1 %
Tris pH 7.4–7.6	20 mM
NaCl	150 mM
NaF	1 mM
EDTA	1 mM
EGTA	1 mM
Glycerolphosphatase	1 mM
SDS	1 %
PMSF	100 mM
protease phosphatase inhibitor cocktail	0.1 %

Sample buffer (6x)

SDS	1 g
Bromophenol blue	4 mg
Glycerol	3.6 ml
2-mercaptoethanol	600 µl

Add ddH₂O up to 12 ml.

Separating gel buffer

Tris-HCL	1.5 M
pH adjusted to 6,6 with HCL.	

Stacking gel buffer

Tris-HCL	500 mM
pH adjusted to 8,8 with HCL.	

Transfer buffer

Tris	12.4 mM
Glycine	0.1 M
Methanol	10 % (v/v)

Blocking buffer I

Tris	500 mM
NaCl	1.3 M
Tween® 20	0.1 % (v/v)

1x Ammoniumchloride/potassium (ACK) buffer

NH ₄ Cl	1.5 M
KHCO ₃	100 mM
EDTA-2Na	100 mM

2.3. Mouse Experiments

All animal experiments were approved by the land of Rhineland-Palatinate (approval number G15-1-051). Mice were bred and housed in the facilities of the Translational Animal Research Center (TARC) Mainz.

2.3.1. *LysM-IL-6^{OE}* Mice

In 1987, Sauer et al. developed the Cre/loxP-system, which can generate genetically modified animals [132, 133]. Marth and Rajewsky further developed this system: either for upregulation or downregulation/knock-out of a gene of interest [127, 134]. Making use of the Cre recombinase from Bacteriophage P1, it is feasible to cut out a specific sequence [134]. The requirement is that loxP sites flank the sequence of interest. It is in consequence possible to use a tissue or cell-specific Cre to induce the gene deletion in a tissue or cell type-specific manner [127, 134].

LysM-IL-6^{OE} mice overexpress IL-6 in all Lysozyme M⁺ (*LysM*⁺) cells. The *LysM* gene is expressed in myeloblasts, immature and mature macrophages, and neutrophils [135, 136]. To generate this mouse strain, *LysM-Cre* mice [136] were crossed to *IL-6^{OE}* mice (generated by S. Karbach and A. Waisman, Jung and Knopp et al submitted to Cardiovasc Res.). *IL-6^{OE}* mice express an additional copy of the IL-6 gene, which is inserted into the ROSA26 locus, combined with a STOP-codon flanked by loxP sites. Through Cre-mediated recombination, the STOP-codon is excised and IL-6 is constantly overexpressed. By using the *LysM-Cre*, IL-6 was overexpressed in all myeloid cells.

2.3.2. *Subtotal vena cava stenosis model*

The vena cava stenosis model was performed in 8-12 week-old mice as described before [137-139]. The bodyweight of the mice was determined and the dosage of the anesthesia was adjusted accordingly. Anesthesia was

applied by intraperitoneal injection of a mixture of fentanyl (0.05 mg/kg; Janssen-Cilag GmbH), medetomidine (0.5 mg/kg; Pfizer Deutschland GmbH), midazolam (5 mg/kg; Ratiopharm GmbH). The hair in the ventral abdominal area was completely removed with depilatory cream and the skin was disinfected with Octeniderm (octenidine dihydrochloride 0.1 g, 1-propanol (Ph.Eur.) 30.0 g, 2-propanol (Ph.Eur.) 45.0 g). To ensure the depth of the anesthesia, the intercalary reflex was tested. The eyes were covered with Bepanthen eye ointment for protection. The mouse was fixed on a 37 °C warming plate in the supine position. Then the abdominal cavity was opened: first, the skin, then the muscle layer, and the peritoneum were opened. A piece of gauze moistened with isotonic saline solution was prepared next to the mouse. Then the intestine was exposed and put out to the right (or left, depending on the surgeon's needs); if necessary, an incision of the duodenocolic ligament was made here. The intestine was kept moist with 0.9% NaCl and the left/right-sided abdominal wall was stretched with a holding thread if necessary. The ligature operation itself was performed by dissecting the inferior vena cava (IVC) (blunt) up to the confluence of the renal vein. With curved forceps, the IVC was tunneled at the level of the confluence, a surgical thread was pulled through (8/0 thread) and a spacer was inserted before tightening. After the ligation, the spacer was removed. At the end, the muscles were sutured using a continuous suture and the skin was sutured with 7/0 thread with a single button suture [140-142]. After the operation, anesthesia antagonization was performed using s.c. injection of atipamezole (0.05 mg/kg) and flumazenil (0.01 mg/kg). The mice remained in the cage on a warming plate until signs of decreasing sedation were observed.

For postoperative analgesic therapy, a single subcutaneous injection of buprenorphine (0.075 mg/kg) was administered directly after the procedure. On the two following days, analgesia was carried out using carprofen (5 mg/kg body weight).

The vena cava stenosis model was performed in cooperation with [REDACTED] who performed here bachelor thesis in our working group.

2.3.3. High-frequency ultrasound

To determine the thrombus formation following IVC ligation in mice, high-frequency ultrasound was performed by using the device Vevo 3100 (Visualsonics) with the transducer 550 (25-55 MHz) [143]. The mice were sedated with isoflurane (mask anesthesia, 0.5-5% in room air) and positioned on their back on a 37 °C warming plate. If necessary, the hair was removed from the abdominal area and contact gel was applied. During the examination, body temperature was monitored with a rectal probe and kept at 37°C. Electrocardiography and respiratory rate were checked non-invasively via the contact electrodes and maintained at 500 beats per minute [141]. The ultrasound head was aligned along the linea alba for duplex sonography of IVC. In the sham group, the vascular wall of the vein was visualized by the more dense structure compared to the surrounding fatty tissue. In the experimental group, the side of the ligation was visualized, and venous thrombi were identified by a high fibrin density which is more compact than blood. The reduction of the blood flow in the vein was quantified by pulse-wave Doppler and color Doppler. With the pulse-wave Doppler (PW-Doppler), the speed of blood flow was analyzed in a selectable sample volume. The PW-Doppler sends short and quick pulses of ultrasound and uses the effect of moving particles changing the innate pulse. These are analyzed with regard to the Doppler-shift, taking into account the return time in which no second ultrasonic wave is emitted [144]. Color Doppler visualizes the flow direction and velocity within a defined area. The direction of flow towards the transducer is usually shown in red, away from the transducer is shown in blue color.

To study the formation of thrombosis, we measured the area and the length three days after ligation. After ultrasound analysis, the mice were transferred back to the cage, to fully awaken within a few minutes.

2.3.4. Tail bleeding assay

The tail bleeding time is an *in vivo* assay in which the interaction of platelets and damaged vessel wall leads to sufficient

plug formation. It is defined as the time after which the bleeding has completely stopped [145, 146]. This assay was performed in 8-12 week old mice. The bodyweight of the mice was determined and the dosage of the anesthesia was adjusted accordingly. Anesthesia was applied by intraperitoneal injection of a mixture of fentanyl (0.05 mg/kg; Janssen-Cilag GmbH), medetomidine (0.5 mg/kg; Pfizer Deutschland GmbH), midazolame (5 mg/kg; Ratiopharm GmbH). Mice were placed in a prone position. A 10 mm long distal piece of tail was removed with a scalpel and the tail was placed in a pre-warmed (37°C) isotonic saline solution. Afterward the mice were monitored over 12 min and bleeding time was recorded as described previously [146].

2.3.5. Adenoviral construct and treatment

The knockdown with an adeno-associated virus (AAV) is an *in vitro* and *in vivo* method to knock down a specific target gene in nearly all cell types [147]. First, the AAV-shRNA vector was constructed as a plasmid in *E. coli* and then transfected into packaging cells using helper plasmids. The plasmid comprises the following components: The vector region lies between the inverted terminal repeats (ITRs). The shRNA expression cassette placed between the two ITRs is introduced into the target cells together with the viral genome. The shRNA is expressed from a U6 promoter. It leads to the degradation of the target gene mRNA in infected cells. When the AAV virus is added to target cells, the single-stranded linear DNA genome is introduced into the cells, where it is converted to double-stranded DNA by the host cell's DNA polymerase machinery. AAV vector DNA forms episomal concatemers in the host cell nucleus. The concatemer remains in non-dividing cells until they die, but dividing cells does dilute the concatemer; hence, the knockdown effect is reversible.

The adenoviral construct was generated by Vector Biolabs (Pennsylvania, USA): AAV8-mCherry-U6-mA2m-shRNA delivered murine small hairpin *A2m* cDNA (RefSeq: NM 175628) under control of an U6 promotor to achieve knockdown of the *A2m* gene. AAV8-mCherry-U6-scrmb-shRNA served as a negative control. 2×10^{11} GC were injected via the tail vein and mice were analyzed after 5 weeks (7).

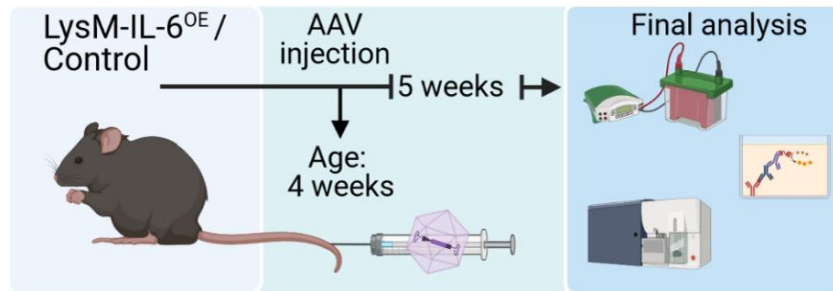


Figure 7 Experimental set-up for treatment with AAV8shRNA *A2m* or AAV8shRNA *scrmb*. Four week old mice were treated with AAV8-mCherry-U6-mA2m-shRNA or AAV8-mCherry-U6-scrmb-shRNA served for five weeks. Afterward, the mice are analyzed regarding the inflammatory and coagulation phenotype. Created with BioRender.com.

2.3.6. Bone marrow transplantation

Bone marrow (BM) chimeras were created by transplanting hematopoietic stem cells from a donor animal to a recipient animal. Wild type C57BL/6 mice carry the leukocyte marker Ly5.2 (CD45.2). C57BL/6 Ly5.1 mice express the marker Ly5.1 (CD45.1), making it easy to identify the adoptively transferred cells in the organs of recipient mice by staining with anti CD45.1 [148-150]. Different amounts of LysM-IL-6^{OE} and control BM were mixed and transferred in order to analyze a dose-dependent effect of transplanted BM. Donor animals were euthanized by an isoflurane overdose and bone marrow was isolated from the femur and tibia. BM mainly consists of pluripotent hematopoietic stem cells, as well as mature hematopoietic cells arising from the lymphoid, and erythroid lineages [151].

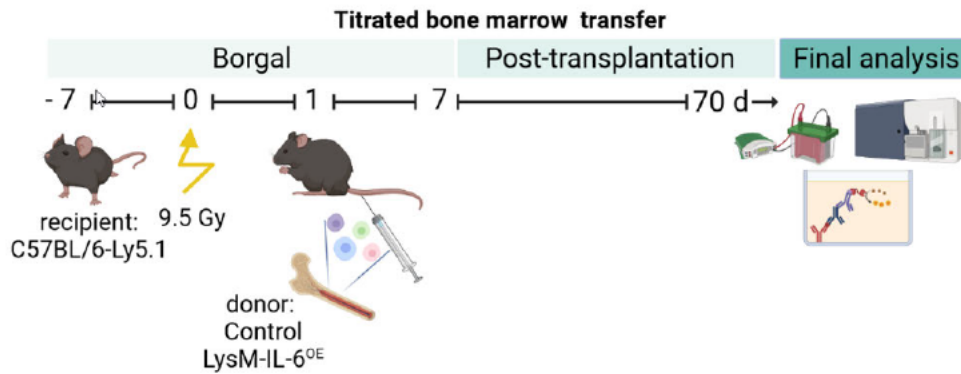


Figure 8 Schematic representation of bone marrow transplantation. C57BL/6-Ly5.1 mice are irradiated on day 0, one day after donor bone marrow is transferred. Before and after irradiation they are treated with Borgal for 7 days. The post-transplant phase is 70 days. Afterward, the mice are analyzed regarding the inflammatory and coagulation phenotype. Created with BioRender.com.

The recipient animals are lethally irradiated (9.5 Gy) 24 h before BM transplant. 5×10^6 cells were transferred into the irradiated recipient animals by intravenous injection into the tail vein (Table 3). The irradiation induces an intermittent immune compromise, animals received antibiotic-containing drinking water (Borgal®; contains: Sulfadoxinum 62.5 mg/ml, Trimethoprimum 12.5 mg/ml) 7 days before the irradiation and up to 7 days after transplantation. The final experiment takes place 70 days after bone marrow transplantation (Figure 8).

Table 3: Transplant scheme

Donor	Recipient
100% Control BM	C57BL/6 Ly5.1
100% LysM-IL-6 ^{OE}	C57BL/6 Ly5.1
10% LysM-IL-6 ^{OE} + 90% Control BM	C57BL/6 Ly5.1

2.3.7. Euthanasia of mice

Mice were sacrificed by inhalation overdose of isoflurane. Organs were collected and were either fixed in PFA or shock frozen in liquid nitrogen. Cells were isolated as described in the following chapter.

2.3.8. Organ isolation und preparation

2.3.8.1. Mouse blood isolation

Whole blood sample were obtained by cardiac puncture of the right ventricle using a 26-gauge needle (Sterican® Gr. 18, G 26 x 1"/ø 0.45 x 25 mm, B.braun, Germany) into syringes containing citrate (ratio 1:10) to prevent coagulation.

To isolate plasma, whole blood was centrifuged at 200 g for 4 min followed by 30 s at 2,000 g at room temperature to obtain platelet rich-plasma (PRP). PRP was stored at -80 °C until further use.

If the blood was used for Thrombin generation or different Platelet assays, platelet count in the obtained PRP was performed using the cell counter KX-21N (Sysmex Corporation). The remaining blood was centrifuged 10 min at 2000 g to obtain PPP (platelet-poor plasma) that was used to adjust to PRP platelet count to 200×10^9 platelets/l.

2.3.8.2. Spleen

Spleen was isolated from mice, minced through a nylon cell strainer (40 µm) and washed with PBS/FCS 2% (v/v). Red blood cells were lysed by adding 1 ml of 1x ACK buffer for 3 min at room temperature and the reaction was stopped by adding 9 ml PBS/FCS 2% (v/v). After centrifugation (300 x g, 6 min, 4 °C), the cell pellet was filtered through gaze to remove fat tissue, resolved in 10 ml PBS/FCS 2% (v/v) and counted.

2.4. Molecular Biology

2.4.1. DNA isolation

Ear biopsies were used to isolate genomic DNA to identify the mouse genotype. For this purpose, biopsies are digested (digestion mix: 100 µl

Lysis-Buffer, 2 μ l proteinase K, 10mg/ml) at 56 °C for 2 h. Isopropanol (100 μ l) was added to precipitate genomic DNA from the remaining cell debris and the samples were centrifuged at 14,000 rpm for 20 minutes. The supernatant was discarded and the pelleted DNA was washed twice with 300 μ l of ethanol (70% (v/v) (centrifugation 14,000 rpm for 10 minutes) and dried at 37 °C for 10 min. Finally, DNA was solved in 300 μ l distilled water and stored at 4 °C.

2.4.2. Quantitative real-time PCR

Quantitative real-time PCR was used to examine the expression of specific genes in the liver. A distinction can be made between a two-step RT-PCR and a one-step RT-PCR. The cDNA reverse transcription (RT) takes place first with RNA as a template in the two-step variant. A sample of this RT reaction is then used in a subsequent PCR, in which the cDNA serves as a template [152]. As a result, the conditions in the two reactions can be optimally adjusted to the enzymes used in each case. In addition, a large number of transcripts (20-100) can be amplified from a single cDNA synthesis [153].

In contrast to the two-step variant, the one-step variant performs the reverse transcription and the PCR in one single reaction [154]. Since one of the two primers is used in the reaction for the cDNA first strand synthesis, sequence-specific primers are an indispensable prerequisite for the one-step RT-PCR. Advantages of the one-step PCR are simple usage and less risk of contaminations since no transfer is necessary between RT and PCR reaction [154, 155].

Either the one-step TaqMan® Gene Expression Assay (Applied Biosystems™, Foster City, CA, USA) or the two-step the PowerUp™ SYBR™ Green Master Mix (Applied Biosystems™, Foster City, CA, USA) was used for quantitative real-time PCR [156, 157]. This was done according to the manufacturer's specifications. All primers used are listed in Table 4 below.

Table 4: Primer used for the Quantitative real-time PCR.

Primer Name	Gene name	Forward	Reverse
<i>FXII</i>	<i>Factor XII</i>	TCC TCC ATC ACC TAC CAG CA	GAT CGC GCA ACT GTT GGT TT
<i>FXI</i>	<i>Factor XI</i>	ACC TAC TAT CCA TCG CAC AG	CTC CCC TCC CAT GAA GTA TT
<i>FIX</i>	<i>Factor IX</i>	TGCTGGTGCCAAGTTGG ATT	TGCTTGCACCTGCCAT TTTT
<i>FVIII</i>	<i>Factor VIII</i>	CAC CAA CAT GTT TGC TAC TTG GTC TC	GCT GGT AAA GAG AGA TTT CAC TCC C
<i>VWF</i>	<i>Von Willebrand Factor</i>	CTT CTG TAC GCC TCA GCT ATG	GCC GTT GTA ATT CCC ACA CAA G
<i>FX</i>	<i>Factor X</i>	TTC CGG ATG AAC GTG GCC CCT	ATG CGT GCG TCC AAA ACC GCT
<i>FV</i>	<i>Factor V</i>	CGA TCT GCT CAA AAT CAA GAA GGT AAC G	CAT GTG CCC CTT GGT ATT GCT GTT TCC
<i>PT</i>	<i>Prothrombin</i>	CTG GTT ATA AAG GGC GGG TGAC	GCC AGC ACA GAA CAT GTT GTC AG
<i>AT</i>	<i>Antithrombin</i>	AGC CAA GTC GCT AAG ATT TCA	AAT CGT TCT TGG AGG GGC AG
<i>Fαchain</i>	<i>Fibrinogen α chain</i>	GCC CAA CGA GAG ACT GTG AT	GTC ATT CAG GCT GCC GAA AC
<i>Fβchain</i>	<i>Fibrinogen β chain</i>	TGA GCC TCC TGA TGT GGT TTC	TGG CAG AGA TGG GCT TAT GT
<i>Fγchain</i>	<i>Fibrinogen γ chain</i>	CCA CGA GAC AAG CAT TCG GT	CAC TTT CTT TGG CGC CCT TG
<i>A2m</i>	<i>α2 Macroglobulin</i>	AGG TGC TGA GGT ATC GGA AC	AGG AGA TCC TGT GTG TTC TGC

2.4.3. Polymerase Chain Reaction (PCR)

The genotype of the mice should be determined by Polymerase Chain Reaction (PCR) [158]. A PCR reaction master mix was used, which contained 2x Taq Plus Mix (2x Taq Plus Master Mix (Dye3 Plus, Vazyme), 2.5 nM specific primer, distilled water and 2 μ l genomic DNA. The PCR reaction was performed in a thermal cycler (Table 5). Here, the double-stranded DNA was first denatured by heating to 94-95 °C for 5 min and followed by 35 amplification cycles that start at 94-95 °C for 30-40 sec, followed by the annealing of the primers to the single stranded DNA at 54-58 °C (corresponding to the specific annealing temperature in Table 5) and the elongation at 70-72 °C for 30-45 sec. The PCR reaction was finished after one final elongation step at 70 °C for 5-10 min [154, 158].

Table 5: List of gene loci, primer name and sequence, annealing temperature and band size. The primers were obtained from Metabion International AG, Martinsried, Germany. Cre = Cre recombinase, fwd = forward, rev = reverse, bp = base pairs, WT = wildtype, TG = transgene.

Gene locus	Primer Name	Sequence	Annealing Temperature	Band size
Cre locus	General Cre fwd.	5'-GGA CAT GTT CAG GGA TCG CCA GGC G-3'	58 °C	250 bp
	General Cre rev.	5'-GCA TAA CCA GTG AAA CAG CAT TGC TG-3'		
Rosa locus	Rosa FA	5'-AAA GTC GCT CTG AGT TGT TAT-3'	58 °C	WT: 624 bp TG: 200 bp
	Rosa RA	5'-GGA GCG GGA GAA ATG GAT ATG-3'		
	SpliAcB	5'-CAT CAA GGA AAC CCT GGA CTA CTG-3'		
LysM Cre	Cre8	5'-CCC AGA AAT GCC AGA TTA CG-3'	54 °C	WT: 350 bp TG: 780 bp
	MLys1	5'-CTT GGG CTG CCA GAA TTT CTC-3'		
	MLys2	5'-TTA CAG TCG GCC AGG CTG AC-3'		
IL-6 ^{ind} transgene	IL-6 fwd.	5'-CTA CTC GGC AAA CCT AGG GCG-3'	58 °C	382 bp
	IL-6 rev.	5'-GCT GCC TGC AAA GGG TCG CTA CAG-3'		

2.4.4. Agarose gel electrophoresis

Agarose gel electrophoresis is used as a standard method to identify DNA fragments [154, 159]. To separate the amplification product, agarose powder was dissolved in TAE buffer to a final concentration of 2%. The agarose suspension was boiled in a microwave and cooled to a temperature of 50-60 °C. Then Midori Green Advance (NIPPON Genetics, Düren, Germany) was added, the suspension was casted to a gel electrophoresis chamber and a comb was used to form wells. After polarization, the gel was placed into the electrophoresis chamber filled with TEA buffer and the comb was carefully removed. The PCR reaction mix was loaded into the wells with an additional well that contains the DNA-marker (100 bp DNA Ladder, New England Biolabs) and an electric field (120-130 V) was applied. Due to its anionic charge, the DNA moves in the electric field from the cathode to the anode. The mobility depends on the molecular size and length. The DNA dye Midori Green Advance binds to the DNA and could be detected by ultraviolet (UV) light in the UV imager (Gel DocTM, Bio-Rad, USA).

2.4.5. RNA isolation and measurement

Isolated liver tissue was pulverized and homogenized in Git buffer. RNA isolation was based on the phenol-chloroform extraction protocol [160]. RNA concentration was measured with NanoDrop™ spectrophotometer (Thermo Fisher) or Tecan's Spark® NanoQuant Plate™ (Tecan Spark, Tecan Inc., Männedorf, Switzerland).

2.5. Cell Biology

2.5.1. Blood count

Complete blood counts and hematocrit were determined with an automatic cell counter VetScan HM5 (Abaxis Europe GmbH, Germany). It uses the impedance technology: Neutrally charged blood cells pass through an electrically charged area, which generates an altered pulse. The number of pulses per minute is measured.

Blood was drawn as described in section 2.3.8.1 and 50 µl of it used immediately afterwards and measured using the VetScan HM5.

2.5.2. Hepatocyte isolation

To prove the successful down-regulation of A2M by the adenoviral construct as described in 2.3.5, primary hepatocytes were isolated, and the mCherry signal was measured. For this purpose, the liver was perfused, and digested with collagenase. The hepatocytes were isolated from other cells, and afterward, the single-cell suspension was cultured. The isolation was performed according to the protocol [161] in cooperation with ██████████

██████████.

2.5.3. Flow cytometry analysis

Single cell solutions of the spleen were stained with fluorogenic antibodies to differentiate between specific cell populations as described recently [162]. First, the pelleted single cells were resuspended in PBS/FCS 2% (v/v) and incubated with anti-CD16/CD32 (Bio X Cell, West Lebanon, USA) to block unspecific binding sites for 10 min at 4°C. Next, cells were washed with 100 µl PBS/FCS 2% (v/v), centrifuged (300 x g, 6 min, 4 °C) and the antibody master mix was added and incubated for 30 min at 4 °C. The used antibodies are listed in Table 6. Afterward, the cells were washed like before, and the stained cells were acquired at the Attune NxT Flow Cytometer (Thermo Fischer Scientific, MA, USA) and analyzed using FlowJo Software (BD, New Jersey, USA).

Table 6 List of antibodies for flow cytometric staining. PerCP = Peridinin-Chlorophyll-protein, APC = Allophycocyanin, PE/Cy7 = Phycoerythrin/ Cyanine dye 7.

Antigen	Fluorophore	Dilution	Clone	Isotype	Supplier
B220/CD45R	PerCP efl.710	1:100	RA3-6B2	Rat IgG2a	eBioscience™
F4/80	APC	1:400	BM8	Rat IgG2a	eBioscience™
Viability dye	efluor780	1:1000	-	-	eBioscience™
Ly6C	efluor450	1:800	HK1.4	Rat IgG2c	eBioscience™
CD45.2	Brilliant Violet 510	1:200	104	Rat IgG2b	eBioscience™
Ly6G	Super Bright 600	1:800	1A8	Rat IgG2a	eBioscience™
CD90.2	Super Bright 645	1:100	53-2.1	Rat IgG2a	eBioscience™
CD11b	PE/Cy7	1:1200	M1/70	Rat IgG2b	eBioscience™

Figure 9 shows the gating strategy to analyze the CD11b⁺ myeloid cells and subdivide the populations into Ly6G⁺Ly6C⁺ neutrophils, Ly6G⁻Ly6C^{high}, or Ly6G⁻Ly6C^{low} monocytes/macrophages. Initially, the doublets were excluded in the upper row of Figure 9. In the next step, CD45⁺ viable cells and all double negative cells for B or T-cells (B220 CD90.2) were gated. All CD11b⁺ cells were then further divided into Ly6G⁺Ly6C⁺ neutrophils, Ly6G⁻Ly6C^{high}, or Ly6G⁻Ly6C^{low} monocytes/macrophages [163].

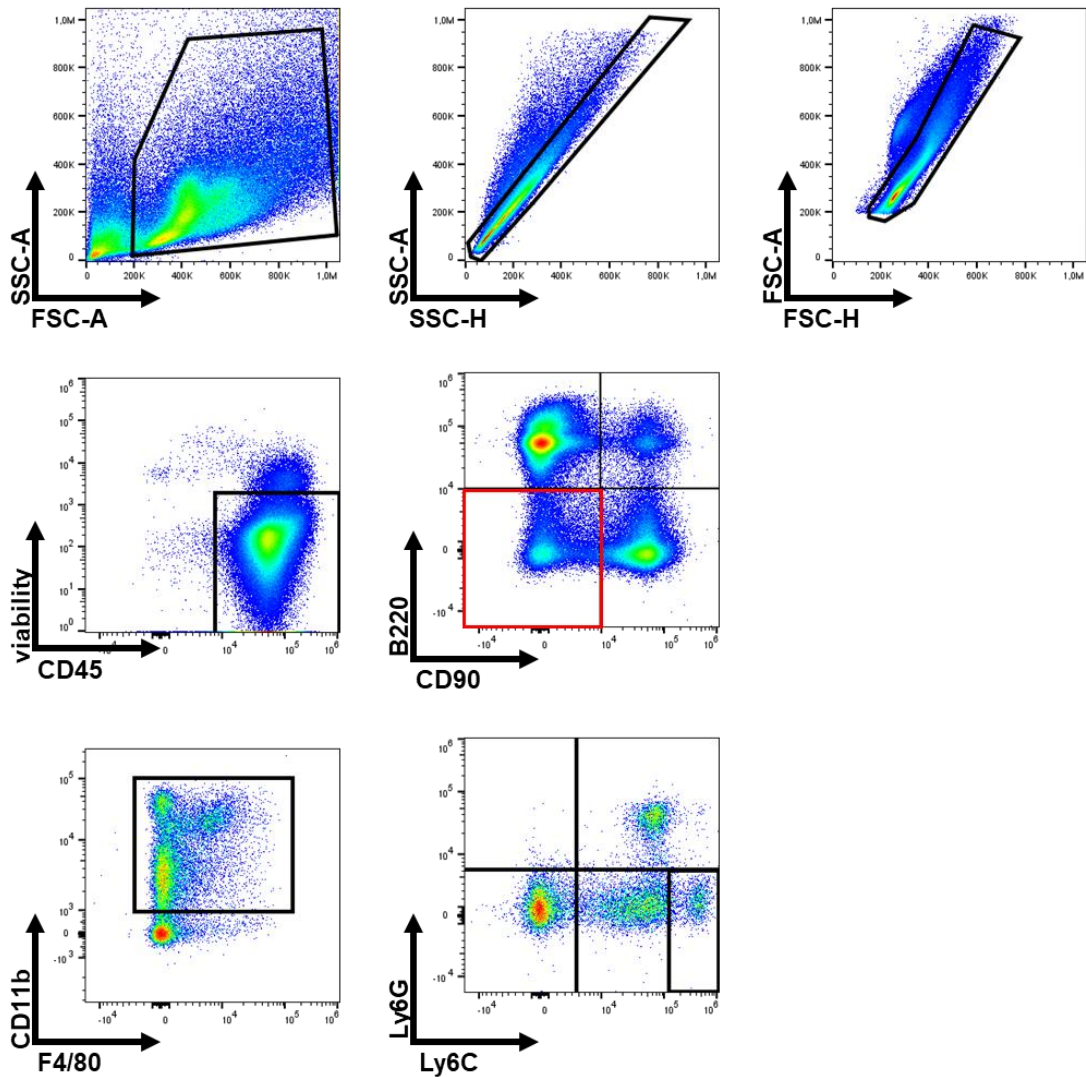


Figure 9 Gating strategy of isolated splenocytes. Spleen cells were gated on doublets (upper row), viable CD45+, B220- CD90.2-(marked red) and expression of CD11b+, Ly6G and Ly6C was examined. Representative plot of LysM-IL-6^{OE} splenocytes is shown.

2.6. Biochemistry

2.6.1. Protein isolation

Isolated liver tissue was pulverized and homogenized in RIPA buffer. The samples were lysed for 15 min on ice and centrifuged at 11000 x g for 15 min at 4 °C. The supernatant, which contains the soluble proteins, was transferred and the protein concentration was determined by Lowry Assay (DC™ Protein Assay, Bio-Rad, USA). The assay was performed according to the manufacturer's instruction and the protein concentration was measured

photometrically at 750 nm with the Tecan Spark® reader (Tecan, Switzerland).

2.6.2. Sodium dodecyl sulfate-polyacrylamide gel electrophoresis (SDS-PAGE)

SDS-PAGE is a widely used method based on the discontinuous SDS-PAGE, first described by Laemmli et al [164]. Proteins are separated in the presence of sodium dodecyl sulfate (SDS) due to their molecular weight in the direction of the anode. By adding an anionic detergent, the intrinsic charge of the proteins is covered, those anionic micelles with a constant net charge per unit of mass are created. β -mercaptoethanol in the sample buffer reduces disulfide bridges in the polypeptide chains. The molecular mass of the proteins is then determined by electrophoresis [154].

Depending on the molecular weight of the protein of interest, gels were prepared according to Table 7. Protein lysates were diluted to an appropriate concentration with 6x sample buffer. Polymerized gels were installed in the electrophoresis tank, filled with 1 x running buffer (10x Tris/Glycine/SDS Electrophoresis Buffer, bio-rad, USA) and samples were loaded into the gel. A prestained protein marker was applied (Prestained Protein Marker BlueStar PLUS, Nippon Genetics, Lab Supplies) to examine the protein regarding to its molecular size. The electrophoresis was performed with the Mini-Protean-III-System (Bio-Rad, USA), by applying a voltage of 80 V till the samples enter the stacking gel. Subsequently, the voltage was changed to 120-140 V till a sufficient separation of the protein marker could be seen.

Table 7: Components of SDS-PAGE gel

Chemical	Separating Gel		Stacking Gel
	7,5 %	10 %	4 %
ddH ₂ O	5,4 ml	4,8 ml	3,2 ml
Stacking gel buffer	2,5 ml	2,5 ml	-
Separating gel buffer	-	-	1,2 ml
Acrylamide/bis-Acrylamide	1,88 ml	3 ml	0,5 ml
10 % (v / v) SDS	100 µl	100 µl	50 µl
10 % (v / v) APS	100 µl	100 µl	50 µl
TEMED	10 µl	10 µl	5 µl

2.6.3. Western blot analyses

Immediately after the gel electrophoresis, the separated proteins were transferred to a protein-binding membrane. The standard method for protein blotting is electrophoretic transfer, whereby the proteins are transferred from the gel to a membrane by applying a voltage. In this work, the wet tank method was used [165]. For this purpose, a 0.2 µm polyvinylidene difluoride (PVDF) membrane was first activated in methanol for 5 min and then incubated in transfer buffer for 5 minutes. The gel was placed onto the PVDF membrane, and both were placed between Whatman™ papers and installed in the transferring cassette. The cassette was filled with transfer buffer and a voltage of 100 V for 90 min was applied [154].

Afterward, the unspecific proteins were blocked by incubating the membrane with blocking buffer I for 1 h at RT. Subsequently, incubation of membranes was performed overnight, at 4°C with A2m (R&D Systems) and α-Actinin (Cell Signaling Technology) primary antibodies followed by incubation with secondary antibodies for 1 h, at room temperature (Sheep IgG HRP-conjugated Antibody, R&D). Bands were detected using the GE Healthcare ECL Western Blotting Detection Reagents (Thermo Scientific Technologies). Relative densitometry was determined using Fusion Fx Imaging System (Vilber Lourmat).

2.6.4. Enzyme-linked immunosorbent assay (ELISA)

Enzyme-linked immunosorbent assay (ELISA) is a well-established immunological assay to detect different proteins [154]. In our case, sandwich ELISA was used, where first an antibody raised against the antigen of interest is captured [154]. Afterward, all antigens in the added sample are bound and can be finally detected by a chromogenic substrate [25].

IL-6 in plasma was determined with mouse IL-6 ELISA Kit (BD Biosciences) and was done according to the manual. D-dimer level was measured in plasma using Mouse D-Dimer (D2D) ELISA Kit (Kamiya Biomedical Company) as well as IgG-1, IgG-3, IgM, and lambda chain (LifeSpan BioSciences) according to the manufacturer's manual.

2.7. Coagulation Biology

2.7.1. Erythrocytes sedimentation rate

The Erythrocytes sedimentation rate (ESR) measures the distance in millimeters which erythrocytes fall within an hour [166, 167]. An increased sedimentation rate is influenced by the increased amount of molecules with a higher weight and asymmetry [166, 167]. These proteins cause the negatively charged red blood cells reject each other. Fibrinogen has an effect that is twice as strong as all other alpha and gamma globulins, while albumin has the weakest effect on ESR [168]. ESR was determined using 200 μ l citrated blood using ESR Stand for Microvette CB 200 sedimentation system (Sarstedt). Sedimentation was measured in mm after 1 and 2 h.

2.7.2. Thrombin-triggered clotting time

Thrombin-triggered clotting time is a self-established coagulation assay to measure the time till a constant amount of thrombin and calcium (CaCl_2)

need to convert fibrinogen to fibrin in whole blood *in vitro*. The time that is necessary for the formation of a stable clot is measured in seconds.

Clotting of 50 μ l of citrated blood was triggered by 100 μ l of CaCl_2 (final concentration 250 mM and 0.1 U/ml of thrombin (Sigma). Clotting was triggered by adding 7.5 μ l of CaCl_2 (final concentration 250 mM) and 0.1 U/ml of thrombin to 100 μ l of whole blood in plastic tube with a metal bead. Tubes were placed on a tube roller SU1400 (Sunlab) (30 rotations per min) with an inclination of 25 degree. Time was stopped once the beads started to make complete rotation in the glass tube. Influence of A2m and IL-6 on the clotting time were evaluated using the same settings in HBS buffer (NaCl 150 mM, HEPES 20 Mm) containing 5 g/l of fibrinogen (Sigma-Aldrich) with or without 20 g/l A2m or with or without 800 pg/ml IL-6.

2.7.3. Analysis of coagulation parameters

International Normalized Ratio (INR), activated Partial Thromboplastin Time (aPTT), VWF and serum albumin levels as well as peripheral liver levels were measured along standard protocols in the Central Laboratory, University Medical Center Mainz, Germany.

2.7.4. Thrombin Generation Assay

Another global coagulation assay is the Thrombin Generation (TG) assay which determines the potential of a given blood sample to form thrombin [169, 170]. The Calibrated automated thrombinography (CAT) (Stago, Gennevilliers, France) measures transient levels of thrombin activity over time in platelet-poor plasma (PPP) or platelet-rich plasma (PRP) by continuously monitoring the cleavage of a fluorogenic thrombin substrate [169, 170]. A low amount of TF triggers coagulation, so the clotting depends on the positive feedback loops, but it is still susceptible to the anticoagulant pathways [169, 170]. TG assay provides information about the process of

prothrombin activation and thrombin degradation [171]. By measuring TG in whole blood the assay is more physiological, because it consists of all circulation blood cells and it already been reported that abnormal functions of blood cells can contribute to coagulation disorders [172, 173].

CAT assay in PRP, PPP and whole blood was performed in a microtiter plate fluorometer (Fluoroskan Ascent, ThermoLabsystems) using a dedicated software program (Thrombinoscope BV) [174]. For PRP and PPP, thrombin generation was triggered by 1 pM tissue factor and 4 μ M phospholipids [175]. Thrombin generation curves were recorded in triplicate. Whole blood CAT was performed as described previously [176]. The parameters calculated by the software were lag time, thrombin peak, time to peak, velocity, time to the tail, and endogenous thrombin potential (ETP), corresponding to the area under the curve. Pipetting time was added to the whole blood lag time [174, 175]. Thrombin Generation assay was performed in cooperation with [REDACTED].

2.8. Histology

2.8.1. Peripheral blood smear

Two slides were used to obtain a monolayer of blood cells. 5 μ l of citrate blood was placed on the end of one and approached with the second slide from the free side until it made wide contact. Then it was swiped back in the other direction so that the blood was thinned out without pressure. As a result, the blood cells were scattered and could be assessed in a better way. The slide were air dried (20 min) and methanol fixed for 10 min.

2.8.2. Pappenheim staining

The staining according to Pappenheim differentiates the different cell types of the blood and allows a distinction to be made between eosinophilic, basophilic and neutrophilic cells [177]. Granulocyte, lymphocytes and

erythrocytes can also be quantitatively determined [177]. The Panoptical Fast Staining Kit was used. Peripheral blood smear was stained for 3 min in staining solution 1. After briefly draining, the samples were stained in solution 2 for 4 min and rinsed in tap water for 1 min. After the peripheral blood smears were air-dried, pictures were taken with the microscope.

2.8.3. Hematoxylin and eosin (H&E) staining

Hematoxylin and eosin (H&E) staining was performed in cooperation with the Core Facility Histology, University Medical Center, Mainz.

2.8.4. Immunofluorescence staining

Methanol fixed blood smears were blocked with 0.05% Tween 20, 1% Bovine serum albumin (BSA) and stained with anti-IL-6 (Host: rabbit, abcam), anti A2m (Host: sheep, R&D Systems) primary antibodies at 4°C overnight [178]. After being washed three times with PBS the slides were incubated with secondary antibodies (Donkey anti-Sheep IgG (H+L) Cross-Adsorbed Secondary Antibody, Thermo Fisher Scientific and Anti Rabbit IgG H&L, Abcam) for 1 h at room temperature in the dark. After three washing steps, slides were counterstained and mounted with ProLong Diamond Antifade Mountant with DAPI (Thermo Fisher Scientific). Analysis was performed with Zeiss LSM710 confocal microscope (Carl Zeiss AG).

2.9. Human patient blood sample

Blood of patients with acute phase of colitis (Crohn's disease, ulcerative colitis or colitis indeterminate) was analyzed (coagulation parameters, blood picture and standard laboratory values and histological analysis of blood smears) and compared to the blood of age- and gender-matched controls without colitis. These analyses were carried out according to the principles of

the declaration of Helsinki and approved by the local ethics committee and the respective national authorities (Landesärztekammer Rheinland-Pfalz Nr. 2019-14135 1 and Nr. 873.199.10 7208).

2.10. Statistical analysis

Statistical analysis was performed with GraphPad Prism software (version 9; GraphPad Software Inc.). Data were analyzed for normal distribution with Kolmogorow–Smirnow test. When normal distribution was given unpaired Student's t-test to compare two experimental groups, and the one-way ANOVA test with Tukey post-hoc test for comparison of more than two groups. If no normal distribution was given,

Two test groups were analyzed with a Mann–Whitney *U* test if no normal distribution was given. The two-way ANOVA with Bonferroni *post hoc* test was used for more than two test groups and more than one measurement, Kruskal-Wallis test with Dunn's multiple comparisons or comparison of selected columns was used as appropriate and indicated in the Figure legends. Survival curves were compared with Log-rank (Mantel-Cox) test.

If no normal distribution was given, Mann–Whitney *U* test was applied for comparison of two groups, and Kruskal–Wallis with Dunn's multiple comparison test to compare more than two groups as indicated in the figure legends. Aortic relaxation curves were compared with two-way ANOVA with Bonferroni post hoc test. Survival curves were compared with Log-rank (Mantel-Cox) test.

P values of <0.001, <0.01, and <0.05 were considered statistically significant and marked by 3, 2, and 1 asterisks (*) or hash sign (#), respectively. Data are presented as mean ± standard error of the mean (SEM).

3. RESULTS

3.1.1. The influence of IL-6 on the coagulation system in mice

As described in Section 1.4, the LysM-IL-6^{OE} mouse strain overexpresses IL-6 in all myeloid cells. In the following figures, the LysM-IL-6^{OE} mouse strain is depicted in bright red. IL-6^{OE} mice, without the Cre-recombinase, were used as littermate control mice. In the following, these mice are referred to as control mice and are shown in grey.

3.1.1. No thrombus formation after subtotal vena cava ligation in LysM-IL-6^{OE} mice

Besides its essential function in inflammation, IL-6 was also described as a potentially pro-thrombotic cytokine [179]. Figure 10A shows no morphological difference in the structure of the inferior vena cava in LysM-IL-6^{OE} mice compared to age-matched control mice. The mice underwent a subtotal IVC ligation [143, 180]. XXXXXXXXXX and I were able to show that no thrombosis formed three days after the operation in LysM-IL-6^{OE} mice compared to the control mice. This could be confirmed by both H&E staining and high-frequency ultrasound examination (Figure 10B) [181]. An average thrombosis size of 5.6 mm in the control group could be detected after the subtotal IVC ligation compared to no thrombus formation in LysM-IL-6^{OE} mice (Figure 10C). Furthermore, it could be observed during the operation that LysM-IL-6^{OE} mice had a greater risk of developing unstoppable bleeding during manipulation compared to the control mice. This unexpected phenotype led us to further investigate the coagulation status in LysM-IL-6^{OE} mice.

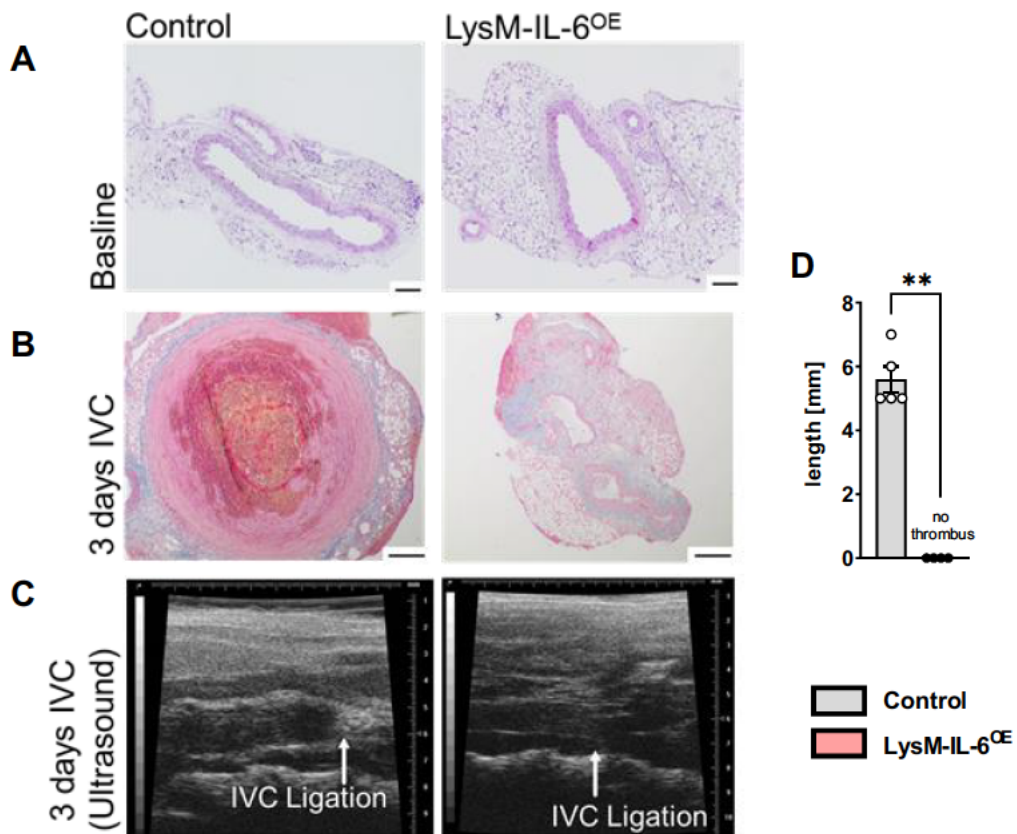


Figure 10 No thrombus formation in LysM-IL-6^{OE} mice compared to control mice. A. H&E staining of isolated IVC of LysM-IL-6^{OE} and control mice and B. three days after subtotal vena cava ligation, representative picture of IVC, n = 3, scale bar represents 200 μ m. C. High-frequency ultrasound analysis of IVC three days after subtotal IVC ligation (lower panel). The arrow shows the site of ligation. Representative image of n = 3 mice per group. D. Quantitative evaluation of IVC three days after subtotal IVC ligation, n = 4-5, Mann-Whitney t-test. Data are presented as mean \pm SEM, ** p < 0.01.

3.1.2. Hematological analysis of blood and coagulation parameters in LysM-IL-6^{OE} mice

The number of white blood cells (WBC) is made up of neutrophils (NEU), lymphocytes (LYM), and monocytes (MON) [18]. To examine the cellular composition of the blood, blood samples were measured using the VetScan HM5 as described in section 2.5.1. As shown in Figure 11A, overexpression of IL-6 in myeloid cells led to an increased WBC number, which can be explained by an increased MON and NEU count. Furthermore, there was a reduced red blood cell (RBC) count and lower hemoglobin (HGB) value which resulted in a decreased mean corpuscular hemoglobin (MCH)

detectable in LysM-IL-6^{OE} mice compared to the control mice (Figure 11B). As seen in the right panel of Figure 11B, LysM-IL-6^{OE} mice showed a possible anisocytosis due to the significantly increased red cell distribution width (RDWs). These data suggest that an increased number of immature erythrocytes without a nucleus, so-called reticulocytes, cycled in the blood of LysM-IL-6^{OE} mice. The total platelet count was unchanged in LysM-IL-6^{OE} mice compared to the control mice, but MPV and PDWs were significantly increased in LysM-IL-6^{OE} mice compared to control mice (Figure 11C). The change in these parameters indicated that the platelets of LysM-IL-6^{OE} mice had been enlarged compared to control mice (Figure 11C) [182]. Constitutive overexpression of IL-6 led to a hematological alteration in LysM-IL-6^{OE} compared to control mice, but this did not explain why the LysM-IL-6^{OE} mice were protected from venous thrombus formation.

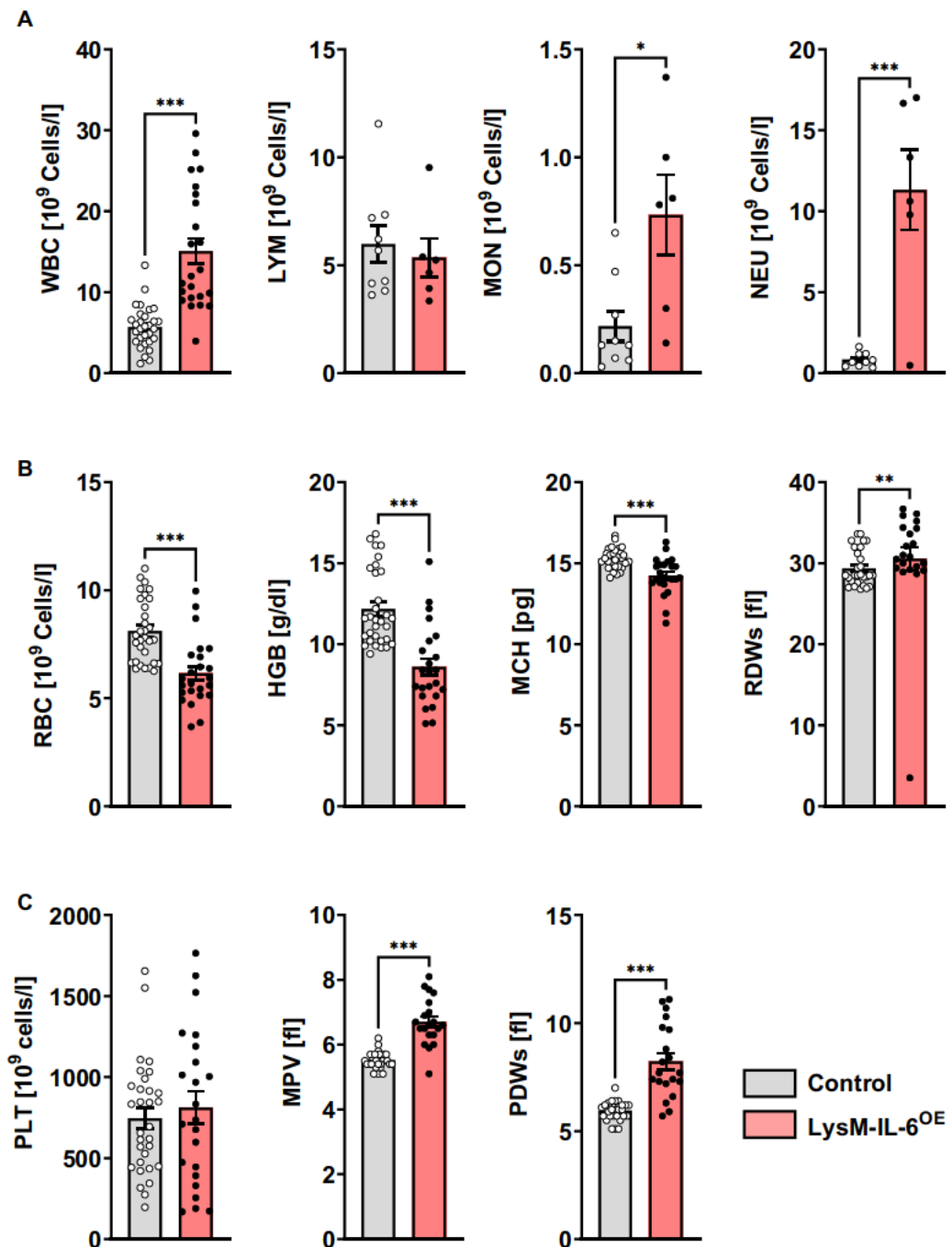


Figure 11 Hematological analysis of LysM-IL-6^{OE} mice compared to control mice. A. White blood cells (WBC) divided into lymphocyte (LYM), monocyte (MON) and neutrophil (NEU) count. B. Red blood cell (RBC) count and the parameters hemoglobin (HGB), mean corpuscular hemoglobin (MCH), and red cell distribution width (RDWs). C. Platelet count (PLT), mean platelet volume (MPV), and platelet distribution width (PDWs); n= 6-28, Mann-Whitney t-test and unpaired Student's t-test, Results as mean ± SEM. * p < 0.5, ** p < 0.01, *** p < 0.001 vs. control.

To get an overview of how IL-6 could influence the coagulation cascade in LysM-IL-6^{OE} mice, the activated Partial Thromboplastin Time (aPTT), the International Normalized Ratio (INR), the tail bleeding time as well as the whole blood thrombin converting time (Figure 12) were analyzed. Figure 12A

shows that aPTT and INR were prolonged in LysM-IL-6^{OE} mice compared to littermate controls. As shown in Figure 12B, a significantly prolonged tail bleeding time compared to control mice could be observed. The experiment had to be terminated after 12 minutes, as the LysM-IL-6^{OE} mice did not stop bleeding. The thrombin-triggered clotting time was also significantly prolonged in LysM-IL-6^{OE} mice compared to control mice (Figure 12C). The mice showed no thrombus formation following subtotal IVC ligation but a delayed aPTT, INR and bleeding time as well as thrombin-triggered clotting time depicting an increased bleeding phenotype.

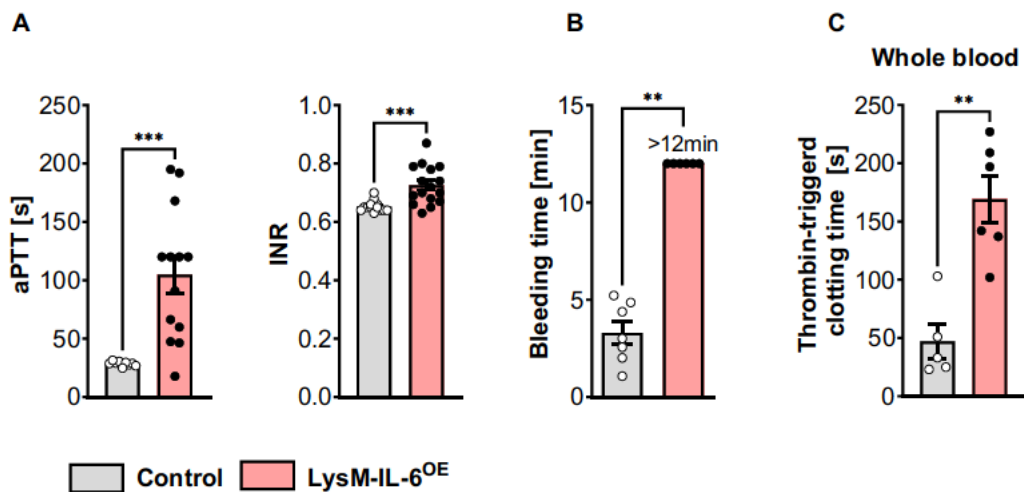


Figure 12 Coagulation parameters in LysM-IL-6^{OE} compared to control mice. A. Left panel: activated Partial Thromboplastin Time (aPTT), $n = 9-13$, unpaired Student's t -test. Right panel: International Normalized Ratio (INR), $n = 13-16$, Mann-Whitney t -test. B. Tail bleeding time in LysM-IL-6^{OE} vs. control mice. $n = 6-7$, Mann-Whitney t -test. C. Thrombin-triggered clotting time in citrated whole blood from LysM-IL-6^{OE} and control mice, $n = 5$, unpaired Student's t -test. ** $p < 0.01$, *** $p < 0.001$. Data are presented as mean \pm SEM.

Due to the prolonged aPTT, the next step was to investigate whether there was a lupus anticoagulant effect. Lupus anticoagulants are antiphospholipid antibodies that interfere with clotting tests. These are IgG or IgM immunoglobulins that bind phospholipids [183]. Since phospholipids are a starting reagent for aPTT, antiphospholipid antibodies may prolong this clotting test [184, 185]. After mixing LysM-IL-6^{OE} whole blood with control whole blood, the clotting was reassessed, and INR and aPTT were normalized in the mixed blood of LysM-IL-6^{OE} mice (Figure 13A). If a clotting inhibitor such as a lupus anticoagulant were present, the inhibitor would interact with the control whole blood and prolonged the clotting time. As the clotting time of the mixed whole blood was normalized in LysM-IL-6^{OE} mice,

the presence of an inhibitor such as the lupus anticoagulant was less likely [183]. However, the experiment showed an insufficient clotting factor amount in LysM-IL-6^{OE} mice supplemented with blood from control mice as it could be normalized by supplementing of control blood. Furthermore, Figure 13B indicates no significant increase in D-dimer level basal or after three days IVC ligation in LysM-IL-6^{OE} compared to control mice, indicating no microthrombus formation.

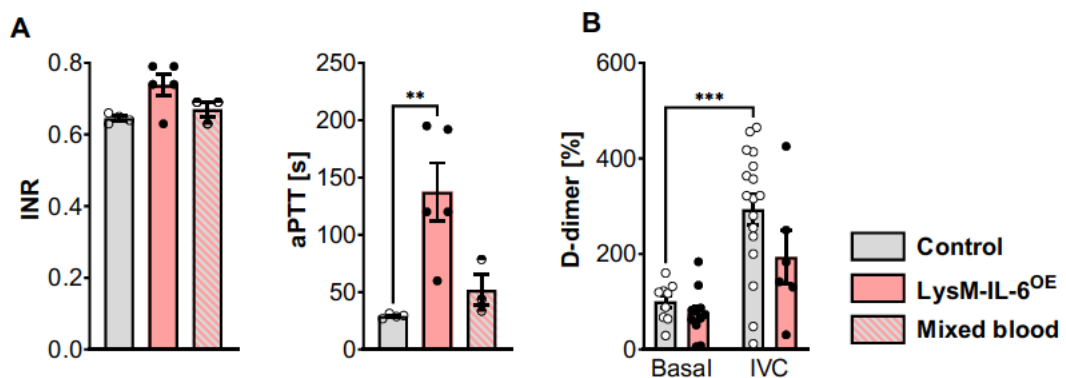


Figure 13 Neither lupus anticoagulant effect nor microthrombus formation in LysM-IL-6^{OE} mice compared to control mice. A. INR (left) and aPTT (right) of LysM-IL-6^{OE}, control mice and mixed blood (1:2). n = 3-5, Kruskal-Wallis test with Dunn's multiple comparisons test. B. D-Dimer detection in LysM-IL-6^{OE} and control mice before and after inferior vena cava ligation (IVC). n = 6-17, One-way analysis of variance and Turkey's post hoc test. ** p < 0.01, *** p < 0.001.

3.1.3. Myeloid IL-6 overexpression leads to delayed thrombin generation

The thrombin generation in Platelet-rich, Platelet-poor plasma and whole blood was tested to understand the cause of prolonged thrombin converting time in the LysM-IL-6^{OE} mice. Figure 14A and C showed a significantly delayed lag time and time to peak of thrombin in Platelet-rich and whole blood in LysM-IL-6^{OE} compared to control mice. The endogenous thrombin potential was increased in Platelet-rich and whole blood in LysM-IL-6^{OE} compared to control mice (Figure 14A and C). In contrast, Platelet-poor plasma displayed a significantly lower endogenous thrombin potential in LysM-IL-6^{OE} compared to control mice (Figure 14B). However, delayed thrombin generation cannot explain the delayed thrombin conversion time in LysM-IL-6^{OE} mice. Furthermore, it did not explain that there was no thrombus

formation in the LysM-IL-6^{OE} mice compared to control mice. For this, a very low ETP would have had to be proven.

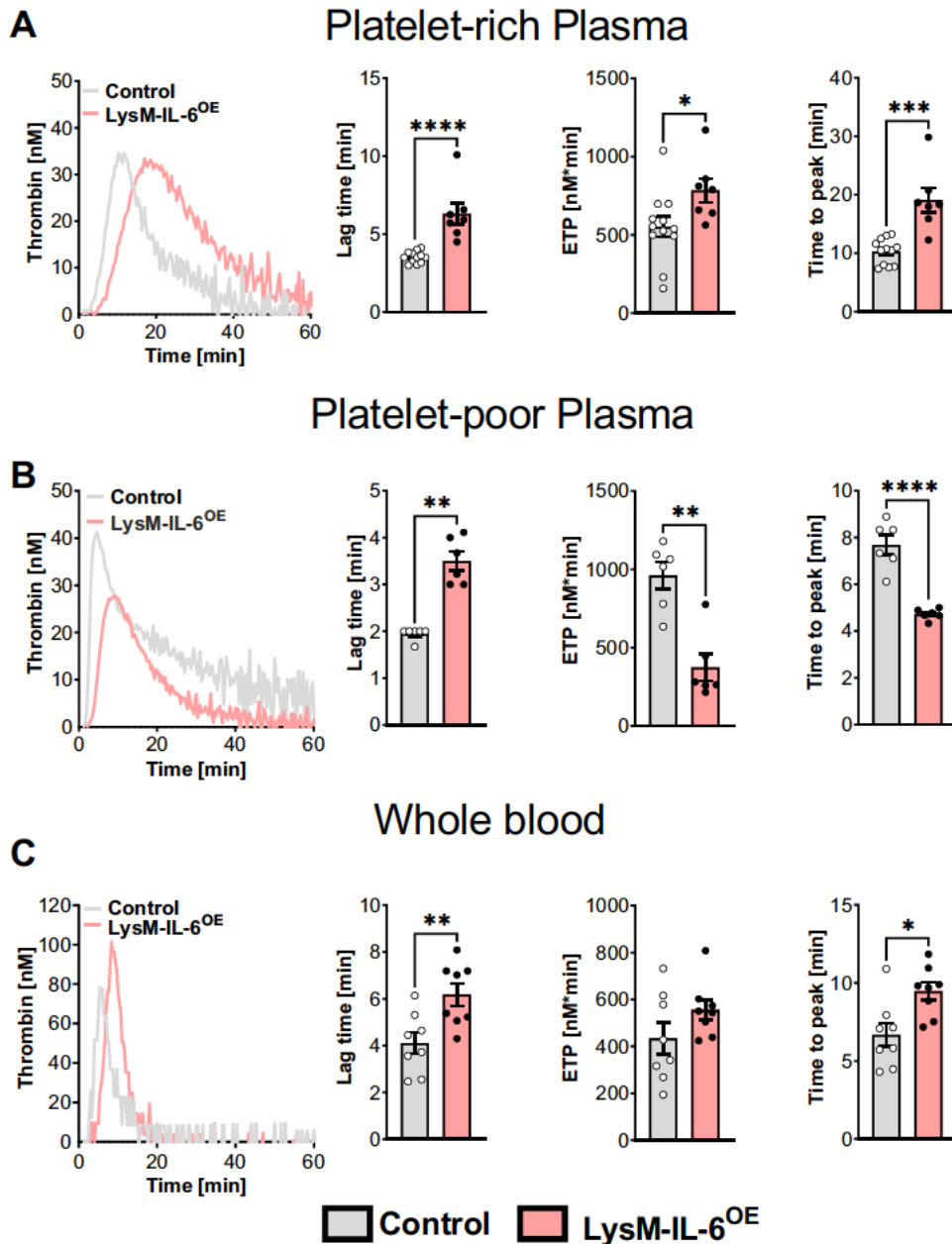


Figure 14 Thrombin generation in LysM-IL-6^{OE} mice. A. Thrombin generation in platelet rich plasma from LysM-IL-6^{OE} compared to control mice. Left panel: representative curves of thrombin generation. Right panel: Calculated lag time, ETP and Time to peak, n = 7-12, unpaired Student's t-test or Mann-Whitney t-test. B. Thrombin generation in platelet poor plasma from LysM-IL-6^{OE} compared to control mice. Left panel: representative curves of thrombin generation. Right panel: Calculated lag time, ETP and Time to peak, n = 6, unpaired Student's t-test or Mann-Whitney t-test. C. Thrombin generation in whole blood from LysM-IL-6^{OE} compared to control mice. Left panel: representative curves of Thrombin generation. Right panel: Calculated lag time, ETP and Time to peak, n = 8, unpaired Student's t-test or Mann-Whitney t-test. * p < 0.05, ** p < 0.01, *** p < 0.001

3.1.4. Coagulation factors and acute phase proteins in *LysM-IL-6^{OE}* mice compared to control mice

As described above, the prolonged thrombin generation did not sufficiently explain the absence of thrombosis because this would have required a lower ETP. Therefore, I analyzed the expression level of the coagulation factors and acute phase in the next step. The coagulation factors *FXI* and *FIX* were reduced in *LysM-IL-6^{OE}* mice compared to littermate control mice, but the expression of *FXII*, *FVIII*, *FX*, *FV*, and *FVII* was not altered (Figure 15).

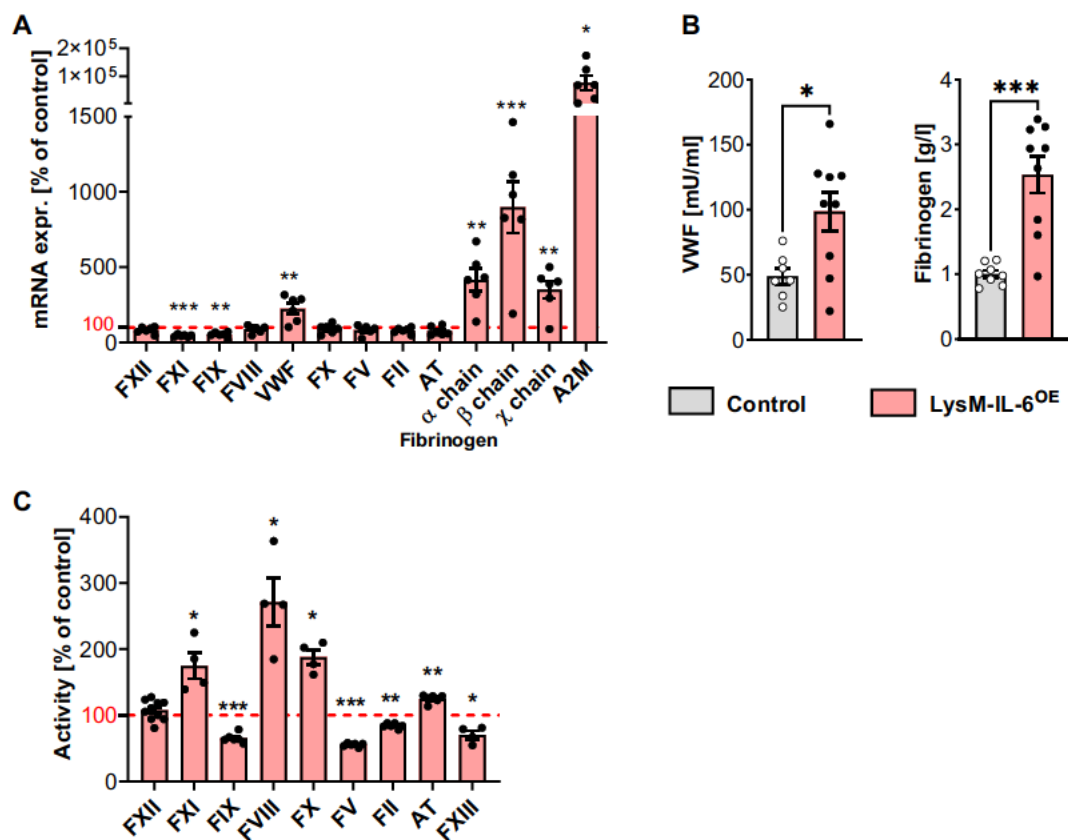


Figure 15 Myeloid IL-6 overexpression influences the expression of coagulation factors and leads to increased hepatic A2m expression. A. Liver mRNA expression of coagulation factors *XII*, *XI*, *IX*, *VIII*, *VWF*, *X*, *V*, *II*, *AT*, *fibrinogen subunit α*, *β*, *γ*, and *A2m* respectively from *LysM-IL-6^{OE}* normalized to control mice (100 % indicated by red dashed line), $n = 5-6$, unpaired Student's t-test or Mann-Whitney t-test. Plasma concentration of (B) VWF, $n = 7-9$, unpaired Student's t-test and (C) fibrinogen. $n = 8-9$, unpaired Student's t-test. C. Activity of coagulation factors *XII*, *XI*, *VIII*, *X*, *V*, *II*, *XIII*, and *AT* in plasma of *LysM-IL-6^{OE}* and control mice. $n = 4-10$. Unpaired Student's t-test or Mann-Whitney t-test. * $p < 0.05$, ** $p < 0.01$, *** $p < 0.001$. Data are presented as mean \pm SEM.

On top, *VWF* and *fibrinogen* subunit expression were significantly increased in the *LysM-IL-6^{OE}* liver, which goes in line with an increased VWF and fibrinogen level in plasma of *LysM-IL-6^{OE}* mice compared to control mice (Figure 15B). In Figure 15C, the increased plasmatic activity of FXI, FVIII,

FX, and antithrombin is shown in LysM-IL-6^{OE} mice, while the plasmatic activity of FIX, FII, and FXIII were significantly decreased in LysM-IL-6^{OE} mice compared to control mice.

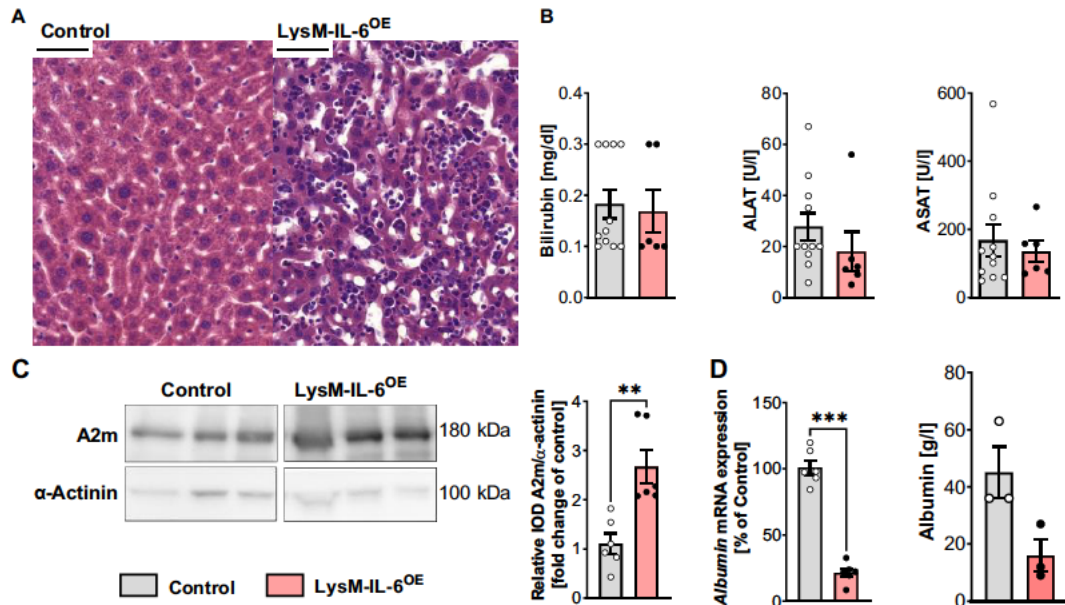


Figure 16 Liver analysis of in LysM-IL-6^{OE} mice compared to control mice. A. H&E staining of liver from LysM-IL-6^{OE} and control mice, scale bar = 50 μ m. B. Measurement of serum alanine aminotransferase (ALAT) and aspartate aminotransferase (ASAT) activity and bilirubin concentration. N = 5-11, Mann-Whitney t-test ** p < 0.01, *** p < 0.001. Data are presented as mean \pm SEM. C. Protein level of A2m in liver of LysM-IL-6^{OE} and control mice. Left panel: representative western blot. Right panel: relative IOD of A2m in relation to α -actinin, n = 6, Mann-Whitney t-test. D. Albumin in LysM-IL-6^{OE} and control mice: Left panel: *Albumin* mRNA expression in liver. Right Panel: Plasma concentration of albumin. n = 3-4, Mann-Whitney t-test.

The liver is one of the most important producers of coagulation factors [186]. Hence, the functionality is essential for an adequate coagulation [186]. LysM-IL-6^{OE} mice showed a mild liver inflammation compared to control mice (Figure 16A), but, Bilirubin, ALAT and ASAT were not altered (Figure 16B). The expression of $\alpha 2$ Macroglobulin (*A2m*) was significantly elevated in LysM-IL-6^{OE} mice compared to control mice and the protein concentration was also increased in the liver of LysM-IL-6^{OE} mice compared to control mice (Figure 15 and Figure 16C). *Albumin* expression and plasma concentration of albumin were decreased in LysM-IL-6^{OE} mice compared to control mice (Figure 16D). These results showed that myeloid derived IL-6 in myeloid cells evokes liver inflammation and impacts on the coagulation factors, but their alteration did not completely explain the absence of thrombus formation or the the increased bleeding tendency after manipulation.

3.1.5. Myeloid IL-6 overexpression results in erythrocyte aggregation

While working with blood samples of LysM-IL-6^{OE} mice, we observed that already five minutes after the blood sample were taken, we could see a clear separation between erythrocytes and plasma (Figure 17A). To quantify this, I determined the erythrocyte sedimentation rate (ESR) and found a significantly increased ESR in LysM-IL-6^{OE} mice than control mice (Figure 17B). To investigate the cause of increased ESR, I performed Pappenheim stainings of LysM-IL-6^{OE} whole blood compared to control whole blood. Here, I detected the formation of erythrocyte aggregates (Figure 17C). The erythrocyte aggregates seems to be the reason for the increased ESR in LysM-IL-6^{OE} compared to control mice. In the presence of certain macromolecules, such as fibrinogen and immunoglobulin erythrocytes tend to aggregate and form cylindrical structures called "erythrocytes rouleaux or money rolls" that resemble coins in a pile [4, 166].

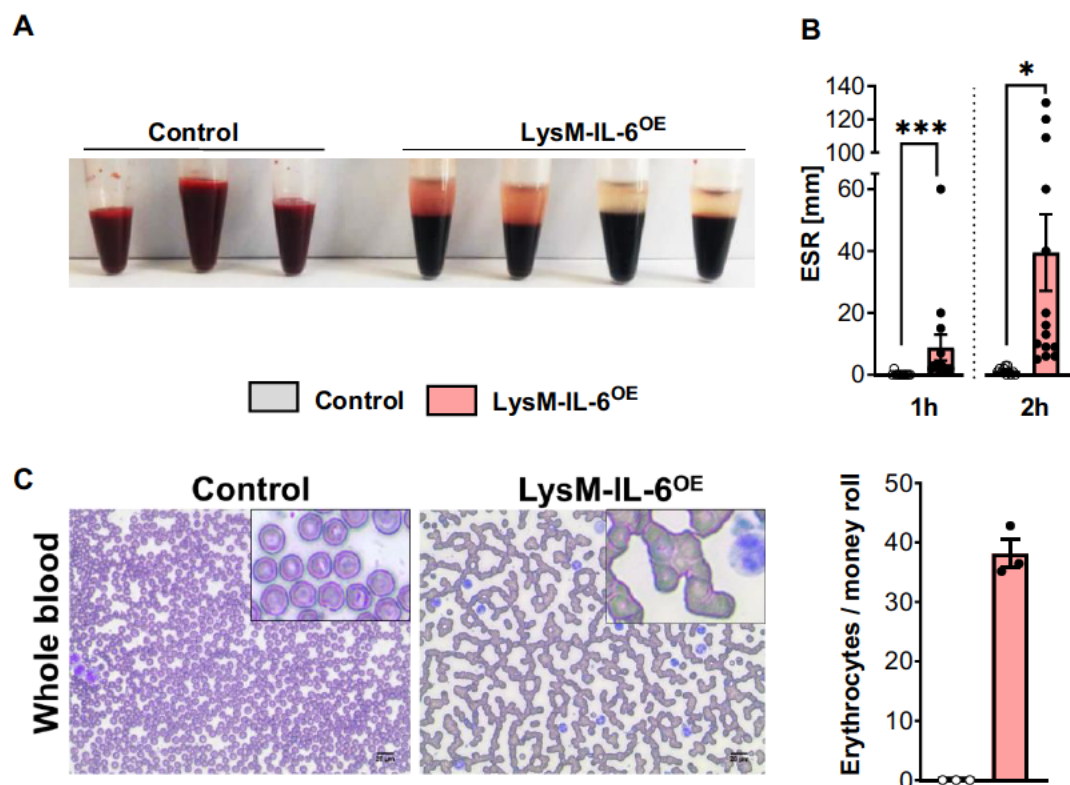


Figure 17 Myeloid IL-6 overexpression leads to an increased erythrocyte sedimentation rate (ESR) and formation of erythrocyte aggregates. A. Representative images of blood samples. B. Erythrocyte sedimentation rate (ESR) after 1 hour and 2 hours from LysM-IL-6^{OE} compared to control mice, n = 11-14, unpaired Student's t-test. C. Pappenheim staining of whole blood from LysM-IL-6^{OE}

and control mice. Representative images of n = 3-7 mice are shown. Scale bar = 20 μ m. Quantification of the relative erythrocytes / money roll proportion (number of erythrocytes per money roll), n = 3. * p < 0.05, ** p < 0.01, *** p < 0.001

Whole blood was diluted in a ratio of 2:3 in order to examine the binding stability of the erythrocyte aggregates. The lower panel of Figure 18A illustrates that the dilution per se was already sufficient to destroy the erythrocyte aggregates in the blood of LysM-IL-6^{OE} mice. In undiluted blood, the thrombin-triggered clotting time was extended in LysM-IL-6^{OE} mice (Figure 12). In diluted blood, the thrombin-triggered clotting time showed the opposite effect and was faster in LysM-IL-6^{OE} compared to control mice (Figure 18). This indicates, on the one hand, that the erythrocyte aggregate formation is a slight binding of erythrocytes in LysM-IL-6^{OE} mice. On the other hand, this findings indicates that erythrocytes seem to influence the thrombin-triggered clotting time.

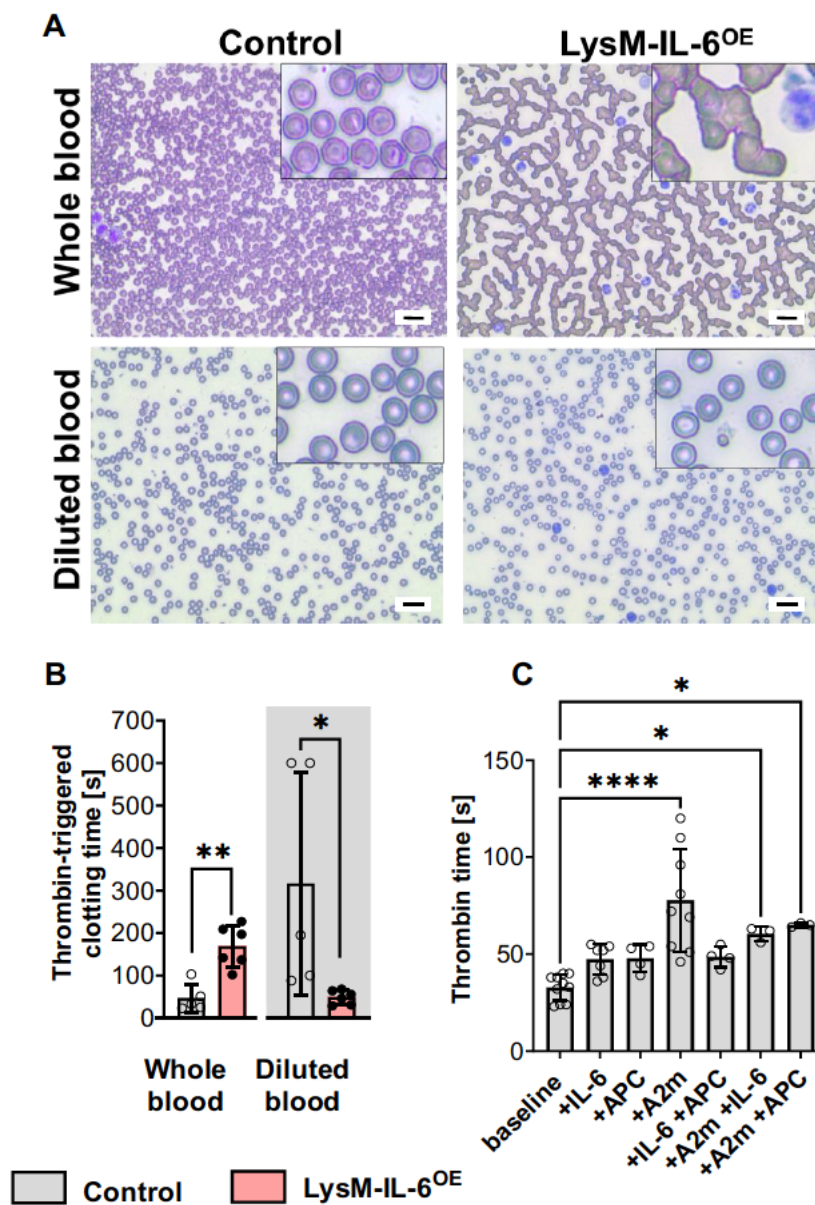


Figure 18 Formation of erythrocyte rouleaux is associated with increased thrombin-triggered clotting time and A2m. A. Pappenheim staining of whole blood (upper panel) and 2/3 diluted blood (lower panel) from LysM-IL-6^{OE} and control mice. Representative images of n = 3-7 mice are shown. Scale bar = 20 μ m. B. Thrombin-triggered clotting time in citrated undiluted blood and in 2/3 diluted blood from LysM-IL-6^{OE} and control mice, n = 5, unpaired Student's t test. * p < 0.05, ** p < 0.01, *** p < 0.001. Data are presented as mean \pm SEM. C. *In vitro* thrombin-triggered clotting time of fibrinogen conversion with or without α -2 macroglobulin (A2m), IL-6, and activated protein C (APC). n = 4-10, Kruskal-Wallis test with Dunn's multiple comparison.

There seems to be a connection between the erythrocyte aggregation and the inhibition of thrombin in LysM-IL-6^{OE} mice leading to the prolonged thrombin-triggered clotting time in LysM-IL-6^{OE} mice. For further investigation, I analyzed different potential thrombin inhibitors *in vitro*. In addition to IL-6 and A2m, APC was also used. APC plays an important role in maintaining homeostasis of thrombosis *in vivo* [187]. APC acts here by proteolytic

inactivation of FVa and FVIIIa, but A2m can also inhibit the activity of APC and thus influence coagulation [110, 116, 188]. Subsequently, the thrombin-triggered clotting time was measured after the addition of A2m (20 mg/ml) to buffer containing fibrinogen, which resulted in a prolongation of the thrombin-triggered clotting time compared to buffer and fibrinogen alone (Figure 18C). The addition of IL-6 or activated protein C (APC) had no additional effect (Figure 18C). The combination of IL-6 and APC had no significant effect, but IL-6 or APC in combination with A2m showed again a prolonged thrombin converting time (Figure 18C).

Based on the *in vitro* experiment results, the next step was to investigate where IL-6 and A2m were localized in the whole blood of LysM-IL-6^{OE} mice. Therefore, blood smears of LysM-IL-6^{OE} mice compared to control mice were prepared. After fixation with methanol, the blood smears were immuno-stained with anti-IL-6, anti-A2m and DAPI for the cell nuclei (Figure 19). The confocal images show that IL-6 was localized on the surface of erythrocyte aggregates of LysM-IL-6^{OE} mice and control mice showed no IL-6 (Figure 19). Furthermore, A2m was partially located around the erythrocytes in LysM-IL-6^{OE} blood smears, but it also formed vesical-like structures (Figure 19). If the immuno-staining was merged, the co-localization of IL-6 and A2m was indicated by an orange signal (Figure 19). So, we were confronted with erythrocyte aggregates combined with collocated IL-6 and A2M in LysM-IL-6^{OE} mice.

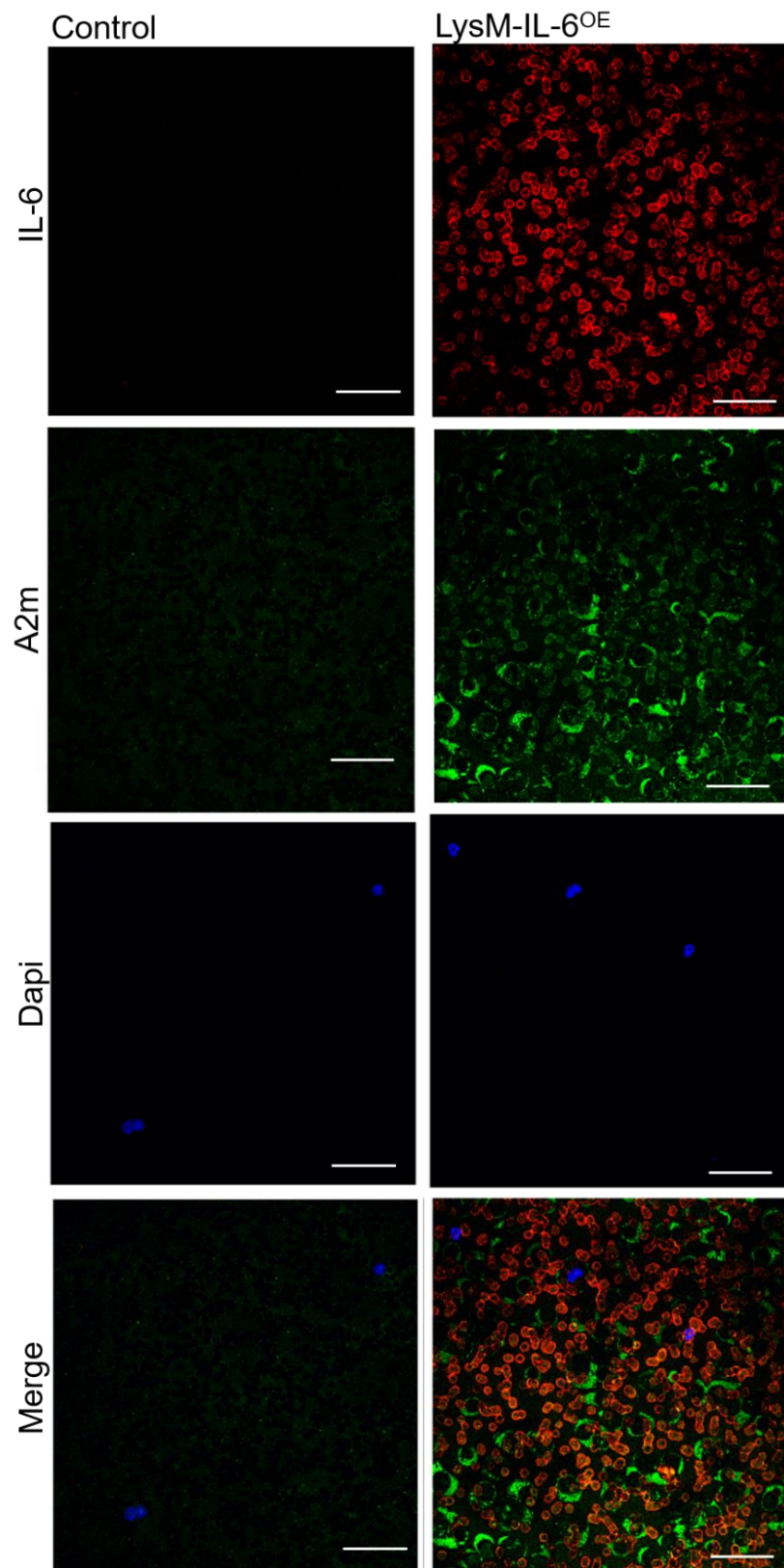


Figure 19 Myeloid IL-6 overexpression leads to formation of erythrocyte aggregates in which IL-6 and A2m are co-localized. Immunofluorescence staining of whole blood smears from LysM-IL-6^{OE} and control mice. (red: IL-6; green: A2m; blue: DAPI). Scale bar represents 30 μ m. Representative images of n = 3 are shown.

The results of this section demonstrated that myeloid cell-derived IL-6 was associated with erythrocyte aggregates formation in whole blood, where IL-6 and A2m are co-localized around erythrocyte complexes (Figure 19). Furthermore, A2m, which is known to inhibit thrombin [85, 117-119], causing a prolonged thrombin-triggered clotting time, might impact the elongated coagulation process in LysM-IL-6^{OE} mice.

3.2. *Myeloid cell-derived IL-6 leads to gut inflammation in LysM-IL-6^{OE} mice compared to control mice*

Rebecca Jung showed that chronic expression of myeloid cell-derived IL-6 led to an increased number of neutrophils, monocytes and macrophages in the spleen, blood, and in the aorta of LysM-IL-6^{OE} mice compared to control mice [189]. This led to the assumption that cell infiltration and inflammation might also occur in other organs. IL-6 plays an important role by the development of autoimmune colitis [190-192], so I examined the colon more closely for signs of inflammation. Figure 20 confirmed that LysM-IL-6^{OE} mice had an inflammation of the colon shown by colonoscopy (performed in cooperation with Romy Mittenzwei) and H&E staining (Core Facility Histology, University Medical Center, Mainz). These results support the relevant role of IL-6 in colitis [192, 193].

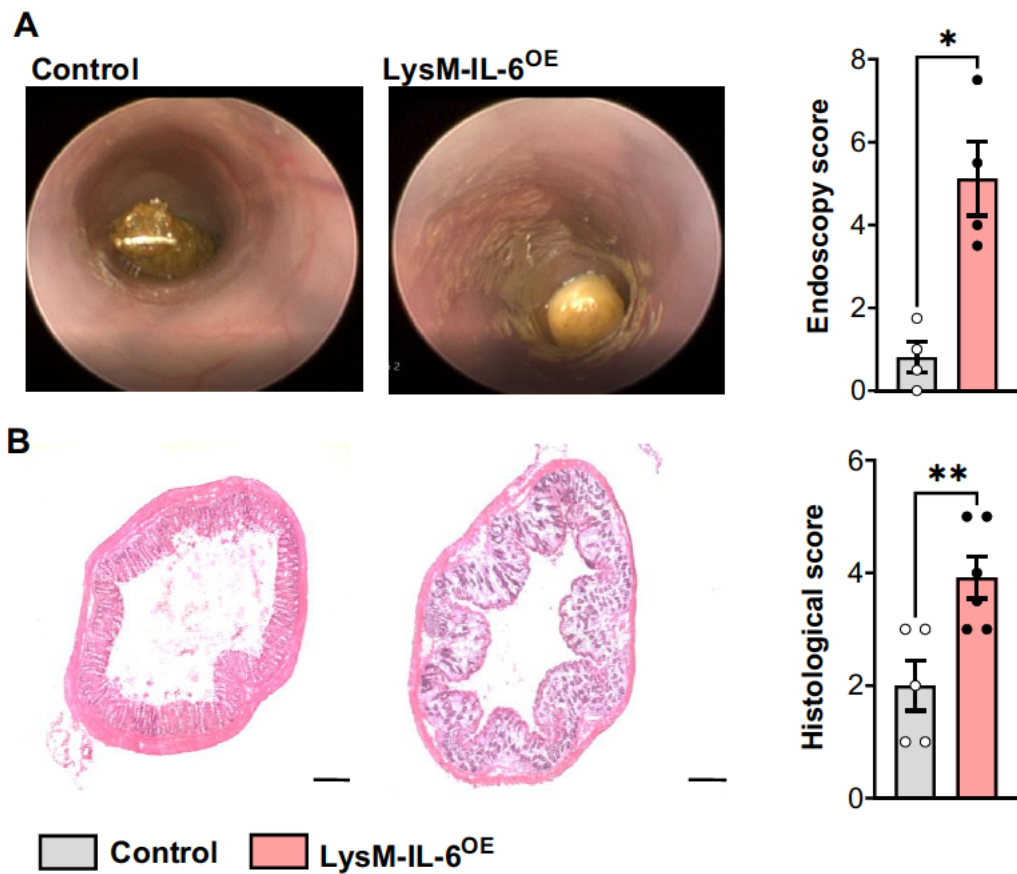


Figure 20 Analysis of colon inflammation in LysM IL-6^{OE} mice compared to control mice. A. Representative image of colon endoscopy (left). Statistical analysis of endoscopy score (right), $n = 4$, Mann-Whitney t-test. B. Histological analysis of gut inflammation in LysM-IL-6^{OE} compared to control mice. Representative picture of H&E staining of colon (left), Statistical analysis of histological score (right), scale bar = 200 μm . $n = 5-6$, Mann-Whitney t-test. * $p < 0.5$, ** $p < 0.01$

3.3. IBD patients with elevated IL-6 levels shows a delayed Thrombin converting time and formation of erythrocyte aggregates in blood

IL-6 is known to be essential for the induction of autoimmune colitis [190-192] and, as I could show in section 3.2., we had found a colitis like phenotype in LysM-IL-6^{OE} mice. Therefore, I analyzed a cohort of IBD patients with acute phase of IBD to investigate the effect of elevated IL-6 levels on the coagulation system. IL-6 and C-reactive protein (CRP) levels were significantly increased in these patients (Figure 21A and B) [194]. Moreover, the IBD patients showed an increase in the INR and ESR compared to age- and gender-matched healthy controls (Figure 21C and D).

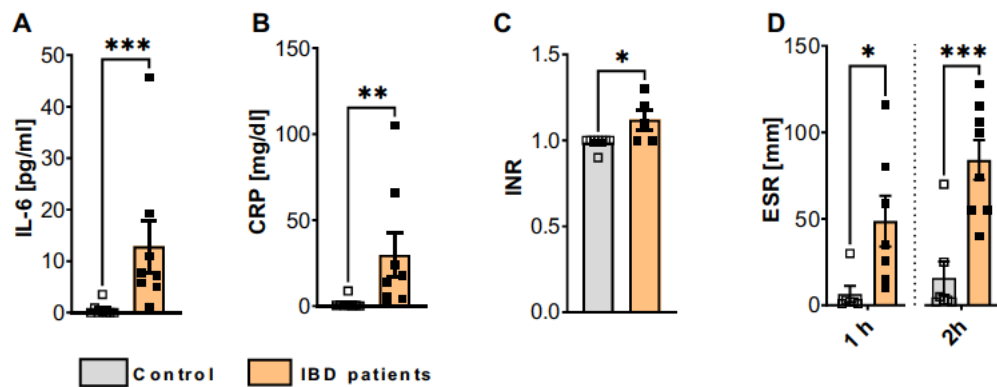


Figure 21 Analyze of the blood from IBD patients. A. Plasma levels of IL-6 and (B) C-reactive protein (CRP) of IBD patients in the acute phase compared to gender and age-matched controls. n = 8, Mann-Whitney t-test. C. INR measurement of IBD patients and healthy controls, n = 4-8, Mann-Whitney t-test. D. Erythrocytes sedimentation rate (ESR) after 1 and 2 hours of IBD patients and healthy controls. n = 7-9, unpaired Student's t-test. * p < 0.05, *** p < 0.001

The increased INR and ESR of IBD patients went in line with the observation in LysM-IL-6^{OE} mice compared to control mice.

In analogy to my mouse experimental approach, blood smears of IBD patients and controls were stained for IL-6, A2M and DAPI using immune-staining (Figure 21). The immune-staining confirmed the increased plasmatic IL-6 level in IBD patients (Figure 21). Apart from IL-6 (red), the proteinase A2M (green) was also elevated in blood smears of IBD patients in the acute phase of IBD compared to the control (Figure 21). Remarkably, blood smears of IBD patients showed also erythrocyte aggregates with a

surface co-localization of IL-6 and A2M (Figure 22). The same co-localization had been detected before in the LysM-IL-6^{OE} mouse model, but the IL-6 A2M erythrocyte co-localization was even more evident in IBD patients (Figure 22 and Figure 19).

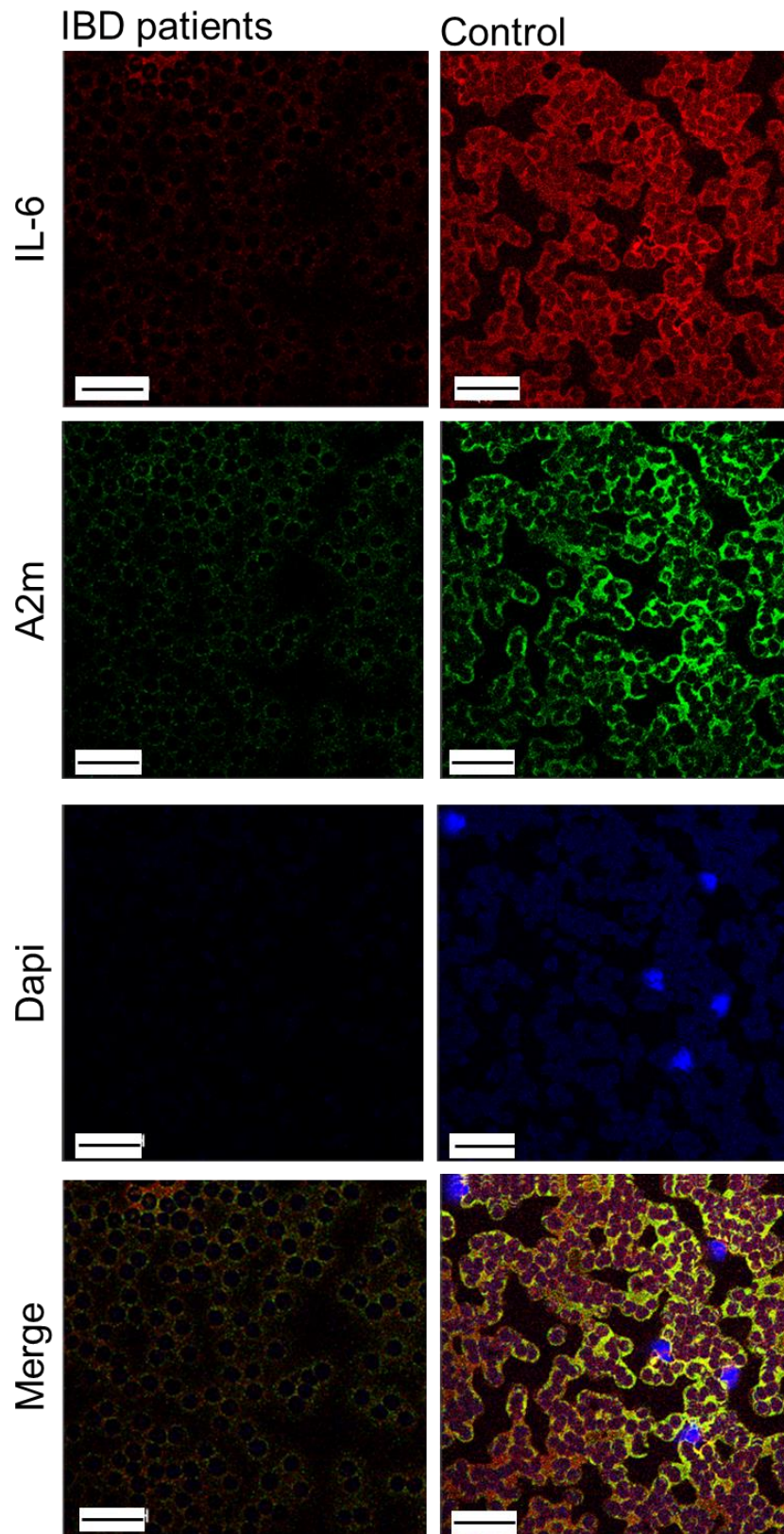


Figure 22 IL-6 and A2m are co-localized in the blood of IBD patients in the acute phase. Immunofluorescence staining of whole blood smears of IBD patients in the acute phase compared to gender and age-matched controls. (red: IL-6; green: A2m; blue: DAPI). Scale bar represents 30 μ m. Representative images of n = 3 are shown.

Whole blood thrombin converting time was significantly delayed in IBD patients, as seen in LysM-IL-6^{OE} mice (Figure 12C mice and Figure 23A). A 2/3 dilution of the blood *in vitro* prevented thrombin-triggered clotting time increase as seen before in LysM-IL-6^{OE} mice (Figure 23). Furthermore, the blood dilution resulted in reduced erythrocyte aggregation (Figure 23).

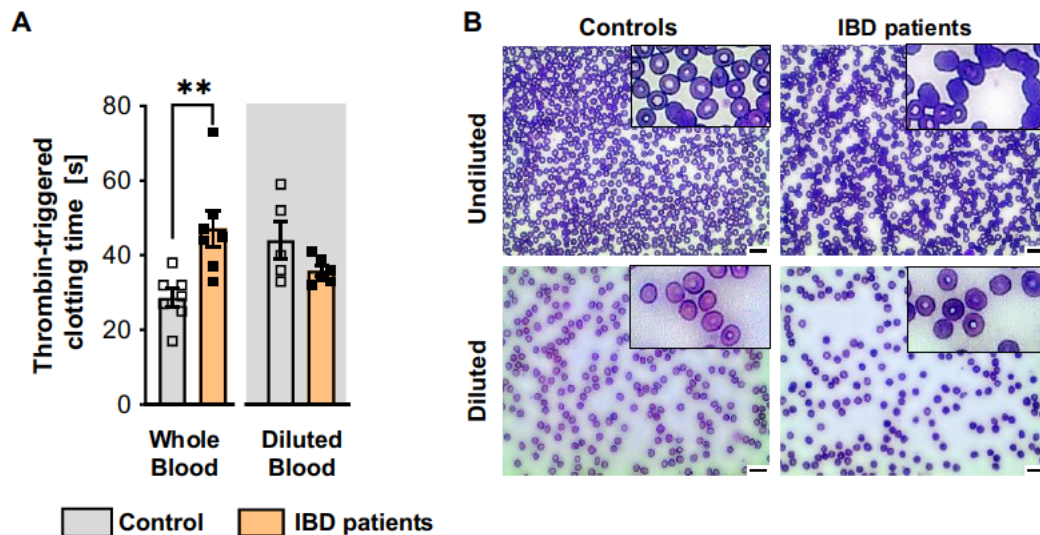


Figure 23 Thrombin converting time and Pappenheim staining of whole blood from IBD patients and control. A. Whole blood thrombin converting time in citrated undiluted whole blood and in 2/3 diluted blood of IBD patients compared to control blood, $n = 5-7$, unpaired Student's t-test. B. Pappenheim staining of whole blood smears of IBD patients and healthy controls (either undiluted or 2/3 diluted). Scale bar represents 20 μm . Representative image of $n = 8$ are shown. ** $p < 0.01$, *** $p < 0.001$. Data are presented as mean \pm SEM.

These findings demonstrate that elevated IL-6 levels were associated with delayed whole blood thrombin converting time and the formation of erythrocyte aggregates with A2m and IL-6 in the blood of the acute phase of human IBD and LysM-IL-6^{OE} mice which also provided a colitis-like phenotype.

3.4. Bone marrow transplant experiments reveal an IL-6 dose-dependent effect on the coagulation system

In the mouse model of myeloid IL-6 overexpression in LysM-IL-6^{OE} mice, I could demonstrate that the systemically increased IL-6 level led to impaired coagulation. This manifested in the absence of thrombosis formation after

subtotal IVC ligation and in a prolonged thrombin-triggered clotting time (Figure 10 and Figure 12). The next step was to check whether there was a correlation between IL-6 levels and the severity of the altered coagulation response. Therefore, bone marrow (BM) chimeric mice with different ratios of BM isolated from LysM-IL-6^{OE} mice mixed with BM of control mice were generated (10% and 100% LysM-IL-6^{OE} BM: 2.3.6 Bone marrow transplantation; Table 3). Seventy days after the transplantation, the animals were examined.

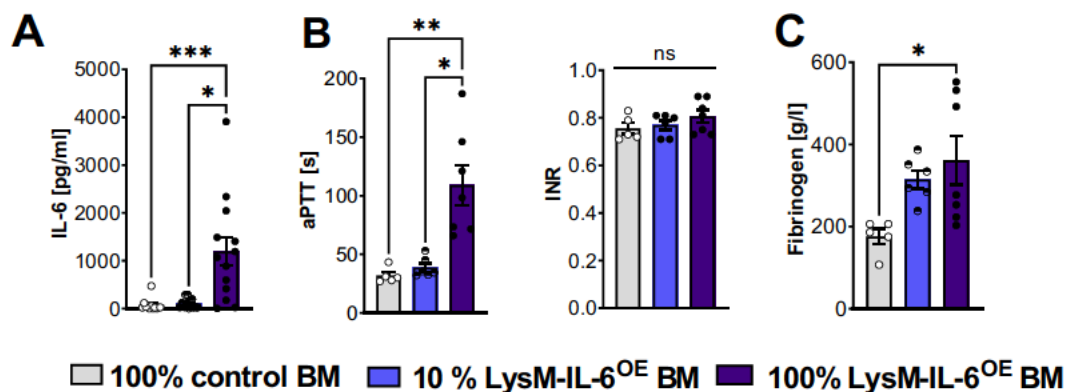


Figure 24 Dose-dependent effect of myeloid cell-derived IL-6 on the coagulation parameters in mice. A. IL-6 plasma level of bone marrow chimeric mice, $n = 12-13$, Kruskal-Wallis test with Dunn's multiple comparisons test. B. aPTT and INR measurement in plasma of bone marrow chimeric mice, $n = 5-7$ mice per group, Kruskal-Wallis test with Dunn's multiple comparisons test or ordinary one-way analysis of variance with Turkey's post-test. C. Fibrinogen concentration in plasma of bone marrow chimeric mice, $n = 5-7$, ordinary one-way analysis of variance with Turkey's post-test.

Figure 24A shows that the more LysM-IL-6^{OE} BM had been transplanted, the higher was the plasma IL-6. In the control group (100% control BM), the mean IL-6 level was 69.77 ± 37.98 pg/ml, and in case 10% LysM-IL-6^{OE} BM had been transplanted, the systemic IL-6 level was slightly increased to 103.7 ± 28.57 pg/ml (Figure 24A). If mice received pure BM from LysM-IL-6^{OE} mice, the plasmatic IL-6 level was significantly increased to 1196 ± 304.1 pg/ml (Figure 24A). Based on these systemic IL-6 levels, I concluded that the systemic IL-6 levels increased with an increasing amount of transplanted LysM-IL-6^{OE} BM. In addition to the elevated systemic IL-6 levels, the aPTT was also prolonged in mice that received pure LysM-IL-6^{OE} BM (Figure 24B). The parameter INR was slightly increased in both groups, received either 10% or 100% LysM-IL-6^{OE} BM, but the difference between the groups was not significant (Figure 24B). Similarly, a significant increase

in plasma fibrinogen could be observed in mice that received 100% LysM-IL-6^{OE} BM (Figure 24C). In mice that had received 10% LysM-IL-6^{OE} BM, fibrinogen only increased by trend (Figure 24C). In summary, there seemed to be an IL 6 concentration-dependent influence on the coagulation.

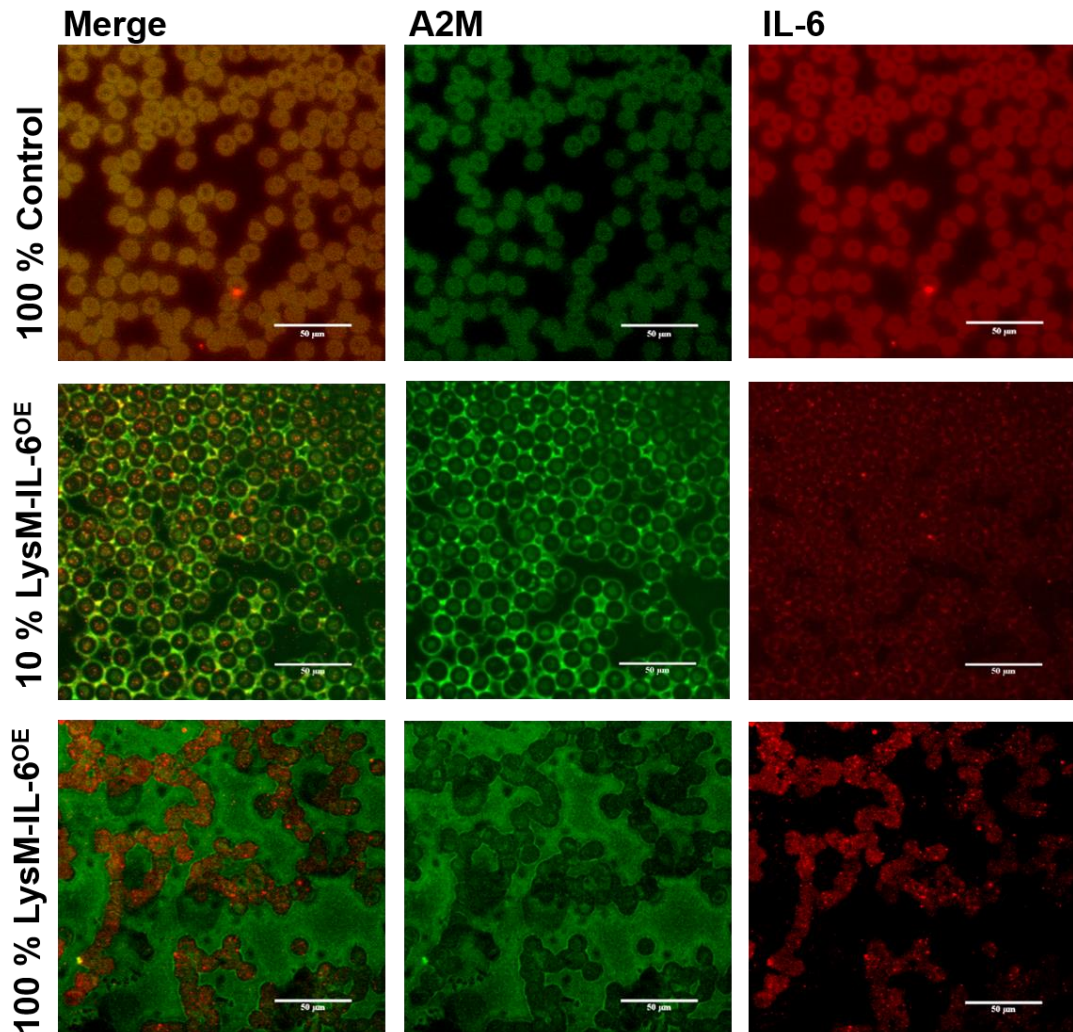


Figure 25 Immunofluorescence staining of blood smears from bone marrow chimeric mice. 100% Control BM, 10% LysM-IL-6^{OE} BM, 100% LysM-IL-6^{OE} BM Red: IL-6; green: A2m, Scale bar represents 50 μ m.

I could confirm by immune-staining of blood smears, on the one hand, that the increased IL-6 (red) level went in line with the percentage of LysM-IL-6^{OE} BM that had been transferred (Figure 24A and Figure 25). On the other hand, there was a hint of difference in intensity between the A2m (green) staining after 10% LysM-IL-6^{OE} BM and 100% LysM-IL-6^{OE} BM transfer (Figure 25). Furthermore, it was already visible in the immune-staining blood smear in mice with 10% LysM-IL-6^{OE} BM transplantation that the erythrocytes started

to form aggregates (Figure 25). In mice that had received 100% LysM-IL-6^{OE} BM, the erythrocyte aggregates were even more clearly visible (Figure 25). This observation was confirmed again by Pappenheim staining, as shown in Figure 26A. In parallel, the whole blood thrombin-triggered clotting time increased with increasing systemic IL-6 levels, which depended on the amount of LysM-IL-6^{OE} BM that had been transferred (Figure 26B).

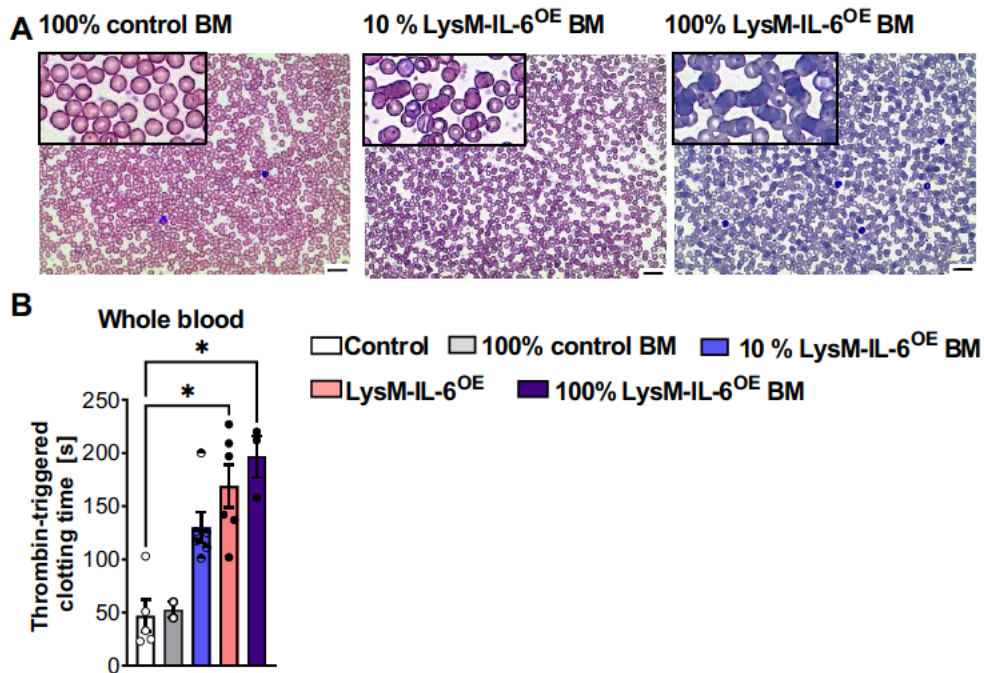


Figure 26 IL-6 dose-dependent effect on the thrombin-triggered clotting and erythrocytes aggregates in mice. A. Pappenheim staining of whole blood from bone marrow chimeric mice. Scale bar represents 200 μ m. Representative image of $n = 3-7$ is shown * $p < 0.5$. (B) Thrombin-triggered clotting time in citrated whole blood from control mice, mice with 100% control bone marrow, mice with 10% LysM-IL-6^{OE} bone marrow, mice with 100% LysM-IL-6^{OE} bone marrow and naïve LysM-IL-6^{OE} mice, $n = 2-6$ mice per group, Kruskal-Wallis test with Dunn's multiple comparisons test.

In summary, the BM transplantation data show that elevated systemic IL-6 levels resulted in a prolongation of thrombin-triggered clotting time in whole blood and led to the formation of erythrocytes aggregates in an IL-6 dose-dependent manner.

3.5. Antagonization of A2m with small hairpin-A2m specific adeno-associated virus in LysM-IL-6^{OE} mice

I found an impaired coagulation in the model of myeloid IL-6 overexpression in mice, partly explained by the IL-6-driven A2m expression and the A2m-mediated inhibition of thrombin. To further confirm this hypothesis, we designed a small hairpin adeno-associated virus that should specifically downregulate the expression of A2m in hepatocytes [147]. Vector Biolabs produced the whole construct. The exact treatment regimen can be found in Figure 7. As a control, the mice were treated with a scrambled virus. This virus contains all the building blocks of the virus but no *cDNA*. The treated LysM-IL-6^{OE} mice, as well as control mice, were examined for inflammation and coagulation five weeks after injection of the small hairpin-A2m / or scrambled specific adeno-associated virus.

3.5.1. Establishing the small hairpin-A2m specific adeno-associated virus in our LysM-IL-6^{OE} mouse model

First of all, I investigated whether the designed construct indeed downregulated the expression of A2m in mice. Therefore, the adeno-associated virus (aav) expressing a short hairpin RNA against *A2m* (AAV8shRNA A2m) was injected *i.v.* into LysM-IL-6^{OE} and control mice to reach hepatocyte-specific A2m knockdown.

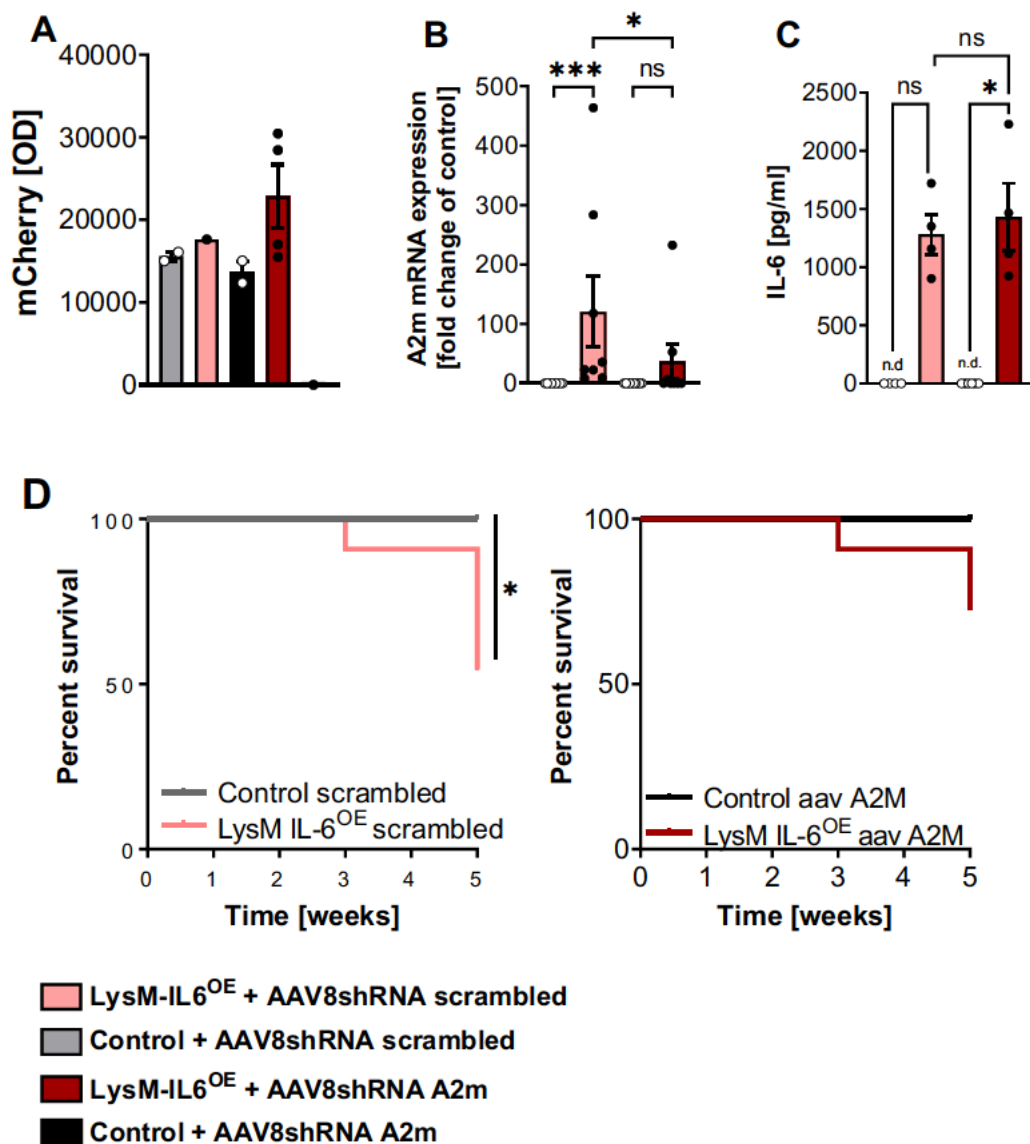


Figure 27 Analysis of LysM-IL-6^{OE} mice treated with small hairpin-A2m specific adeno-associated virus. A. mCherry expression in isolated hepatocyte of LysM-IL-6^{OE} and control mice treated with AAV8shRNA A2m B. A2m mRNA expression in the liver of LysM-IL-6^{OE} and control mice after 5 weeks of treatment with adeno-associated virus 8 small hairpin RNA against A2m (AAV8shRNA A2m) or AAV8shRNA scrambled. n = 7-10, Kruskal-Wallis test with Dunn's multiple comparisons test. C. IL-6 plasma levels in AAV8shRNA A2m or AAV8shRNA scrambled treated LysM-IL-6^{OE} compared to control mice. n = 4-6, Kruskal-Wallis test with Dunn's multiple comparisons test. D. Kaplan-Meier survival curve of LysM-IL-6^{OE} and control mice treated with AAV8shRNA A2m (right) or AAV8shRNA scrambled treated (left). n = 9-12, Log-rank (Mantel-Cox) test, * p < 0.5, *** p < 0.001.

In a first approach, hepatocytes of LysM-IL-6^{OE} compared to control mice treated with AAV8shRNA A2m or AAV8shRNA scrambled were isolated. If the knockdown was successful, then, in addition to the reduced expression of A2m, the expression of mCherry would also occur in hepatocytes. Figure 27A shows that all aav treated groups expressed the mCherry protein but not in the untreated control mice. It was consistent with A2m mRNA expression in

the liver which was significantly decreased in AAV8shRNA *A2m* treated LysM-IL-6^{OE} compared to AAV8shRNA scrambled treated LysM-IL-6^{OE} mice (Figure 27B). In addition, the aav treatment did not alter the plasma IL-6 level (Figure 27C). Treatment with AAV8shRNA *A2m* resulted in a slightly improved survival rate of LysM-IL-6^{OE} mice - AAV8shRNA *A2m* treated LysM-IL-6^{OE} mice had no longer a reduced survival compared to AAV8shRNA *A2m* treated control mice whereas in the *scrambled* vector treated groups there was a reduced survival of LysM-IL-6^{OE} mice compared to control mice (Figure 27D). In summary, the results of this section show that treatment with AAV8shRNA *A2m* led to a hepatocyte-specific *A2m* knockdown in mice.

3.5.2. Inflammatory analysis after treatment with small hairpin-A2m specific adeno-associated virus in LysM-IL-6^{OE} mice

The proteinases inhibitor A2m is known to bind different cytokines including IL-6 [195]. However, the activity of IL-6 bound to A2m does not have to be impaired [196]. In order to ensure that the hepatocyte-specific A2m knockdown only affects the coagulation and does not affect inflammation, the infiltration of cells into the spleen was investigated.

Figure 28A shows that there were no difference in the elevated number of myeloid cells in LysM-IL-6^{OE} mice, no matter if they were treated with AAV8shRNA *A2m* or with AAV8shRNA *scrambled* (Control+AAV8shRNA *scrambled*). The increased splenic monocytes/macrophages compartment in LysM-IL-6^{OE} mice was not altered after AAV8shRNA *A2m* treatment (Figure 28). However, there was no change in the percentage of neutrophils between LysM-IL-6^{OE} mice treated with AAV8shRNA *A2m* or AAV8shRNA *scrambled* (Figure 28).

In summary, the data showed that the knockdown of *A2m* had no effect on the severity of inflammation in myeloid IL-6 overexpression in LysM-IL-6^{OE} mice.

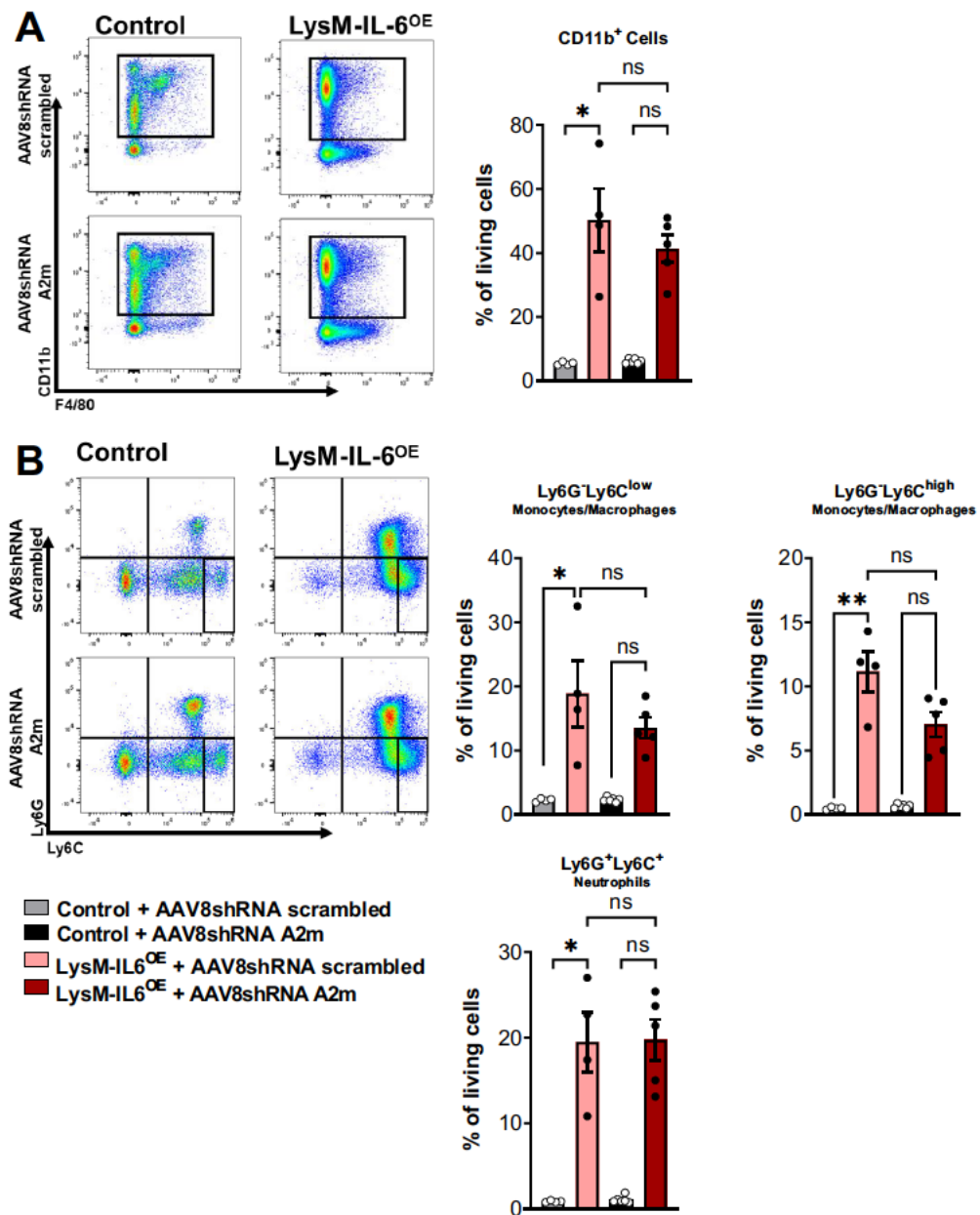


Figure 28 Inflammatory cell analysis of LysM-IL-6^{OE} mice treated with AAV8shRNA A2m or AAV8shRNA scrambled. Representative flow cytometry plots of myeloid surface staining from LysM-IL-6^{OE} spleen treated with AAV8shRNA A2m or AAV8shRNA scrambled. Pre-gated on living cells, CD45.2⁺, CD11b⁺ and F4/80⁺, and gated on and either Ly6G⁺Ly6C⁺ Neutrophils, Ly6G⁻Ly6C^{high} or Ly6G⁻Ly6C^{low} monocytes/macrophages. Quantification of Ly6G⁺Ly6C⁺ Neutrophils, Ly6G⁻Ly6C^{high} or Ly6G⁻Ly6C^{low} Monocytes/Macrophages in the spleen, n = 4-7, Kruskal-Wallis test with Dunn's multiple comparisons test * p < 0.5, *** p < 0.001.

3.5.3. Analyzing the impact of A2m on the coagulation in mice

As upregulated A2m seemed to directly impact on the ability to convert fibrinogen to fibrin in LysM-IL-6^{OE} mice, I analysed the coagulation parameters aPTT and INR in LysM-IL-6^{OE} and control mice after treatment with AAV8shRNA *A2m* versus AAV8shRNA *scrambled*. Figure 29 shows that the AAV8shRNA *A2m* treatment did not affect aPTT in LysM-IL-6^{OE} mice compared to LysM-IL-6^{OE} AAV8shRNA *scrambled* mice: LysM-IL-6^{OE} mice displayed still a significantly prolonged aPTT (Figure 29A). Furthermore, INR increased by a trend in LysM-IL-6^{OE} mice treated either with AAV8shRNA *A2m* or AAV8shRNA *scrambled* (Figure 29B). Plasmatic fibrinogen showed the same effect as aPTT: the levels were significantly elevated in LysM-IL-6^{OE} compared with control with either AAV8shRNA *A2m* or AAV8shRNA *scrambled* adeno-associated virus (Figure 29C). So there was no effect between LysM-IL-6^{OE} treated with AAV8shRNA *A2m* or AAV8shRNA *scrambled*. These data support the idea that the myeloid IL-6 overexpression might mediate the inflammatory effect on the coagulation cascade and not A2m alone in LysM-IL-6^{OE} mice.

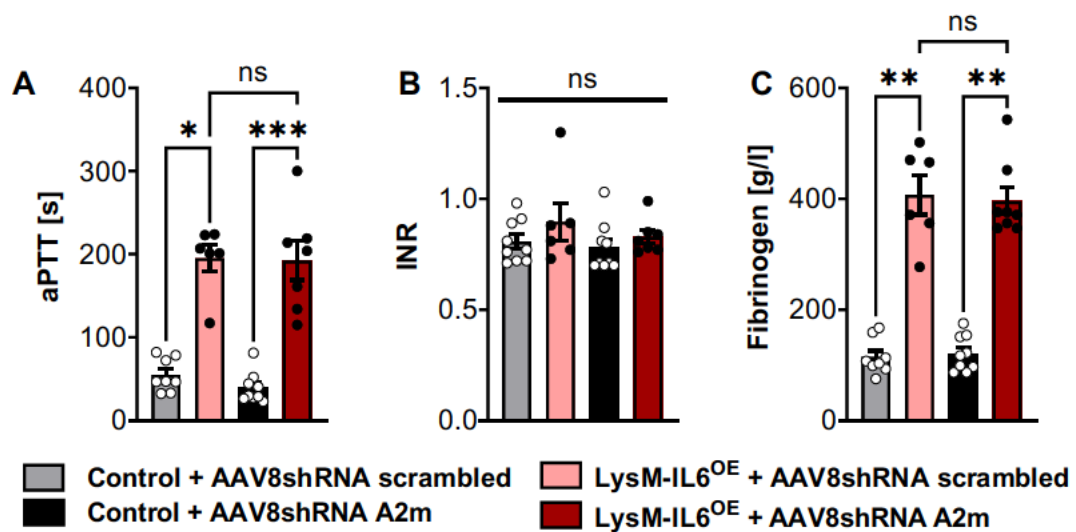


Figure 29 Coagulation Parameter analysis of LysM-IL-6^{OE} mice treated with AAV8shRNA A2m or AAV8shRNA scrambled. A. aPTT and INR (B) from LysM-IL-6^{OE} vs. control mice after 5 weeks of treatment with adeno-associated virus 8 small hairpin RNA against A2m (AAV8shRNA A2m) or AAV8shRNA scrambled, n = 7-8, unpaired Student's t-test. (B) Plasma concentration of Fibrinogen, n= 6-9, Kruskal-Wallis test with Dunn's multiple comparisons test. * p <0.5, ** p <0.01, *** p < 0.001. Data are presented as mean ± SEM.

To elucidate the effect of A2m on the hepatic *Factors XII, XI, IX, VIII, VWF, X, V, Prothrombin, AT, Fibrinogen subunit β and γ* expression: LysM-IL-6^{OE} mice treated with AAV8shRNA A2m and AAV8shRNA scrambled has been normalized to control mice treated with AAV8shRNA scrambled. The control mice treated with AAV8shRNA A2m were also normalized to control mice treated with AAV8shRNA scrambled (Figure 29).

First of all, the data showed that the treatment of the control mice with AAV8shRNA A2m or AAV8shRNA scrambled had no effect on the expression of the coagulation factors in the liver (Figure 29). The coagulation factors *IX, FX* and *Prothrombin* were significantly upregulated in the liver of LysM-IL-6^{OE} AAV8shRNA A2m mice compared to control AAV8shRNA scrambled mice (Figure 29C, F and H). *FIX* and *Prothrombin* expression was also significantly upregulated compared between LysM-IL-6^{OE} AAV8shRNA A2m mice compared to LysM-IL-6^{OE} AAV8shRNA scrambled mice (Figure 29C and H). The expression still tended to be low if one compares the AAV8shRNA scrambled-treated group between LysM-IL-6^{OE} and control mice. Comparing the AAV8shRNA A2m-treated LysM-IL-6^{OE} with AAV8shRNA A2m-treated control mice, the expression still tended to be low

(Figure 29B). Figure 29A and D show that the *FXII* and *FVIII* expression was unchanged between all groups. The treatment with AAV8shRNA *A2m* in LysM-IL-6^{OE} mice increased the hepatocyte *FV* expression compared to the *A2m*-treated control mice by trend. The treatment with AAV8shRNA *A2m* did not alter the expression *vWF* and *Fibrinogen subunit β* and *γ* expression; after the treatment, there was still an increased *mRNA* expression in LysM-IL-6^{OE} mice compared to control mice (Figure 29E, J and K).

The results show that the change in the expression of the coagulation factors could not be attributed to the increased *A2m* expression alone. Rather, it can be confirmed by this that IL-6 overexpressing has a strong influence on the expression of *vWF* and *Fibrinogen*.

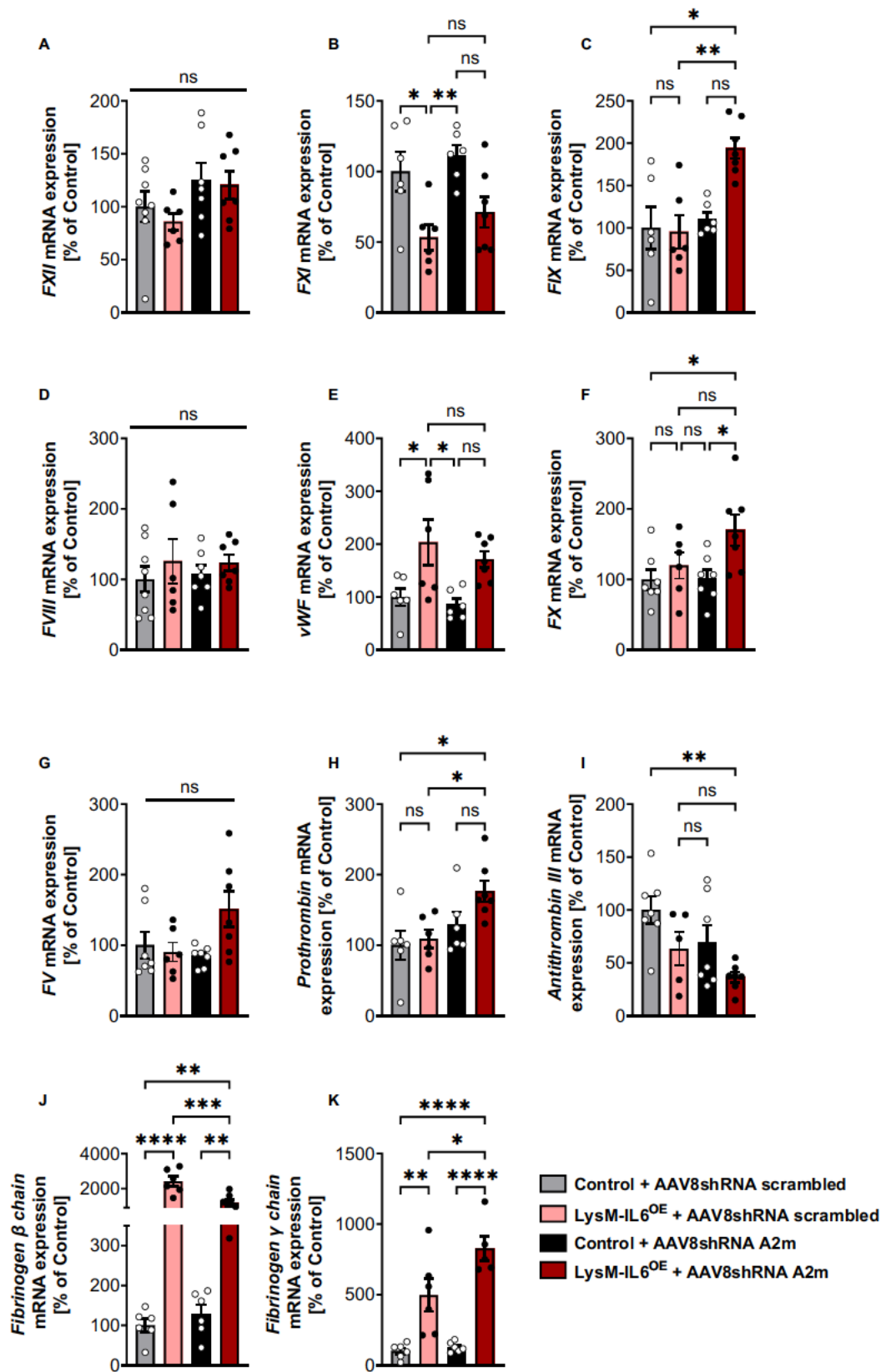


Figure 30 Liver mRNA expression of coagulation factors of LysM-IL6^{OE} mice treated with AAV8shRNA A2m. XII, XI, IX, VIII, VWF, X, V, II, AT, fibrinogen subunit β , γ expression from AAV8shRNA A2m treated LysM-IL6^{OE} mice normalized to LysM-IL6^{OE} mice treated with AAV8shRNA scrambled, n = 8, unpaired Student's t-test or Mann-Whitney t-test. * p < 0.05, ** p < 0.01, Data are presented as mean \pm SEM.

Additionally, hepatocyte-specific *A2m* knockdown did not prevent erythrocyte aggregate formation in *LysM-IL-6^{OE}* treated with AAV8shRNA *A2m* compared to AAV8shRNA *scrambled* treated *LysM-IL-6^{OE}* mice (Figure 31A). A detailed analysis of money roll length shows a significant reduction of erythrocytes per money roll in *LysM-IL-6^{OE}* mice treated with AAV8shRNA *A2m* compared to AAV8shRNA *scrambled* treated mice (Figure 31A). Hepatocyte-specific *A2m* knockdown prevented thrombin converting time delay in *LysM-IL-6^{OE}* mice compared to *LysM-IL-6^{OE}* mice AAV8shRNA *scrambled*. The *LysM-IL-6^{OE}* mice treated with AAV8shRNA *scrambled* showed a significant increase in thrombin converting time compared to AAV8shRNA *scrambled* treated control mice (Figure 31B). In summary, these data show that the thrombin converting time could be indeed directly related to the increased *A2m* level.

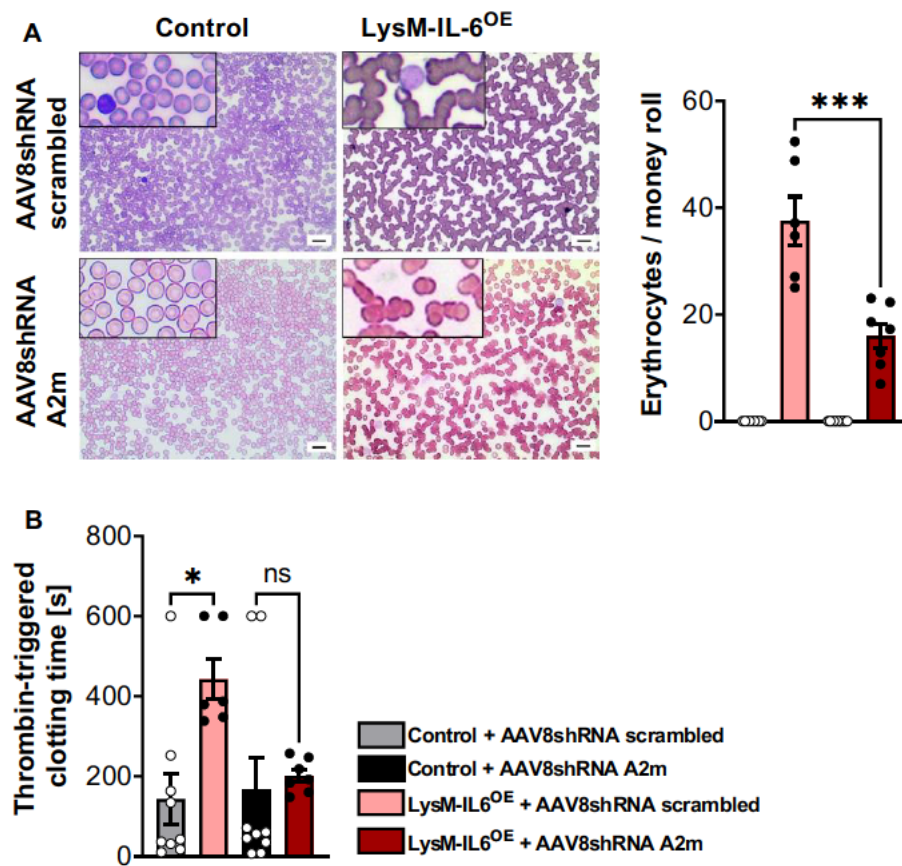


Figure 31 Pappenheim staining and Thrombin converting time of LysM-IL-6^{OE} mice treated with AAV8shRNA A2m or AAV8shRNA scrambled. (A) Pappenheim staining of blood smears of LysM-IL-6^{OE} and control mice treated with AAV8shRNA A2m or AAV8shRNA scrambled. Scale bar represents 20 μ m. Representative image of n = 6-11 are shown. Right: Quantification of the relative erythrocytes / money roll proportion, n = 6-11. Comparison of LysM-IL-6^{OE} treated with AAV8shRNA A2m or AAV8shRNA scrambled with one-way ANOVA with Sidak's multiple comparisons test. (B) Thrombin-triggered clotting time in citrated whole blood of LysM-IL-6^{OE} and control mice treated with AAV8shRNA A2m or AAV8shRNA scrambled. n = 6-7 mice per group, Kruskal-Wallis test with Dunn's multiple comparisons test. * p < 0.5, ** p < 0.01, Data are presented as mean \pm SEM.

4. DISCUSSION

4.1. The role of IL-6 during coagulation

The cytokine IL-6 is a key player in inflammation and supports and amplifies the inflammatory response in infections [34, 182]. However, IL-6 had also been described to alter coagulation differently, which is still not understood [76, 183].

As part of my thesis, I initially wanted to investigate the potentially pro-thrombotic effect of IL-6. Libby *et al.* summarized the evidence that inflammation and thrombosis are linked [197]. Furthermore, he hypothesizes that anti-inflammatory therapies could limit thrombosis and that antithrombotic therapies could reduce vascular inflammation [197]. As IL-6 is a key player in inflammation, I used a genetic mouse model based on a myeloid cell-dependent IL-6 overexpression (LysM-IL-6^{OE} mice). Schüler *et al.* showed that LysM-IL-6^{OE} mice had a plasma IL-6 level of approximately 483.4 ± 87.9 pg/ml (Figure 6 and [126]). These increased levels show that the LysM-IL-6^{OE} mice do not have acute sepsis (IL-6 level > 60000 pg/ml). These values are not comparable to the IL-6 values in acute sepsis [126, 129]. Thus, the LysM-IL-6^{OE} mice are more a chronic inflammatory mouse model rather than an acute one. Interestingly, LysM-IL-6^{OE} mice overexpressing IL-6 in myeloid cells showed no thrombus formation following subtotal IVC ligation compared to control mice (Figure 10). This was extremely surprising since IL-6 was described as a pro-thrombotic cytokine in literature [198]. The increased number and reactivity of platelets, increased monocyte TF production or fibrinogen concentration associated with IL-6 pointed to a pro-thrombotic environment [71, 77, 78, 83, 84]. However, the chronic inflammation present in the LysM-IL-6^{OE} mouse model did not increase the risk of thrombosis after subtotal IVC ligation but revealed an increased risk for bleeding after manipulation.

Based on these observations, the scientific focus was placed on the impact of IL-6 on the coagulation and its hematological components. The elevated IL-6 levels in LysM-IL-6^{OE} mice resulted in a strong chronic inflammatory

phenotype, leading to increased proliferation of myeloid cells in the blood of LysM-IL-6^{OE} mice compared to control mice. This is consistent with IL-6 being able to recruit and activate myeloid cells (Figure 11) [34]. Furthermore, chronic inflammation can manifest in anemia as longterm effect [199, 200], which was also seen in LysM-IL-6^{OE} mice compared to control mice based on the decreased RBC, HGB, and MCH (Figure 11). Williams et al. described that IL-6 stimulated megakaryocytopoiesis in the bone marrow, resulting in an increased platelet count [201]. Contrary to the common literature, the myeloid overexpression of IL-6 in our mouse model did not increase platelet count in the circulation compared to control mice, but enlarged platelets were detected (Figure 11). Elevated MPV indicates usually increased PLT size [202]. This could mean that mainly younger PLTs were present in LysM-IL-6^{OE} mice compared to control mice, implying a faster production of PLTs, but at the same time also consumption or degradation of the PLTs since the number of PLTs itself was not increased [84, 130]. The fact that the D-dimer was not increased in LysM-IL-6^{OE} mice compared to the controls speaks against consumption by bleeding or thrombus formation (Figure 13B) [203]. Another explanation would be that due to the underlying inflammatory processes, there was an increased intracellular synthesis of pro-coagulant and pro-inflammatory factors and degranulation of granules, leading to hyperactivity of platelets and an increased risk of clot formation [204]. However, this was not seen in LysM-IL-6^{OE} mice. In contrast, a prolonged aPTT, a prolonged bleeding time and longer thrombin-triggered clotting time indicate impaired coagulation (Figure 12). Prolonged aPTT and INR can be due to congenital and acquired factor deficiencies such as hemophilia A (FVIII), hemophilia B (FIX), von Willebrand disease with FVIII deficiency, congenital deficiency of intrinsic pathway factors (FXI, FXII, prekallikrein) or the common end route (fibrinogen, FII, FV, FX) [205-208]. However, the prolonged aPTT and INR also indicated autoimmune diseases with lupus inhibitors (antiphospholipid antibodies) or inhibitors against coagulation factors [208]. Using the plasma mixing test, it was possible to rule out that a lupus anticoagulant was present (Figure 13A) [183, 184]. Likewise, the analysis of the expression of the coagulation factors in the liver shows that no hemophilia which could explain the disturbed coagulation in LysM-IL-6^{OE}

mice compared to control mice (Figure 15A). Furthermore, the hepatic expression of *vWF* and *fibrinogen* again showed a pro-thrombotic tendency in LysM-IL-6^{OE} mice compared to control mice, making the absence of thrombosis formation difficult to explain at first sight. However, it is consistent with the current state of the literature, describing that IL-6 can upregulate the *vWF* and *fibrinogen* expression (Figure 15A and B) [72, 131]. Due to the prolonged thrombin-triggered clotting time in whole blood, I investigated whether IL-6 influenced thrombin generation. If there was a very low ETP, this could explain the lack of thrombosis formation in LysM-IL-6^{OE} mice compared to control mice. First, I investigated the thrombin generation in PRP and PPP to see the influence of the platelets on the thrombin generation. It turned out that thrombin generation occurred in PRP and PPP and that the platelets contributed to the generation of thrombin (Figure 14A and B). This was reflected in lower ETP in PPP of LysM-IL-6^{OE} mice compared to the control, but it could also be seen in the comparison between PRP and PPP that the LysM-IL-6^{OE} mice platelets contributed to the generation of thrombin (Figure 14A and B). Nevertheless, the overexpression of IL-6 in myeloid cells resulted in a delayed lag time in PPP and PRP compared to control mice (Figure 14A and B). Furthermore, the data show that in the presence of PLT (PRP), it took longer to reach the time to peak in LysM-IL-6^{OE} mice compared to the control. This could be due to the delayed response of the PLT to thrombin activation and results in a slower expression of procoagulant coagulation factors (FV, FXI, fibrinogen), delaying the positive feedback loop. However, not only platelets influence the coagulation, erythrocytes can act on the coagulation by phosphatidylserine and the membrane triggers the contact activation [209-211]. Also, leukocytes can express tissue factor, release procoagulant components and activate platelets [211]. Therefore, I analysed TG in whole blood to see if these cells acted on the thrombin generation. Whole blood TG showed that the ETP in LysM-IL-6^{OE} mice compared to the control was increased by trend (Figure 14C) and the lag time and time to peak was significantly delayed in LysM-IL-6^{OE} mice compared to the control mice. This suggests that not the RBC or Leukocytes impacted on the ETP but the platelets. In addition, the

data showed a delay in the response (Lag time and time to peak) in LysM-IL-6^{OE} mice compared to the control mice (Figure 14).

The cytokine IL-6 is also of central importance in the SARS-CoV2 pandemic: A complex interaction between IL-6, inflammation and coagulation has been shown here [212]. SARS-CoV2 is associated with an increased rate of thrombotic events, often determining clinical outcomes and contributing to poor survival. However, bleeding complications have also been reported [213]. De la Morena-Barrio and colleagues could show that in PPP of SARS-CoV2 patients with an increased IL-6 level have a prolonged lag-time and reduced ETP [214], what is exactly what we could also see in the LysM-IL-6^{OE} mice compared to control mice. These data so far presented the complexity of the interaction between IL-6 and the coagulation system. However, neither the expression of the different coagulation factors nor the thrombin generation could explain the prolonged bleeding time in LysM-IL-6^{OE} mice.

Because IL-6 activated the inflammatory process, the expression of acute-phase proteins also increases [167, 168]. This can influence the ESR by many factors like inflammation, size, shape, and the number of red blood cells as well as levels of serum fibrinogen and immunoglobulins [4, 167]. An increased ESR, in turn, correlates with rouleaux formation [4]. Boss et al. pointed out a correlation between increased IL-6 plasma levels, CRP and ESR in rheumatoid arthritis patients [215]. This fits to our observations in the LysM-IL-6^{OE} mice showing the increased ESR compared to control mice (Figure 17). The increased fibrinogen plasma levels could be a possible cause of erythrocyte rouleaux formation (Figure 15B). Bedell et al. summarized that fibrinogen had the strongest effect on the rouleaux formation because of its molecular weight and the asymmetric structure [167]. However, not only fibrinogen is a possible cause, alpha and gamma globulins also influence the charge of the erythrocytes [167]. Thus, the elevated A2m levels might also contribute to the erythrocyte rouleaux formation because of its molecular weight and the structure (Figure 15A and Figure 16C). In the further course of the project, it would be useful to

consider the serum alpha and gamma globulins level of LysM-IL-6^{OE} mice compared to control mice, as these are also possible candidates which can influence the erythrocyte rouleaux formation. As myeloid IL-6 overexpression was associated with the rouleaux formation, the question arised whether the bound erythrocytes also might influence coagulation. This could be confirmed by dilution of the blood leading to disaggregation of erythrocyte rouleaux and to an acceleration of thrombin-triggered clotting time. This means that clot formation should occurs again more quickly. In addition, A2m and IL-6 were found to accumulate on the surface of erythrocytes of LysM-IL-6^{OE} mice compared to control mice, which further enhanced the rouleaux formation (Figure 19). Erythrocytes express the IL-6 receptor as well as gp130 [83]. This explains why IL-6 most likely can binds to the surface of erythrocytes. The data show that IL-6 did not only induce inflammation, but also led to rouleaux formation associated with the accumulation of IL-6 and A2M and thus erythrocytes semm to influence thrombin-triggered clotting time in LysM-IL-6^{OE} mice compared to control mice.

To dissect in detail the influence of IL-6 on coagulation and erythrocyte rouleaux formation, we generated chimeric bone marrow (BM) mice with different ratios of BM isolated from LysM-IL-6^{OE} mice mixed with BM from control mice. The results of these experiments showed that on the one hand, with increasing IL-6 levels also aPTT, fibrinogen and the thrombin-triggered clotting time increased by trend (Figure 24B, C and Figure 26B). On the other hand, the erythrocyte rouleaux formation was also related to the IL-6 levels (Figure 26A). The same was seen concerning the accumulation of IL-6 and A2m on the erythrocytes. This coincides with the observation that with the increase in IL-6, the ESR and thus the erythrocyte rouleaux formation also increased. So, there was a direct connection between the IL-6 levels and its effect on the rouleaux formation and the coagulation.

The present data show that myeloid overexpression of IL-6 activates inflammatory processes, including the increased expression of the proteinase A2m. Yoo et al. showed that IL-6 can activate the Jak pathway and Stat3, which bind to the A2m gene promotor and upregulates the expression of A2m [99]. This explains the increased concentration of A2m both at mRNA

and protein level in the liver of LysM-IL-6^{OE} mice compared to control mice (Figure 15 A and Figure 16C). A2m can impact on the coagulation itself as well as on fibrinolysis at various points in the cascade [85, 112, 115, 117-119, 124]. The activity of the coagulation factors also shows that A2m may have a negative influence on FXIII and FII in LysM-IL-6^{OE} mice compared to control mice (Figure 15C). According to the literature, A2m is a potent thrombin inhibitor [85, 117-119]. I could confirm this by showing that A2m alone was able to have the most potent effect on thrombin *in vitro* in the context of the thrombin-triggered clotting time (Figure 18C). Furthermore, I showed that when other proteins are present, such as IL-6 or APC, the thrombin-triggered clotting time was not significantly delayed compared to the controls, but the effect is weakened. A possible explanation could be that A2m has no preference which protein it will bind.

Finally, I could show that by inhibiting *A2m* RNA expression using a specific adeno-associated virus, the thrombin-triggered clotting time in LysM-IL-6^{OE} mice was normalized (Figure 31). The presented data shows that the increased A2m expression negatively influenced the thrombin-triggered clotting time in AAV8shRNA *A2m*-treated LysM-IL-6^{OE} mice compared to AAV8shRNA *A2m*-treated control mice. As a consequence it should be impossible to form a stable clot by cleaving fibrinogen into fibrin [85, 117, 120, 121]. However, it is also clear that the coagulation phenotype of the LysM-IL-6^{OE} mice cannot only be reduced to A2m overexpression. The parameters apTT and INR were not normalized in AAV8shRNA *A2m*-treated LysM-IL-6^{OE} mice compared to AAV8shRNA *A2m*-treated control mice, just like the expression of the different coagulation factors (Figure 29 and Figure 30). It shows that the IL-6-mediated influence on coagulation factors is more complex. It would be of great interest to study the activity of the coagulation factors after treatment with *A2m* adeno-associated virus to investigate the possible influence of A2m on the coagulation factors in LysM-IL-6^{OE}. Furthermore, the assumption was confirmed, by Pappenheim staining of whole blood, that A2m also influences the erythrocyte rouleaux formation in LysM-IL-6^{OE} mice compared to control mice (Figure 31). In total the data

suggest that the interaction of IL-6 and A2M can influence thrombin and thus influence also the clot formation

4.2. The complex interplay of IL-6 and coagulation in human diseases.

Interleukin-6 is a key player in the process of inflammation and therefore also plays a role in various diseases. Elevated IL-6 levels have been found in inflammatory processes such as rheumatoid arthritis [44], Crohn's disease [47, 48], ulcerative colitis [47, 48], fever [21], and sepsis [21]. Furthermore, elevated IL-6 levels are associated with poorer myocardial infarction survival [216]. IL-6 is a predictor of long-term cardiovascular mortality in patients with acute coronary syndrome [217], is implicated in heart failure [218], and is predictive of coronary artery disease [219]. In addition, IL-6 also promotes tumor growth [220]. IL-6 is of central importance in SARS-CoV2 disease: This again could reflect the complex interaction between IL-6, inflammation and coagulation [212, 213]. In the context of the present work, I wanted to check whether elevated A2m levels also occur in humans with chronic, moderately elevated IL-6, influencing the thrombin-triggered clotting time.

IBD patients such as Crohn's disease and ulcerative colitis have elevated IL-6 levels. Which goes in line with the fact, that LysM-IL-6^{OE} mice show a colitis-like phenotype (Figure 20). Therefore, patients with this condition were examined more closely [47, 48]. Patients with an acute phase of IBD showed a prolonged INR (Figure 29) and increased fibrinogen levels. Furthermore, erythrocyte rouleaux formation in the blood went in line with increased ESR (Figure 31). Alper et al. could show a correlation of ESR and C-reactive protein with pediatric IBD activity [221]. After closer analysis of the blood smears, accumulation of IL-6 and A2m on the surface of erythrocytes could also be shown (Figure 22). This fits to our observations in the LysM-IL6^{OE} mice where we found the same accumulation of IL-6 and A2m on erythrocytes (Figure 19). The thrombin-triggered clotting time was significantly delayed in IBD patients as previously shown in the LysM-IL-6

mice as well. (Figure 23 and Figure 11). It is noteworthy that dilution could reverse the erythrocyte rouleaux formation and the prolonged thrombin-triggered clotting time also in human blood. IBD alone counts as a risk factor for venous thromboembolism but conversely, bleeding from the intestinal tract is one of the most common signs of IBD [222, 223]. A typical symptom of IBD is the defect in the barrier function in the intestinal epithelium [224]. The damage can vary in severity, but results in the loss of the protective function of the barrier and an imbalance between the microbes and the host's immune system [224]. This triggers compensatory immune reactions. In addition to the immune response, a destroyed intestinal endothelium also has effects on the coagulation [224]. Endothelial cells express anticoagulant factors such as tissue factor pathway inhibitor (TFPI) and proteins that enable PC activation such as thrombomodulin and endothelial PC receptor (EPCR) [225-227]. In physiological conditions, these are expressed on the surface of endothelial cells and prevent activation of the extrinsic signaling pathway [225-227]. Inflammation leads to activation and dysfunction resulting in the release of TFPI and EPCR [225-227]. This leads to a disturbed endothelial anticoagulation function [225-227]. In a population-based study, Murthy was able to show that IBD patients have a sevenfold increased risk of developing venous thromboembolism or pulmonary embolism [69]. Besides, there are reports that various treatment methods also increase the risk of venous thromboembolism [70, 228]. Sandborn's study indicates that treatment with the JAK inhibitor Tofacitinib can lead to increased pulmonary embolism and venous thromboembolism [229]. A possible explanation for this could be the Stat3-mediated *A2m* expression: There is no Stat3 expression when the Jack pathway is inhibited leading to no increased *A2m* expression. And a hypothesis could be, that the organism tries to counteract the increased risk of thrombosis by *A2m*-induced thrombin inhibition. If this process is interfered with by Tofacitinib administration, it could lead to an increased prothrombotic environment and venous thromboembolism risk increases. This could be an example of the potentially important role of IL-6-driven overexpression of *A2m* in maintaining hemostasis.

As already mentioned, IL-6 is also of crucial relevance in SARS-CoV2 disease [212, 213]. SARS-CoV2 is associated with an increased risk of thrombotic events and this risk also determines the clinical outcome and may contribute to a reduced chance of survival [230]. However, also bleeding complications have also been reported [213]. Schramm and colleagues have hypothesized that higher levels of A2m in childhood might contribute to a more favorable course of SARS-CoV2 disease in children compared to adults [231]. Within their recent publication, they refer to the finding that A2m has been detected on the surface of endothelial cells [231-233]. If A2m attaches itself to the surface of the vessel wall, this could have a protective effect on the vascular endothelium. It could serve as a protective layer between blood cells and the vessel wall [233]. This could protect the endothelium from circulating proteins secreted during inflammation or hemostatic events. In turn, this could have a positive effect on the course of SARS-CoV2 disease [231-233]. In total, this underlines how important the analysis of the crosstalk between IL-6 and A2m in regard to the coagulation and hemostasis are.

4.3. Conclusion

The LysM-IL-6^{OE} mouse model shows that chronically and moderately elevated IL-6 levels led to chronic inflammation but did not lead to spontaneous thrombosis or bleeding basal. In case the coagulation cascade was activated, such as following vena cava ligation we found that no thrombus was formed and that there was a much greater tendency to bleed after stimulation.

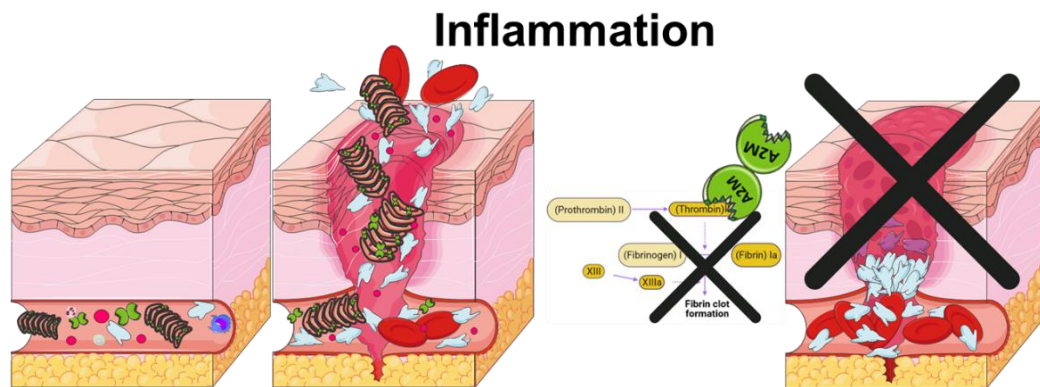


Figure 32 Scheme of the impact of IL-6-driven A2m overexpression on clot formation. When coagulation is activated during IL-6-mediated inflammation, such as by injury, A2m prevents the bleeding from stopping.

In total, the data of my theses suggest that chronic moderate IL-6 elevation activated a vicious circle. IL-6 activated myeloid cells to produce more IL-6. This stimulates the inflammatory cycle and impacts on the coagulation cascade in a complex way. IL-6 mediated JAK/STAT activation binds the A2m gene promoter region in the liver. This results in increased A2m expression in hepatocytes. A2m is secreted into the bloodstream. Increased levels of IL-6 and A2m lead to the erythrocyte rouleaux formation, with an accumulation of IL-6 and A2m on the surface of the erythrocytes (Figure 33). The increased occurrence of A2m has the consequence that it influences the coagulation cascade by inhibition of thrombin.

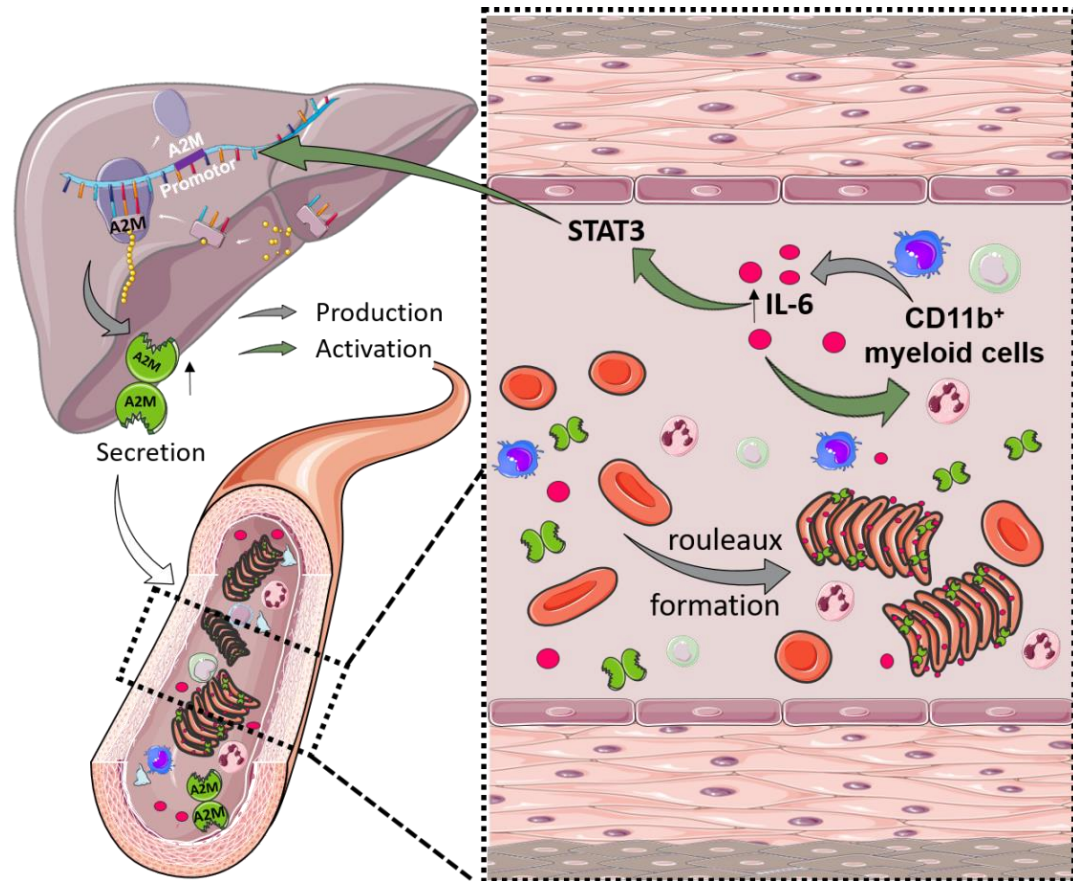


Figure 33 Scheme of the impact of IL-6 on erythrocyte rouleaux formation, myeloid cells and **A2m**. Increased IL-6 levels activate the STAT3 signaling pathway. STAT3 leads to increased expression of *A2m* in the liver. A2m influences coagulation and, together with IL-6, influences, among other things, the rouleaux formation of erythrocytes.

5. SUMMARY

In summary, my thesis points out the complex crosstalk between chronically moderate elevated Interleukin-6 levels and the coagulation cascade.

I analyzed the impact of myeloid cell-dependent chronic IL-6 overexpression, focusing on the coagulation system. Mice overexpressing IL-6 in the myeloid cells (LysM-IL-6^{OE}) had a moderately increased IL-6 level which surprisingly resulted in no thrombus formation following subtotal IVC ligation. Instead, myeloid-derived IL-6 overexpression led to a prolonged aPTT, INR and thrombin-triggered clotting time. This was also reflected in a prolonged tail bleeding time. The IL-6-driven inflammation was mirrored in the blood cell composition: There was an increased number of white blood cells, neutrophils and leukocytes in the blood but with no alteration of platelet count compared to control mice. The expression and activity of some coagulation factors, such as Factor XI and IX, were altered in LysM-IL-6^{OE} mice compared to control mice, but this did not explain the missing thrombus formation after subtotal IVC ligation and the bleeding tendency after activation of the coagulation cascade. The thrombin generation in LysM-IL-6^{OE} mice showed that the thrombin formation is possible in PPP, PRP and whole blood with a slight delay in the lag time and time to peak.

Myeloid-derived IL-6 resulted in chronic inflammation and a colitis-like phenotype and it also led to increased hepatic *A2m* expression via STAT3 signaling. The IL-6-mediated inflammation was associated with the erythrocyte rouleaux formation and prolonged ESR. The erythrocyte rouleaux formation could be driven by the increased plasmatic fibrinogen levels and by the hepatic overexpression of *A2m*. In *in vitro* experiments, the rouleaux formation could be removed by dilution of the blood, resulting in a faster thrombin-triggered clotting time. The proteinase A2m led to reduced thrombin activity and was colocalized with IL-6 on the surface of erythrocytes in LysM-IL-6^{OE} mice compared to control mice.

In a bench-to-bedside approach, I could show that moderately elevated IL-6 levels in IBD patients had a similar impact on the coagulation cascade as

seen in LysM-IL-6^{OE} mice compared to control mice: There was an increased INR and a delayed thrombin-triggered clotting time in IBD patients. The effect of inflammation on erythrocyte rouleaux formation and ESR was also evident. Remarkably, IBD patients also show an accumulation of A2m and IL-6 on the surface of erythrocytes. Suggesting that A2m might play an important role in maintaining hemostasis because it neutralizes the prothrombotic environment associated with inflammation.

The impact of myeloid cell-dependent IL-6 overexpression on the coagulation system depended strongly on the systemic IL-6 level. I could show this by generating BM chimeric mice with different ratios of BM isolated from LysM-IL-6^{OE} mice mixed with BM of control mice. Already 10% LysM-IL-6^{OE} BM was sufficient to increase the plasmatic fibrinogen levels compared to control mice. Besides, a beginning rouleaux formation and the accumulation of A2m and IL-6 on the erythrocyte surface were already evident. I could also show that 10% LysM-IL-6^{OE} BM was sufficient to delay the thrombin-triggered clotting time and could thus harm clot formation. However, if 100% LysM-IL-6^{OE} BM was transplanted, a significantly increased thrombin-triggered clotting time was found, as seen before in the LysM-IL-6^{OE} mice.

In the last part of my thesis, I used an adeno-associated virus expressing a short hairpin RNA against A2m (AAV8shRNA *A2m*) to inhibit the hepatic expression of *A2m*. With this experimental approach, I could show in a straight-forward approach that A2m strongly influenced the thrombin-triggered clotting time LysM-IL-6^{OE} mice compared to control mice. By treating the LysM-IL-6^{OE} mice with AAV8shRNA *A2m*, the thrombin-triggered clotting time could be almost normalized, and the rouleaux formation was also decreased.

In conclusion, myeloid cell-dependent chronic IL-6 overexpression increased hepatic A2m expression, which contributed to delayed thrombin-triggered clotting time and inhibited venous thrombus formation in mice. These data illustrate a new facet of the ability of IL-6 to modulate hemostasis.

6. Zusammenfassung

Zusammenfassend weisen die Daten meiner Dissertation auf die komplexe Wechselwirkung zwischen chronisch moderat erhöhten Interleukin-6-Spiegeln und der Gerinnungskaskade hin.

Ich habe den Einfluss von myeloiden Zellen abstammendem IL-6 analysiert, mit Hilfe von Mäusen (LysM-IL-6^{OE}), die IL-6 in myeloiden Zellen überexpressieren, wobei der Schwerpunkt auf dem Gerinnungssystem lag. Mäuse, die IL-6 in den myeloiden Zellen überexpressieren, hatten einen moderat erhöhten IL-6-Spiegel. Dies hatte überraschenderweise zur Folge, dass keine venösen Thromben durch IVC-Ligation induziert werden konnten. Vielmehr zeigte sich, dass eine IL-6-Überexpression zu einer verlängerten aPTT und INR im Plasma, sowie einer verzögerten Thrombin-getriggerten Gerinnungszeit im Vollblut führte. Dies konnte durch eine verlängerte Schwanzblutungszeit bestätigt werden. Die IL-6-gesteuerte Entzündung spiegelte sich in der Blutzusammensetzung wider: Es gab eine erhöhte Anzahl von weißen Blutkörperchen, Neutrophilen und Leukozyten im Blut, aber ohne Veränderung der Blutplättchenzahl im Vergleich zu Kontrollmäusen. Die Expression und Aktivität einiger Gerinnungsfaktoren, wie Faktor XI und IX, waren in LysM-IL-6^{OE} Mäusen im Vergleich zu Kontrollmäusen verändert. Dies erklärte jedoch nicht die fehlende Thrombusbildung nach subtotaler IVC-Ligation und die Blutungsneigung nach Aktivierung der Gerinnungskaskade. Die Thrombin Generierung zeigte, dass die Bildung von Thrombin in PPP, PRP und Vollblut mit einer leichten Verzögerung in der lag time and time to peak möglich war.

Myeloide IL-6 Überexpression führte im Mausmodell zu einer chronischen Entzündung und einem Colitis-ähnlichen Phänotyp. Es führte auch zu einer erhöhten hepatischen *A2m*-Expression über STAT3-Signalisierung. Die IL-6-vermittelte Entzündung führte zur Erythrocyten Rouleaux-Bildung (Geldrollenbildung) und war mit einer verlängerten ESR verbunden. Die Rouleaux-Bildung von Erythrozyten könnte durch die erhöhten plasmatischen Fibrinogenspiegel und die hepatische Überexpression von *A2m* begünstigt worden sein. Durch Verdünnung des Blutes konnte die Rouleaux-Bildung

aufgelöst werden, was zu einer schnelleren Thrombin-getriggerten Gerinnungszeit führte. Die Proteinase A2m führte zu einer verminderten Aktivität von Thrombin und war mit IL-6 auf der Oberfläche von Erythrozyten lokalisiert.

In einem Bench-to-Bedside-Ansatz konnte ich zeigen, dass moderat erhöhte IL-6-Spiegel bei Patienten mit einer chronisch-entzündlichen Darmerkrankung einen ähnlichen Einfluss auf die Gerinnungskaskade zu haben wie bei LysM-IL-6^{OE} im Vergleich zu Kontrollmäusen. Es zeigte sich einen erhöhte INR und eine verzögerte Thrombin-getriggerte Gerinnungszeit. Der Entzündungseinfluss auf die Rouleaux-Bildung und ESR war ebenfalls ersichtlich. Bemerkenswerterweise zeigten Patienten mit chronisch-entzündliche Darmerkrankung auch eine Akkumulation von A2m und IL-6 auf der Oberfläche von Erythrozyten. Dies deutete darauf hin, dass A2m eine wichtige Rolle bei der Aufrechterhaltung der Hämostase, als auch bei der Neutralisierung des mit Entzündungen verbundene pro-thrombotische Milieus spielt.

Die Auswirkung der myeloischen zellabhängigen IL-6-Überexpression auf das Gerinnungssystem hing stark vom IL-6-Spiegel ab. Ich konnte dies zeigen, indem ich Knochenmarkchimäre mit unterschiedlichen Verhältnissen von Knochenmark erzeugte. Hierzu wurde Knochenmark aus LysM-IL-6^{OE}-Mäusen mit Knochenmark von Kontrollmäusen gemischt. Bereits 10 % LysM-IL-6^{OE} Knochenmark reichte aus, um die plasmatischen Fibrinogen spiegel im Vergleich zu Kontrollmäusen zu erhöhen. Außerdem war bereits eine beginnende Rouleaux-Bildung und die Akkumulation von A2m und IL-6 auf der Erythrozytenoberfläche erkennbar. Ich konnte auch zeigen, dass 10 % LysM-IL-6^{OE} Knochenmark ausreichten, um die Thrombin-getriggerte Gerinnungszeit zu beeinflussen und somit der Blutgerinnung zu schaden. Wenn jedoch 100 % LysM-IL-6^{OE} Knochenmark transplantiert wurde, wurde eine signifikant verlängerte Thrombin-getriggerte Gerinnungszeit gefunden, wie es zuvor bei den LysM-IL-6^{OE} -Mäusen beobachtet werden konnte.

Im letzten Teil meiner Doktorarbeit habe ich ein Adeno-assoziiertes Virus verwendet, das eine kurze Haarnadel-RNA gegen A2m (AAV8shRNA A2m)

exprimiert, um die hepatische Expression von *A2m* zu hemmen. Mit diesem experimentellen Ansatz konnte ich zeigen, dass *A2m* einen starken Einfluss auf die Thrombin-getriggerte Gerinnungszeit hat. Durch die Behandlung der Mäuse konnte die Thrombin-induzierte Gerinnungszeit nahezu normalisiert werden, es zeigte sich aber auch, dass die Erythrocyten-Rouleaux-Bildung abnahm.

Zusammenfassend führte die von myeloiden Zellen abhängige chronische IL-6-Überexpression zu einer erhöhten hepatischen *A2m*-Expression, die zu einer verzögerten Thrombin-angestimmten Gerinnungszeit beitrug und die venöse Thrombusbildung bei Mäusen hemmte. Diese Daten veranschaulichen eine neue Facette der Fähigkeit von IL-6, die Hämostase zu beeinflussen.

7. REFERENCES

1. Grover, S.P. and N. Mackman, *Intrinsic pathway of coagulation and thrombosis: Insights from animal models*. Arteriosclerosis, thrombosis, and vascular biology, 2019. **39**(3): p. 331-338.
2. Smith, S.A., R.J. Travers, and J.H. Morrissey, *How it all starts: Initiation of the clotting cascade*. Critical reviews in biochemistry and molecular biology, 2015. **50**(4): p. 326-336.
3. Kemkes-Matthes, B. and G. Oehler, *Blutgerinnung und Thrombose*. 2001: Georg Thieme Verlag.
4. Skalak, R., et al., *Mechanics of rouleau formation*. Biophysical journal, 1981. **35**(3): p. 771-781.
5. Hoffbrand, A.V. and D.P. Steensma, *Hoffbrand's essential haematology*. 2019: John Wiley & Sons.
6. van Montfoort, M.L. and J.C. Meijers, *Recent insights into the role of the contact pathway in thrombo-inflammatory disorders*. Hematology 2014, the American Society of Hematology Education Program Book, 2014. **2014**(1): p. 60-65.
7. Revenko, A.S., et al., *Selective depletion of plasma prekallikrein or coagulation factor XII inhibits thrombosis in mice without increased risk of bleeding*. Blood, The Journal of the American Society of Hematology, 2011. **118**(19): p. 5302-5311.
8. Visser, M., et al., *Role of factor XIa and plasma kallikrein in arterial and venous thrombosis*. Thrombosis and haemostasis, 2020. **120**(06): p. 883-993.
9. Bendapudi, P.K., et al., *Stimulated platelets but not endothelium generate thrombin via a factor XIa-dependent mechanism requiring phosphatidylserine exposure*. Blood, 2016. **128**(22): p. 258.
10. Esmon, C.T., *The roles of protein C and thrombomodulin in the regulation of blood coagulation*. J Biol Chem, 1989. **264**: p. 4743-4746.
11. Esmon, C.T. *Inflammation and the activated protein C anticoagulant pathway*. in *Seminars in thrombosis and hemostasis*. 2006. Copyright© 2006 by Thieme Medical Publishers, Inc., 333 Seventh Avenue, New York, NY 10001, USA., 2006. S. 049-060.
12. Grover, S.P. and N. Mackman, *Tissue factor: an essential mediator of hemostasis and trigger of thrombosis*. Arteriosclerosis, thrombosis, and vascular biology, 2018. **38**(4): p. 709-725.
13. Wilcox, J.N., et al., *Localization of tissue factor in the normal vessel wall and in the atherosclerotic plaque*. Proceedings of the National Academy of Sciences, 1989. **86**(8): p. 2839-2843.
14. Darbousset, R., et al., *Tissue factor-positive neutrophils bind to injured endothelial wall and initiate thrombus formation*. Blood, The Journal of the American Society of Hematology, 2012. **120**(10): p. 2133-2143.
15. Macfarlane, R., *An enzyme cascade in the blood clotting mechanism, and its function as a biochemical amplifier*. Nature, 1964. **202**(4931): p. 498-499.
16. Rijken, D. and H. Lijnen, *New insights into the molecular mechanisms of the fibrinolytic system*. Journal of thrombosis and haemostasis, 2009. **7**(1): p. 4-13.
17. Carmeliet, P., et al., *Physiological consequences of loss of plasminogen activator gene function in mice*. Nature, 1994. **368**(6470): p. 419-424.
18. Colman, R.W., *Hemostasis and thrombosis: basic principles and clinical practice*. 2006: Lippincott Williams & Wilkins.

19. Colman, R.W., *Activation of plasminogen by human plasma kallikrein*. Biochemical and biophysical research communications, 1969. **35**(2): p. 273-279.
20. D'Angelo, G.J.J.B.D., *Inflammation and coagulation: a "continuum" between coagulation activation and prothrombotic state*. 2015. **2**(1): p. 1023.
21. Patel, P., et al., *Markers of inflammation and infection in sepsis and disseminated intravascular coagulation*. 2019. **25**: p. 1076029619843338.
22. Ridker, P.M.J.N.r., *Inflammatory biomarkers and risks of myocardial infarction, stroke, diabetes, and total mortality: implications for longevity*. 2007. **65**(suppl 3): p. S253-S259.
23. Lindsberg, P.J. and A.J.J.S. Grau, *Inflammation and infections as risk factors for ischemic stroke*. 2003. **34**(10): p. 2518-2532.
24. Ridker, P.M., et al., *C-reactive protein and other markers of inflammation in the prediction of cardiovascular disease in women*. 2000. **342**(12): p. 836-843.
25. Murphy, K. and C. Weaver, *Janeway's immunobiology*. 2016: Garland science.
26. Levi, M., T. van der Poll, and H.R.J.C. Büller, *Bidirectional relation between inflammation and coagulation*. 2004. **109**(22): p. 2698-2704.
27. Ozeren, A., et al., *Levels of serum IL-1 β , IL-2, IL-8 and tumor necrosis factor- α in patients with unstable angina pectoris*. 2003. **12**(6): p. 361-365.
28. Mohamed-Ali, V., et al., *Subcutaneous adipose tissue releases interleukin-6, but not tumor necrosis factor- α , in vivo*. 1997. **82**(12): p. 4196-4200.
29. Jirik, F., et al., *Bacterial lipopolysaccharide and inflammatory mediators augment IL-6 secretion by human endothelial cells*. 1989. **142**(1): p. 144-147.
30. Van Snick, J., *Interleukin-6: an overview*. Annual review of immunology, 1990. **8**: p. 253-278.
31. Heinrich, P.C., J.V. Castell, and T. Andus, *Interleukin-6 and the acute phase response*. Biochemical journal, 1990. **265**(3): p. 621-636.
32. Scheller, J., et al., *The pro- and anti-inflammatory properties of the cytokine interleukin-6*. Biochimica et biophysica acta, 2011. **1813**(5): p. 878-888.
33. Aarden, L.A., et al., *Production of hybridoma growth factor by human monocytes*. European journal of immunology, 1987. **17**(10): p. 1411-1416.
34. Tanaka, T., M. Narazaki, and T.J.C.S.H.p.i.b. Kishimoto, *IL-6 in inflammation, immunity, and disease*. 2014. **6**(10): p. a016295.
35. Akira, S., T. Taga, and T.J.A.i.i. Kishimoto, *Interleukin-6 in biology and medicine*. 1993. **54**: p. 1-78.
36. Scheller, J., et al., *The pro-and anti-inflammatory properties of the cytokine interleukin-6*. Biochimica et Biophysica Acta (BBA)-Molecular Cell Research, 2011. **1813**(5): p. 878-888.
37. Dienz, O. and M. Rincon, *The effects of IL-6 on CD4 T cell responses*. Clinical immunology, 2009. **130**(1): p. 27-33.
38. Gabay, C., *Interleukin-6 and chronic inflammation*. Arthritis research & therapy, 2006. **8**(2): p. 1-6.
39. Screpanti, I., et al., *Inactivation of the IL-6 gene prevents development of multicentric Castleman's disease in C/EBP beta-deficient mice*. The Journal of experimental medicine, 1996. **184**(4): p. 1561-1566.
40. Lattanzio, G., et al., *Defective development of pristane-oil-induced plasmacytomas in interleukin-6-deficient BALB/c mice*. The American journal of pathology, 1997. **151**(3): p. 689.
41. Campbell, I.L., et al., *Trans-signaling is a dominant mechanism for the pathogenic actions of interleukin-6 in the brain*. Journal of Neuroscience, 2014. **34**(7): p. 2503-2513.

42. Jones, S.A., *Directing transition from innate to acquired immunity: defining a role for IL-6*. The Journal of Immunology, 2005. **175**(6): p. 3463-3468.
43. Dayer, J.-M. and E. Choy, *Therapeutic targets in rheumatoid arthritis: the interleukin-6 receptor*. Rheumatology, 2010. **49**(1): p. 15-24.
44. Kotake, S., et al., *Interleukin-6 and soluble interleukin-6 receptors in the synovial fluids from rheumatoid arthritis patients are responsible for osteoclast-like cell formation*. Journal of Bone and Mineral Research, 1996. **11**(1): p. 88-95.
45. Kvalvik, A., M. Jones, and D. Symmons, *Mortality in a cohort of Norwegian patients with rheumatoid arthritis followed from 1977 to 1992*. Scandinavian journal of rheumatology, 2000. **29**(1): p. 29-37.
46. Podolsky, D.K., *Inflammatory Bowel Disease*. New England Journal of Medicine, 1991. **325**(13): p. 928-937.
47. Atreya, R. and M.F. Neurath, *Involvement of IL-6 in the pathogenesis of inflammatory bowel disease and colon cancer*. Clinical Reviews in Allergy & Immunology, 2005. **28**(3): p. 187-195.
48. Lust, J.A., et al., *Isolation of an mRNA encoding a soluble form of the human interleukin-6 receptor*. Cytokine, 1992. **4**(2): p. 96-100.
49. Hibi, M., et al., *Molecular cloning and expression of an IL-6 signal transducer, gp130*. Cell, 1990. **63**(6): p. 1149-1157.
50. Yamasaki, K., et al., *Cloning and expression of the human interleukin-6 (BSF-2/IL-6) receptor*. Science, 1988. **241**(4867): p. 825-828.
51. Romano, M., et al., *Role of IL-6 and its soluble receptor in induction of chemokines and leukocyte recruitment*. Immunity, 1997. **6**(3): p. 315-325.
52. Peters, M., et al., *Extramedullary expansion of hematopoietic progenitor cells in interleukin (IL)-6-sIL-6R double transgenic mice*. The Journal of experimental medicine, 1997. **185**(4): p. 755-766.
53. Mülberg, J., et al., *The soluble interleukin-6 receptor is generated by shedding*. European journal of immunology, 1993. **23**(2): p. 473-480.
54. Rose-John, S., *IL-6 trans-signaling via the soluble IL-6 receptor: importance for the pro-inflammatory activities of IL-6*. International journal of biological sciences, 2012. **8**(9): p. 1237-1247.
55. Wolf, J., S. Rose-John, and C. Garbers, *Interleukin-6 and its receptors: a highly regulated and dynamic system*. Cytokine, 2014. **70**(1): p. 11-20.
56. Suzuki, M., et al., *Anti-inflammatory mechanism of tocilizumab, a humanized anti-IL-6R antibody: effect on the expression of chemokine and adhesion molecule*. Rheumatology international, 2010. **30**(3): p. 309-315.
57. Scheller, J. and S. Rose-John, *Interleukin-6 and its receptor: from bench to bedside*. Medical microbiology and immunology, 2006. **195**(4): p. 173-183.
58. Poredos, P. and M. Jezovnik, *The role of inflammation in venous thromboembolism and the link between arterial and venous thrombosis*. International angiology, 2007. **26**(4): p. 306.
59. Levi, M. and T. van der Poll, *Endothelial injury in sepsis*. Intensive care medicine, 2013. **39**(10): p. 1839-1842.
60. Schouten, M., et al., *Inflammation, endothelium, and coagulation in sepsis*. Journal of leukocyte biology, 2008. **83**(3): p. 536-545.
61. Takemoto, C.M., *Venous thromboembolism in cystic fibrosis*. Pediatric pulmonology, 2012. **47**(2): p. 105-112.
62. Olson, N.C., et al., *Inflammation markers and incident venous thromboembolism: the REGARDS cohort*. Journal of Thrombosis and Haemostasis, 2014. **12**(12): p. 1993-2001.
63. Monn, M.F., et al., *Infection and venous thromboembolism in patients undergoing colorectal surgery: what is the relationship?* Diseases of the colon and rectum, 2014. **57**(4): p. 497.

64. Matta, F., et al., *Risk of venous thromboembolism with rheumatoid arthritis*. *Thrombosis and haemostasis*, 2009. **101**(01): p. 134-138.
65. Kim, S.C., et al., *Risk of venous thromboembolism in patients with rheumatoid arthritis*. *Arthritis care & research*, 2013. **65**(10): p. 1600-1607.
66. Lagrange, J., et al., *Shedding light on hemostasis in patients with inflammatory bowel diseases*. *Clinical Gastroenterology and Hepatology*, 2021. **19**(6): p. 1088-1097. e6.
67. Yuhara, H., et al., *Meta-analysis: the risk of venous thromboembolism in patients with inflammatory bowel disease*. *Alimentary pharmacology & therapeutics*, 2013. **37**(10): p. 953-962.
68. Belaiche, J., et al., *Acute lower gastrointestinal bleeding in Crohn's disease: characteristics of a unique series of 34 patients*. *The American journal of gastroenterology*, 1999. **94**(8): p. 2177-2181.
69. Murthy, S.K., G.C.J.O.j.o.t.A.C.o.G. Nguyen, and ACG, *Venous thromboembolism in inflammatory bowel disease: an epidemiological review*. 2011. **106**(4): p. 713-718.
70. Fumery, M., et al., *Thromboembolic events and cardiovascular mortality in inflammatory bowel diseases: a meta-analysis of observational studies*. 2014. **8**(6): p. 469-479.
71. Amrani, D., *Regulation of fibrinogen biosynthesis: glucocorticoid and interleukin-6 control*. *Blood coagulation & fibrinolysis: an international journal in haemostasis and thrombosis*, 1990. **1**(4-5): p. 443-446.
72. Liu, Z. and G.M. Fuller, *Detection of a Novel Transcription Factor for the A α Fibrinogen Gene in Response to Interleukin-6 (*)*. *Journal of Biological Chemistry*, 1995. **270**(13): p. 7580-7586.
73. Zhang, Z. and G.M. Fuller, *Interleukin 1 β inhibits interleukin 6-mediated rat γ fibrinogen gene expression*. *Blood, The Journal of the American Society of Hematology*, 2000. **96**(10): p. 3466-3472.
74. Luc, G., et al., *C-reactive protein, interleukin-6, and fibrinogen as predictors of coronary heart disease: the PRIME Study*. *Arteriosclerosis, thrombosis, and vascular biology*, 2003. **23**(7): p. 1255-1261.
75. Tracy, R.P., *Inflammation markers and coronary heart disease*. *Current opinion in lipidology*, 1999. **10**(5): p. 435-441.
76. Koenig, W., *Fibrin (ogen) in cardiovascular disease: an update*. *Thrombosis and haemostasis*, 2003. **89**(04): p. 601-609.
77. Osterud, B. and S.I. Rapaport, *Activation of factor IX by the reaction product of tissue factor and factor VII: additional pathway for initiating blood coagulation*. *Proceedings of the National Academy of Sciences*, 1977. **74**(12): p. 5260-5264.
78. Neumann, F.-J., et al., *Effect of human recombinant interleukin-6 and interleukin-8 on monocyte procoagulant activity*. *Arteriosclerosis, thrombosis, and vascular biology*, 1997. **17**(12): p. 3399-3405.
79. Cermak, J., et al., *C-reactive protein induces human peripheral blood monocytes to synthesize tissue factor*. 1993.
80. Hollen, C.W., et al., *Elevated serum interleukin-6 levels in patients with reactive thrombocytosis*. *British Journal of Haematology*, 1991. **79**(2): p. 286-290.
81. Asano, S., et al., *In vivo effects of recombinant human interleukin-6 in primates: stimulated production of platelets*. *Blood*, 1990. **75**(8): p. 1602-1605.
82. Ishibashi, T., et al., *Interleukin-6 is a potent thrombopoietic factor in vivo in mice*. *Blood*, 1989. **74**(4): p. 1241-1244.
83. Bester, J. and E. Pretorius, *Effects of IL-1 β , IL-6 and IL-8 on erythrocytes, platelets and clot viscoelasticity*. *Scientific reports*, 2016. **6**: p. 32188-32188.

84. Peng, J., et al., *Alteration of platelet function in dogs mediated by interleukin-6*. 1994.
85. Abildgaard, U., *Inhibition of the thrombin-fibrinogen reaction by α 2-macroglobulin, studied by N-terminal analysis*. Thrombosis and Haemostasis, 1969. **21**(02): p. 173-180.
86. Harpel, P.C., *HUMAN PLASMA ALPHA 2-MACROGLOBULIN : AN INHIBITOR OF PLASMA KALLIKREIN*. The Journal of Experimental Medicine, 1970. **132**(2): p. 329-352.
87. Holmberg, L., I. Lecander, and B. Astedt, *Binding of urokinase to plasma proteinase inhibitors*. Scandinavian journal of clinical and laboratory investigation, 1980. **40**(8): p. 743-747.
88. Koj, A., *Comparison of synthesis and secretion of plasma albumin, fibrinogen and alpha 2-macroglobulin by slices of Morris hepatomas and rat liver*. British journal of experimental pathology, 1980. **61**(3): p. 332.
89. Isaac, L., et al., *Murine alpha-2-macroglobulin increase during inflammatory responses and tumor growth*. Inflammation Research, 1999. **48**(8): p. 446-452.
90. Makis, A.C., et al., *Alpha-2-macroglobulin and interleukin-6 levels in steady-state sickle cell disease patients*. Acta haematologica, 2000. **104**(4): p. 164-168.
91. French, K., J.J. Yerbury, and M.R. Wilson, *Protease activation of α 2-macroglobulin modulates a chaperone-like action with broad specificity*. Biochemistry, 2008. **47**(4): p. 1176-1185.
92. Wu, S.M., D.D. Patel, and S.V. Pizzo, *Oxidized α 2-macroglobulin (α 2M) differentially regulates receptor binding by cytokines/growth factors: implications for tissue injury and repair mechanisms in inflammation*. The Journal of Immunology, 1998. **161**(8): p. 4356-4365.
93. Gourine, A.V., et al., *Role of alpha(2)-macroglobulin in fever and cytokine responses induced by lipopolysaccharide in mice*. American journal of physiology. Regulatory, integrative and comparative physiology, 2002. **283**(1): p. R218-R226.
94. Sottrup-Jensen, L., et al., *The α -macroglobulin bait region: sequence diversity and localization of cleavage sites for proteinases in five mammalian α -macroglobulins*. Journal of Biological Chemistry, 1989. **264**(27): p. 15781-15789.
95. Iwaki, D., et al., *Molecular Cloning of Limulus α 2-Macroglobulin*. European journal of biochemistry, 1996. **242**(3): p. 822-831.
96. Sottrup-Jensen, L., et al., *Sequence similarity between alpha 2-macroglobulin from the horseshoe crab, Limulus polyphemus, and proteins of the alpha 2-macroglobulin family from mammals*. Comparative biochemistry and physiology. B, Comparative biochemistry, 1990. **96**(3): p. 621-625.
97. Armstrong, P.B. and J.P. Quigley, *α 2-macroglobulin: an evolutionarily conserved arm of the innate immune system*. Developmental & Comparative Immunology, 1999. **23**(4-5): p. 375-390.
98. Hattori, M., et al., *Acute-phase reaction induces a specific complex between hepatic nuclear proteins and the interleukin 6 response element of the rat alpha 2-macroglobulin gene*. Proceedings of the National Academy of Sciences, 1990. **87**(6): p. 2364-2368.
99. Yoo, J.-Y., et al., *Synergistic activity of STAT3 and c-Jun at a specific array of DNA elements in the α 2-macroglobulin promoter*. Journal of Biological Chemistry, 2001. **276**(28): p. 26421-26429.
100. Zhang, X. and J.E. Darnell, Jr., *Functional importance of Stat3 tetramerization in activation of the alpha 2-macroglobulin gene*. The Journal of biological chemistry, 2001. **276**(36): p. 33576-33581.

101. Cater, J.H., M.R. Wilson, and A.R. Wyatt, *Alpha-2-macroglobulin, a hypochlorite-regulated chaperone and immune system modulator*. Oxidative medicine and cellular longevity, 2019. **2019**.
102. Hovi, T., D. Mosher, and A. Vaheri, *Cultured human monocytes synthesize and secrete alpha2-macroglobulin*. The Journal of experimental medicine, 1977. **145**(6): p. 1580-1589.
103. Mosher, D.F. and D.A. Wing, *Synthesis and secretion of alpha2-macroglobulin by cultured human fibroblasts*. The Journal of experimental medicine, 1976. **143**(2): p. 462-467.
104. Feldman, S.R., S.L. Gonias, and S.V. Pizzo, *Model of alpha 2-macroglobulin structure and function*. Proceedings of the National Academy of Sciences, 1985. **82**(17): p. 5700-5704.
105. Harpel, P.C., *STUDIES ON HUMAN PLASMA α 2-MACROGLOBULIN-ENZYME INTERACTIONS : EVIDENCE FOR PROTEOLYTIC MODIFICATION OF THE SUBUNIT CHAIN STRUCTURE*. The Journal of Experimental Medicine, 1973. **138**(3): p. 508-521.
106. Jenner, L., et al., *Crystal structure of the receptor-binding domain of α 2-macroglobulin*. Structure, 1998. **6**(5): p. 595-604.
107. Wu, S.M., C.M. Boyer, and S.V. Pizzo, *The binding of receptor-recognized α 2-macroglobulin to the low density lipoprotein receptor-related protein and the α 2M signaling receptor is decoupled by oxidation*. Journal of Biological Chemistry, 1997. **272**(33): p. 20627-20635.
108. Kristensen, T., et al., *Evidence that the newly cloned low-density-lipoprotein receptor related protein (LRP) is the α 2-macroglobulin receptor*. Febs Letters, 1990. **276**(1-2): p. 151-155.
109. Lagrange, J., et al., *Alpha-2-macroglobulin in hemostasis and thrombosis: an underestimated old double-edged sword*. Journal of Thrombosis and Haemostasis, 2022.
110. Heeb, M.J., A. Gruber, and J.H. Griffin, *Identification of divalent metal ion-dependent inhibition of activated protein C by alpha 2-macroglobulin and alpha 2-antiplasmin in blood and comparisons to inhibition of factor Xa, thrombin, and plasmin*. Journal of Biological Chemistry, 1991. **266**(26): p. 17606-17612.
111. Wagenvoord, R., et al., *The paradoxical stimulation by a reversible thrombin inhibitor of thrombin generation in plasma measured with thrombinography is caused by α 2-macroglobulin-thrombin*. Journal of Thrombosis and Haemostasis, 2010. **8**(6): p. 1281-1289.
112. Meijers, J.C., P.N. Tijburg, and B.N. Bouma, *Inhibition of human blood coagulation factor Xa by. alpha. 2-macroglobulin*. Biochemistry, 1987. **26**(18): p. 5932-5937.
113. Ellis, V., et al., *Inhibition of human factor Xa by various plasma protease inhibitors*. Biochimica et Biophysica Acta (BBA)-Protein Structure and Molecular Enzymology, 1982. **701**(1): p. 26-31.
114. Fuchs, H. and S. Pizzo, *Regulation of factor Xa in vitro in human and mouse plasma and in vivo in mouse. Role of the endothelium and plasma proteinase inhibitors*. The Journal of clinical investigation, 1983. **72**(6): p. 2041-2049.
115. Cvirn, G., S. Gallistl, and W. Muntean, *Alpha-2-macroglobulin inhibits the anticoagulant action of activated protein C in cord and adult plasma*. Pathophysiology of Haemostasis and Thrombosis, 2001. **31**(1): p. 1-11.
116. Martos, L., et al., *α 2-macroglobulin is a significant in vivo inhibitor of activated protein C and low APC: α 2M levels are associated with venous thromboembolism*. Thrombosis and haemostasis, 2018. **47**(04): p. 630-638.
117. Straight, D.L. and P. McKee, *Characterization of thrombin binding to alpha 2-macroglobulin*. Journal of Biological Chemistry, 1984. **259**(2): p. 1272-1278.

118. Vogel, C.N., H.S. Kingdon, and R.L. Lundblad, *Correlation of in vivo and in vitro inhibition of thrombin by plasma inhibitors*. The Journal of laboratory and clinical medicine, 1979. **93**(4): p. 661-673.
119. Fischer, A., et al., *Respective roles of antithrombin III and alpha 2 macroglobulin in thrombin inactivation*. Thrombosis and haemostasis, 1981. **45**(01): p. 051-054.
120. Downing, M.R., J.W. Bloom, and K.G. Mann, *Comparison of the inhibition of thrombin by three plasma protease inhibitors*. Biochemistry, 1978. **17**(13): p. 2649-2653.
121. Sottrup-Jensen, L., et al., *Primary structure of the 'bait' region for proteinases in α 2-macroglobulin: Nature of the complex*. FEBS letters, 1981. **127**(2): p. 167-173.
122. Mosher, D.F., *Action of fibrin-stabilizing factor on cold-insoluble globulin and alpha2-macroglobulin in clotting plasma*. Journal of Biological Chemistry, 1976. **251**(6): p. 1639-1645.
123. Singh, S., et al., *Identification of potential novel interacting partners for coagulation factor XIII B (FXIII-B) subunit, a protein associated with a rare bleeding disorder*. International journal of molecular sciences, 2019. **20**(11): p. 2682.
124. Korninger, C. and D. Collen, *Neutralization of human extrinsic (tissue-type) plasminogen activator in human plasma: no evidence for a specific inhibitor*. Thrombosis and haemostasis, 1981. **46**(07): p. 662-665.
125. De Boer, J., et al., *Alpha-2-macroglobulin functions as an inhibitor of fibrinolytic, clotting, and neutrophilic proteinases in sepsis: studies using a baboon model*. Infection and immunity, 1993. **61**(12): p. 5035-5043.
126. Schüler, R., *Interleukin-17A and Interleukin-6 in the Development of Vascular Inflammation*, in *Faculty of Biology*. 2019, Johannes Gutenberg-Universität Mainz. p. 136.
127. Gu, H., Y.-R. Zou, and K. Rajewsky, *Independent control of immunoglobulin switch recombination at individual switch regions evidenced through Cre-loxP-mediated gene targeting*. Cell, 1993. **73**(6): p. 1155-1164.
128. Croxford, A.L., et al., *IL-6 regulates neutrophil microabscess formation in IL-17A-driven psoriasiform lesions*. Journal of Investigative Dermatology, 2014. **134**(3): p. 728-735.
129. Bosmann, M., N.F. Russkamp, and P.A. Ward, *Fingerprinting of the TLR4-induced acute inflammatory response*. Experimental and molecular pathology, 2012. **93**(3): p. 319-323.
130. Burstein, S.A., et al., *Cytokine-induced alteration of platelet and hemostatic function*. Stem cells, 1996. **14**(S1): p. 154-162.
131. Zhang, Z., N.L. Fuentes, and G.M. Fuller, *Characterization of the IL-6 responsive elements in the gamma fibrinogen gene promoter*. The Journal of biological chemistry, 1995. **270**(41): p. 24287-24291.
132. Sauer, B., *Functional expression of the cre-lox site-specific recombination system in the yeast Saccharomyces cerevisiae*. Molecular and cellular biology, 1987. **7**(6): p. 2087-2096.
133. Sauer, B. and N. Henderson, *Site-specific DNA recombination in mammalian cells by the Cre recombinase of bacteriophage P1*. Proceedings of the National Academy of Sciences, 1988. **85**(14): p. 5166-5170.
134. Orban, P.C., D. Chui, and J.D. Marth, *Tissue- and site-specific DNA recombination in transgenic mice*. Proceedings of the National Academy of Sciences, 1992. **89**(15): p. 6861-6865.
135. Cross, M., et al., *Mouse lysozyme M gene: isolation, characterization, and expression studies*. Proceedings of the National Academy of Sciences, 1988. **85**(17): p. 6232-6236.

136. Clausen, B., et al., *Conditional gene targeting in macrophages and granulocytes using LysMcre mice*. Transgenic research, 1999. **8**(4): p. 265-277.
137. Burnand, K., et al., *The role of the monocyte in the generation and dissolution of arterial and venous thrombi*. Cardiovascular Surgery, 1998. **6**(2): p. 119-125.
138. Diaz, J.A., et al., *Thrombogenesis with continuous blood flow in the inferior vena cava*. Thrombosis and haemostasis, 2010. **104**(08): p. 366-375.
139. Cooley, B.C., et al., *A murine model of deep vein thrombosis Characterization and validation in transgenic mice*. Thrombosis and haemostasis, 2005. **94**(09): p. 498-503.
140. Diaz, J.A., et al., *Inferior vena cava branch variations in C57BL/6 mice have an impact on thrombus size in an IVC ligation (stasis) model*. Journal of thrombosis and haemostasis : JTH, 2015. **13**(4): p. 660-664.
141. Brandt, M., et al., *Deep vein thrombus formation induced by flow reduction in mice is determined by venous side branches*. Clinical hemorheology and microcirculation, 2014. **56**(2): p. 145-152.
142. Diaz, J.A., et al., *Critical review of mouse models of venous thrombosis*. Arteriosclerosis, thrombosis, and vascular biology, 2012. **32**(3): p. 556-562.
143. Schönfelder, T., S. Jäckel, and P. Wenzel, *Mouse models of deep vein thrombosis*. Gefässchirurgie, 2017. **22**(1): p. 28-33.
144. Böhmeke, T. and K. Weber, *Checkliste Echokardiographie*. 1998: Thieme.
145. Johansen, P.B., et al., *Automated registration of tail bleeding in rats*. Thrombosis and haemostasis, 2008. **99**(11): p. 956-962.
146. Liu, Y., et al., *Standardizing a simpler, more sensitive and accurate tail bleeding assay in mice*. World journal of experimental medicine, 2012. **2**(2): p. 30-36.
147. Grimm, D., K. Pandey, and M.A. Kay, *Adeno-associated virus vectors for short hairpin RNA expression*. Methods in enzymology, 2005. **392**: p. 381-405.
148. Shen, F., et al., *Cloning of Ly-5 cDNA*. Proceedings of the National Academy of Sciences, 1985. **82**(21): p. 7360-7363.
149. Spangrude, G.J., S. Heimfeld, and I.L. Weissman, *Purification and characterization of mouse hematopoietic stem cells*. Science, 1988. **241**(4861): p. 58-62.
150. Scheid, M.P. and D. Triglia, *Further description of the Ly-5 system*. Immunogenetics, 1979. **9**(1): p. 423-433.
151. Duran-Struuck, R. and R.C. Dysko, *Principles of bone marrow transplantation (BMT): providing optimal veterinary and husbandry care to irradiated mice in BMT studies*. Journal of the American Association for Laboratory Animal Science : JAALAS, 2009. **48**(1): p. 11-22.
152. Veres, G., et al., *The molecular basis of the sparse fur mouse mutation*. Science, 1987. **237**(4813): p. 415-417.
153. Van Gelder, R.N., et al., *Amplified RNA synthesized from limited quantities of heterogeneous cDNA*. Proceedings of the National Academy of Sciences, 1990. **87**(5): p. 1663-1667.
154. Aigner, A., *Gentechnische Methoden: eine Sammlung von Arbeitsanleitungen für das molekularbiologische Labor*. 2011: Springer-Verlag.
155. Taylor, J.M., R. Illmensee, and J. Summers, *Efficient transcription of RNA into DNA by avian sarcoma virus polymerase*. Biochimica et Biophysica Acta (BBA)-Nucleic Acids and Protein Synthesis, 1976. **442**(3): p. 324-330.
156. Holland, P.M., et al., *Detection of specific polymerase chain reaction product by utilizing the 5'----3'exonuclease activity of Thermus aquaticus DNA*

- polymerase*. Proceedings of the National Academy of Sciences, 1991. **88**(16): p. 7276-7280.
157. Morrison, T.B., J.J. Weis, and C.T. Wittwer, *Quantification of low-copy transcripts by continuous SYBR Green I monitoring during amplification*. Biotechniques, 1998. **24**(6): p. 954-8, 960, 962.
158. Saiki, R.K., et al., *Primer-directed enzymatic amplification of DNA with a thermostable DNA polymerase*. Science, 1988. **239**(4839): p. 487-491.
159. Ausubel, F.M., *Current protocols in molecular biology*. Vol. 1. 1987: Greene Pub. Associates and Wiley-Interscience.
160. Henke, D.C., S. Kouzan, and T.E. Eling, *Analysis of leukotrienes, prostaglandins, and other oxygenated metabolites of arachidonic acid by high-performance liquid chromatography*. Analytical biochemistry, 1984. **140**(1): p. 87-94.
161. Shen, Y., et al., *Protocol for visualizing newly synthesized proteins in primary mouse hepatocytes*. STAR Protocols, 2021. **2**(3): p. 100616.
162. Cossarizza, A., et al., *Guidelines for the use of flow cytometry and cell sorting in immunological studies*. European journal of immunology, 2019. **49**(10): p. 1457-1973.
163. Knopp, T., et al., *Effects of Dietary Protein Intake on Cutaneous and Systemic Inflammation in Mice with Acute Experimental Psoriasis*. Nutrients, 2021. **13**(6): p. 1897.
164. Laemmli, U.K., *Cleavage of structural proteins during the assembly of the head of bacteriophage T4*. nature, 1970. **227**(5259): p. 680-685.
165. Towbin, H., T. Staehelin, and J. Gordon, *Electrophoretic transfer of proteins from polyacrylamide gels to nitrocellulose sheets: procedure and some applications*. Proc Natl Acad Sci U S A, 1979. **76**(9): p. 4350-4.
166. Fåhræus, R., *The suspension stability of the blood*. Physiological reviews, 1929. **9**(2): p. 241-274.
167. Bedell, S.E. and B.T. Bush, *Erythrocyte sedimentation rate. From folklore to facts*. The American journal of medicine, 1985. **78**(6): p. 1001-1009.
168. Talstad, I., *The mechanism of the erythrocyte sedimentation rate (ESR)*. Acta Medica Scandinavica, 1971. **190**(1-6): p. 11-16.
169. Hemker, H.C., et al., *Calibrated automated thrombin generation measurement in clotting plasma*. Pathophysiology of haemostasis and thrombosis, 2003. **33**(1): p. 4-15.
170. Hemker, H., et al., *The calibrated automated thrombogram (CAT): a universal routine test for hyper-and hypocoagulability*. Pathophysiology of haemostasis and thrombosis, 2002. **32**(5-6): p. 249-253.
171. Lippi, G. and E.J. Favaloro, *Hemostasis practice: state-of-the-art*. Journal of Laboratory and Precision Medicine, 2018. **3**.
172. Ninivaggi, M., et al., *Whole-blood thrombin generation monitored with a calibrated automated thrombogram-based assay*. Clinical chemistry, 2012. **58**(8): p. 1252-1259.
173. Prior, S.M., et al., *Continuous thrombin generation in whole blood: New applications for assessing activators and inhibitors of coagulation*. Analytical biochemistry, 2018. **551**: p. 19-25.
174. Regnault, V., et al., *Phenotyping the haemostatic system by thrombography-potential for the estimation of thrombotic risk*. Thromb Res, 2004. **114**(5-6): p. 539-45.
175. Dargaud, Y., et al., *Monitoring platelet dependent thrombin generation in mice*. Thromb Res, 2010. **126**(5): p. 436-41.
176. Ninivaggi, M., et al., *Whole-blood thrombin generation monitored with a calibrated automated thrombogram-based assay*. Clin Chem, 2012. **58**(8): p. 1252-9.

177. Binder, T., et al., *Pappenheim-Färbung: Beschreibung einer hämatologischen Standardfärbung – Geschichte, Chemie, Durchführung, Artefakte und Problemlösungen/Pappenheim Stain: Description of a hematological standard stain – history, chemistry, procedure, artifacts and problem solutions*. *Laboratoriumsmedizin*, 2012. **36**(5): p. 293-309.
178. Efentakis, P., et al., *Tubulin-folding cofactor E deficiency is associated with vascular dysfunction and endoplasmic reticulum stress of vascular smooth muscle cells*. *European Heart Journal*, 2021. **42**(Supplement 1): p. ehab724. 3360.
179. Burstein, S.A., et al., *Cytokine-induced alteration of platelet and hemostatic function*. *Stem cells (Dayton, Ohio)*, 1996. **14 Suppl 1**: p. 154-162.
180. Westrick, R.J., M.E. Winn, and D.T. Eitzman, *Murine Models of Vascular Thrombosis*. 2007. **27**(10): p. 2079-2093.
181. Ridder, F.L., *The deep vein thrombosis induced by inferior vena cava ligation in C57BL/6 mice is analysed with the focus on myelomonocytic cells and the cytokine IL-6*, in *Biomedical Chemistry*. 2016, Johannes Gutenberg-University Mainz: Unpublished Thesis. p. 88.
182. Riley, R.S., et al., *Reticulocytes and reticulocyte enumeration*. *Journal of clinical laboratory analysis*, 2001. **15**(5): p. 267.
183. Devreese, K.M., *Interpretation of normal plasma mixing studies in the laboratory diagnosis of lupus anticoagulants*. *Thrombosis research*, 2007. **119**(3): p. 369-376.
184. Rasool, Z.S. and V. Tiwari, *Biochemistry, Lupus Anticoagulant*. 2019.
185. Lanzkowsky, P., *Manual of pediatric hematology and oncology*. 2005: Elsevier.
186. Kasuda, S., et al., *Expression of coagulation factors from murine induced pluripotent stem cell-derived liver cells*. *Blood Coagulation & Fibrinolysis*, 2011. **22**(4): p. 271-279.
187. Esmon, C.T., *The protein C pathway*. *Chest*, 2003. **124**(3): p. 26S-32S.
188. Rezaie, A.R., et al., *Protein C Inhibitor Is a Potent Inhibitor of the Thrombin-Thrombomodulin Complex (*)*. *Journal of Biological Chemistry*, 1995. **270**(43): p. 25336-25339.
189. Schüler, R., *Interleukin-17A and Interleukin-6 in the Development of Vascular Inflammation*, in *Faculty of Biology*. 2019, Johannes Gutenberg-Universität Mainz. p. 136.
190. Lee, S.H., J. eun Kwon, and M.-L. Cho, *Immunological pathogenesis of inflammatory bowel disease*. *Intestinal research*, 2018. **16**(1): p. 26.
191. Hosokawa, T., et al., *Interleukin-6 and soluble interleukin-6 receptor in the colonic mucosa of inflammatory bowel disease*. *Journal of gastroenterology and hepatology*, 1999. **14**(10): p. 987-996.
192. Ito, H., et al., *A pilot randomized trial of a human anti-interleukin-6 receptor monoclonal antibody in active Crohn's disease*. *Gastroenterology*, 2004. **126**(4): p. 989-996.
193. Mudter, J. and M.F. Neurath, *Il-6 signaling in inflammatory bowel disease: Pathophysiological role and clinical relevance*. *Inflammatory Bowel Diseases*, 2007. **13**(8): p. 1016-1023.
194. Solem, C.A., et al., *Correlation of C-reactive protein with clinical, endoscopic, histologic, and radiographic activity in inflammatory bowel disease*. *Inflammatory bowel diseases*, 2005. **11**(8): p. 707-712.
195. Matsuo, K., et al., *Venous thromboembolism, interleukin-6 and survival outcomes in patients with advanced ovarian clear cell carcinoma*. *European journal of cancer (Oxford, England : 1990)*, 2015. **51**(14): p. 1978-1988.
196. Matsuda, T., et al., *Identification of alpha 2-macroglobulin as a carrier protein for IL-6*. *The Journal of Immunology*, 1989. **142**(1): p. 148.

197. Libby, P. and D.I. Simon, *Inflammation and thrombosis: the clot thickens*. 2001, Am Heart Assoc. p. 1718-1720.
198. Mutlu, G.M., et al., *Ambient particulate matter accelerates coagulation via an IL-6-dependent pathway*. The Journal of clinical investigation, 2007. **117**(10): p. 2952-2961.
199. Atkins, M.B., et al., *Interleukin-6-associated anemia: determination of the underlying mechanism*. 1995.
200. van Gameren, M.M., et al., *Effects of recombinant human interleukin-6 in cancer patients: a phase I-II study*. 1994.
201. Williams, N., et al. *The role of interleukin 6 in megakaryocyte formation, megakaryocyte development and platelet production*. in *Ciba Foundation Symposium 167-Polyfunctional Cytokines: IL-6 and LIF: Polyfunctional Cytokines: IL-6 and LIF: Ciba Foundation Symposium 167*. 2007. Wiley Online Library.
202. Schmoeller, D., et al., *Mean platelet volume and immature platelet fraction in autoimmune disorders*. Frontiers in medicine, 2017. **4**: p. 146.
203. Wells, P.S., et al., *Evaluation of D-dimer in the diagnosis of suspected deep-vein thrombosis*. New England Journal of Medicine, 2003. **349**(13): p. 1227-1235.
204. Kamath, S., A. Blann, and G. Lip, *Platelet activation: assessment and quantification*. European heart journal, 2001. **22**(17): p. 1561-1571.
205. Baudo, F., T. Caimi, and F. De Cataldo, *Diagnosis and treatment of acquired haemophilia*. Haemophilia, 2010. **16**(102): p. 102-106.
206. Bowyer, A., S. Kitchen, and M. Makris, *The responsiveness of different APTT reagents to mild factor VIII, IX and XI deficiencies*. International journal of laboratory hematology, 2011. **33**(2): p. 154-158.
207. Kitchens, C., *To bleed or not to bleed? Is that the question for the PTT?* Journal of Thrombosis and Haemostasis, 2005. **3**(12): p. 2607-2611.
208. Kapiotis, S., et al., *Anticardiolipin antibodies in patients with venous thrombosis*. Pathophysiology of Haemostasis and Thrombosis, 1991. **21**(1): p. 19-24.
209. Van Der Meijden, P., et al., *Platelet-and erythrocyte-derived microparticles trigger thrombin generation via factor XIIa*. Journal of thrombosis and haemostasis, 2012. **10**(7): p. 1355-1362.
210. Noubouossie, D.F., et al., *Red blood cell microvesicles activate the contact system, leading to factor IX activation via 2 independent pathways*. Blood, The Journal of the American Society of Hematology, 2020. **135**(10): p. 755-765.
211. Swystun, L.L. and P.C. Liaw, *The role of leukocytes in thrombosis*. Blood, The Journal of the American Society of Hematology, 2016. **128**(6): p. 753-762.
212. Aziz, M., R. Fatima, and R. Assaly, *Elevated interleukin-6 and severe COVID-19: a meta-analysis*. Journal of medical virology, 2020.
213. Kong, R., N. Hutchinson, and K. Görlinger, *Hyper-and hypocoagulability in COVID-19 as assessed by thromboelastometry-two case reports*. Korean Journal of Anesthesiology, 2021. **74**(4): p. 350.
214. de la Morena-Barrio, M.E., et al., *Prognostic value of thrombin generation parameters in hospitalized COVID-19 patients*. Scientific reports, 2021. **11**(1): p. 1-11.
215. Boss, B. and G. Neeck, *Correlation of IL-6 with the classical humoral disease activity parameters ESR and CRP and with serum cortisol, reflecting the activity of the HPA axis in active rheumatoid arthritis*. Zeitschrift für Rheumatologie, 2000. **59**(2): p. 1162-1164.
216. Fanola, C.L., et al., *Interleukin-6 and the risk of adverse outcomes in patients after an acute coronary syndrome: observations from the SOLID-TIMI 52*

- (stabilization of plaque using darapladib—thrombolysis in myocardial infarction 52) trial. *Journal of the American Heart Association*, 2017. **6**(10): p. e005637.
217. Gager, G.M., et al., *Interleukin-6 level is a powerful predictor of long-term cardiovascular mortality in patients with acute coronary syndrome*. *Vascular Pharmacology*, 2020. **135**: p. 106806.
218. Markousis-Mavrogenis, G., et al., *The clinical significance of interleukin-6 in heart failure: results from the BIostat-CHF study*. *European journal of heart failure*, 2019. **21**(8): p. 965-973.
219. Wainstein, M.V., et al., *Elevated serum interleukin-6 is predictive of coronary artery disease in intermediate risk overweight patients referred for coronary angiography*. *Diabetology & metabolic syndrome*, 2017. **9**(1): p. 1-7.
220. Mudter, J. and M.F.J.I.b.d. Neurath, *Il-6 signaling in inflammatory bowel disease: pathophysiological role and clinical relevance*. 2007. **13**(8): p. 1016-1023.
221. Alper, A., et al., *Correlation of erythrocyte sedimentation rate and C-reactive protein with pediatric inflammatory bowel disease activity*. 2017. **65**(2): p. e25-e27.
222. Pepe, M., et al., *Inflammatory bowel disease and acute coronary syndromes: from pathogenesis to the fine line between bleeding and ischemic risk*. 2021. **27**(5): p. 725-731.
223. Goh, I.Y., et al., *Thromboembolism in active ulcerative colitis*. 2017. **2017**: p. bcr-2016-218608.
224. Vancamelbeke, M. and S. Vermeire, *The intestinal barrier: a fundamental role in health and disease*. *Expert review of gastroenterology & hepatology*, 2017. **11**(9): p. 821-834.
225. Schlagenhauf, A., et al., *Children with inflammatory bowel disease exhibit insensitivity to tissue factor pathway inhibitor*. 2018, American Society of Hematology Washington, DC.
226. He, H.-L., J.-B. Zhang, and Q. Li, *Clinical significance of expression of tissue factor and tissue factor pathway inhibitor in ulcerative colitis*. *World Journal of Gastroenterology: WJG*, 2014. **20**(23): p. 7461.
227. Cibor, D., et al., *Levels of tissue factor pathway inhibitor in patients with inflammatory bowel disease*. *Pol Arch Intern Med*, 2019. **129**(4): p. 253-258.
228. Sandborn, W.J., et al., *Tofacitinib, an oral Janus kinase inhibitor, in active ulcerative colitis*. 2012. **367**(7): p. 616-624.
229. Sandborn, W.J., et al., *Venous thromboembolic events in the tofacitinib ulcerative colitis clinical development programme*. 2019. **50**(10): p. 1068-1076.
230. Miesbach, W., M.J.C. Makris, and a. thrombosis/hemostasis, *COVID-19: coagulopathy, risk of thrombosis, and the rationale for anticoagulation*. 2020. **26**: p. 1076029620938149.
231. Schramm, W., et al., *COVID-19-associated coagulopathy-Hypothesis: Are Children protected due to enhanced thrombin inhibition by higher α 2-Macroglobulin (α 2-M)?* 2020.
232. Seitz, R., et al., *Thromboinflammation in COVID-19: Can α 2-macroglobulin help to control the fire?* 2021. **19**(2): p. 351-354.
233. Becker, C. and P. Harpel, *alpha2-Macroglobulin on human vascular endothelium*. *The Journal of experimental medicine*, 1976. **144**(1): p. 1-9.

8. LISTS

8.1. Tables

Table 1: List of chemicals	15
Table 2: List of Instruments and equipment	16
Table 3: Transplant scheme	25
Table 4: Primer used for the Quantitative real-time PCR.....	28
Table 5: List of gene loci, primer name and sequence, annealing temperature and band size.	29
Table 6 List of antibodies for flow cytometric staining.	31
Table 7: Components of SDS-PAGE gel.....	34

8.2. Figures

Figure 1 Schematic overview of the coagulation cascade.....	1
Figure 2 Overview of some of the IL-6 producer and effects of IL-6 [34].	4
Figure 3 Schematic overview of the IL-6 signaling pathway.	6
Figure 4 Biological function of A2M adapted from [101].	8
Figure 5 Influence of A2M on coagulation and fibrinolysis cascades.....	10
Figure 6 IL-6 overexpression in myeloid cells leads to a reduced live expectancy. .	12
Figure 7 Experimental set-up for treatment with AAV8shRNA A2m or AAV8shRNA scrmb.....	24
Figure 8 Schematic representation of bone marrow transplantation.....	25
Figure 9 Gating strategy of isolated splenocytes.....	32
Figure 10 No thrombus formation in LysM-IL-6 ^{OE} mice compared to control mice. .	41
Figure 11 Hematological analysis of LysM-IL-6 ^{OE} mice compared to control mice. .	43
Figure 12 Coagulation parameters in LysM-IL-6 ^{OE} compared to control mice.	44
Figure 13 Neither lupus anticoagulant effect nor microthrombus formation in LysM-IL-6 ^{OE} mice compared to control mice	45
Figure 14 Thrombin generation in LysM-IL-6 ^{OE} mice.....	46
Figure 15 Myeloid IL-6 overexpression influences the expression of coagulation factors and leads to increased hepatic A2m expression.....	47
Figure 16 Liver analysis of in LysM-IL-6 ^{OE} mice compared to control mice.	48
Figure 17 Myeloid IL-6 overexpression leads to an increased erythrocyte sedimentation rate (ESR) and formation of erythrocyte aggregates.	49
Figure 18 Formation of erythrocyte rouleaux is associated with increased thrombin-triggered clotting time and A2m.	51
Figure 19 Myeloid IL-6 overexpression leads to formation of erythrocyte aggregates in which IL-6 and A2m are co-localized.....	53
Figure 20 Analysis of colon inflammation in LysM IL-6 ^{OE} mice compared to control mice.....	55
Figure 21 Analyze of the blood from IBD patients.	56
Figure 23 IL-6 and A2m are co-localized in the blood of IBD patients in the acute phase.....	58

Figure 23 Thrombin converting time and Pappenheim staining of whole blood from IBD patients and control.....	59
Figure 24 Dose-dependent effect of myeloid cell-derived IL-6 on the coagulation parameters in mice.	60
Figure 25 Immunofluorescence staining of blood smears from bone marrow chimeric mice.....	61
Figure 26 IL-6 dose-dependent effect on the thrombin-triggered clotting and erythrocytes aggregates in mice.	62
Figure 27 Analysis of LysM-IL-6 ^{OE} mice treated with small hairpin-A2m specific adeno-associated virus	64
Figure 28 Inflammatory cell analysis of LysM-IL-6 ^{OE} mice treated with AAV8shRNA A2m or AAV8shRNA scrambled.	66
Figure 29 Coagulation Parameter analysis of LysM-IL-6 ^{OE} mice treated with AAV8shRNA A2m or AAV8shRNA scrambled	68
Figure 30 Liver mRNA expression of coagulation factors of LysM-IL-6 ^{OE} mice treated with AAV8shRNA A2m.....	70
Figure 31 Pappenheim staining and Thrombin converting time of LysM-IL-6 ^{OE} mice treated with AAV8shRNA A2m or AAV8shRNA <i>scrambled</i>	72
Figure 32 Scheme of the impact of IL-6-driven A2m overexpression on clot formation.	82
Figure 33 Scheme of the impact of IL-6 on erythrocyte rouleaux formation, myeloid cells and A2m.	83

9. ACKNOWLEDGEMENTS

10. VERSICHERUNG

Hiermit versichere ich gemäß § 11, Abs. 3d der Promotionsordnung vom 01.04.2018, dass ich die vorliegende Arbeit selbstständig und nur mit zur Hilfenahme der angegebenen Quellen angefertigt habe. Die vorgelegte Arbeit wurde nicht als Prüfungsarbeit für eine andere Prüfung eingereicht. Weiterhin wurde die Arbeit nicht, auch nicht in Auszügen, als Dissertation an einer anderen Fakultät bzw. Fachbereich eingereicht. Teile der Arbeit wurden bereits für eine Veröffentlichung verwendet und sind entsprechend gekennzeichnet.

Bern, den 27.08.2022

Tanja Knopp

11. CURRICULUM VITAE

12. PUBLIKATIONEN UND VORTRÄGE

Publikationen

Knopp T., Lagrange J., Jung R., Ridder F., Bieler T., Joumana M., Reißig S., Wild J., Reinhardt C., Spronk H., Munder M., Schattenberg J., Bechman I., Rossman H., Jurk K., Wunderlich F., Hövelmeyer N., Lämmle B., Münzel T., Ruf W., Wenzel P., Waisman A., Karbach S., CHRONICALLY ELEVATED INTERLEUKIN-6 LEADS TO IMPAIRED COAGULATION VIA ACCUMULATION OF ALPHA2-MACROGLOBULIN ON ERYTHROCYTES (Manuscript in preperation)

Jung R.*, **Knopp T.***, Efentakis P., Wild J., Bieler T., Garlapati V.S., Molitor M., Bochenek M., Lagrange J., Masri J., Randriamboavonjy V., Wunderlich T., Hövelmeyer N., Oelze M., Daiber A., Bosmann B., Schäfer K., Fleming I., Münzel T., Wenzel P., Waisman A., Karbach S., MYELOID CELL DERIVED INTERLEUKIN-6 DRIVES VASCULAR DYSFUNCTION AND ENHANCES VASCULAR INFLAMMATION BUT DOES NOT LEAD TO HYPERTENSION, (Masuscript submitted to CVR)

Molitor M.*, Bayo Jimenez MT.*, Hahad O., Witzler C., Finger S., Galapati V., Kalinovic S., **Knopp T.**, Bieler T., Aluia M., Lagrange J., Blessing R., Rapp S., Schulz., Kleinert H., Karbach S., Steven S., Wild P., Daiber A., Münzel T.*, Wenzel P.*, Aircraft noise exposure induces pro-inflammatory vascular conditioning and amplifies vascular dysfunction and impairment of cardiac function after myocardial infarction, European Heart Journal, 2022 (**under revision**)

Hasselwander S., Xia N., Ascher S., Mimmler M., **Knopp T.**, Reifenberg G., Karbach S., Ruf W., Reinhardt C., Li H., B LYMPHOCYTE-DEFICIENCY IN

MICE PROMOTES VENOUS THROMBOSIS, Heliyon, 2022 (**under revision**)

Brandt M.*, Dörschmann H.*, Khraisat S., **Knopp T.**, Ringen J., Kalinovic S., Garlapati V., Siemer S., Molitor M., Göbler S., Stauber R., Karbach S., Münzel T., Daiber A., Wenzel., TELOMERE SHORTENING IN HYPERTENSIVE HEART DISEASE DEPENDS ON NOX2-MEDIATED OXIDATIVE DNA DAMAGE AND PREDICTS IMPAIRED RECOVERY OF CARDIAC FUNCTION, Hypertension, 2022

Wild J.*, Ringen J.*, Bieler T., **Knopp T.**, Lagrange J., Molitor M., Kropp A., Keller K., Daiber A., Münzel T., Rauh M., Waisman A., Wenzel P., Titze J., Karbach S., IMIQUIMOD-INDUCED SKIN INFLAMMATION: SYSTEMIC AND PHYSIOLOGICAL EFFECTS, Journal of Investigative Dermatolog, 2022

Knopp T.*, Bieler T.*, Jung R., Ringen J., Molitor M., Jurda A., Münzel T., Waisman A., Wenzel P., Karbach SH., Wild J., EFFECTS OF DIETARY PROTEIN INTAKE ON CUTANEOUS AND SYSTEMIC INFLAMMATION IN MICE WITH ACUTE EXPERIMENTAL PSORIASIS. Nutrients, **2021**.

Wild J., Jung R., **Knopp T.**, Efentakis P., Benaki D., Grill A., Wegner J., Molitor M., Garlapati V., Rakova N., Markó L., Marton A., Mikros E., Münzel T., Kossmann S., Rauh M., Nakano D., Kitada K., Luft F., Waisman A., Wenzel P., Titze J., Karbach S., AESTIVATION MOTIFS EXPLAIN HYPERTENSION AND MUSCLE MASS LOSS IN MICE WITH PSORIATIC SKIN BARRIER DEFECT. Acta Physiologica, **2021**.

Molitor M., Rudi WS., Garlapati V., Finger S., Schüler R., Kossmann S., Lagrange J., Nguyen TS., Wild J., **Knopp T.**, Karbach SH., Knorr M., Ruf W., Münzel T., Wenzel P., NOX2+ MYELOID CELLS DRIVE VASCULAR INFLAMMATION AND ENDOTHELIAL DYSFUNCTION IN HEART FAILURE AFTER MYOCARDIAL INFARCTION VIA ANGIOTENSIN II RECEPTOR TYPE 1. *Cardiovascular Research*, **2021**.

Chen W., Werner F., Illerhaus A., **Knopp T.**, Völker K., Potapenko T., Hofmann U., Frantz S., Baba HA., Rösch M., Zerneck A., Karbach S., Wenzel P., Kuhn M., STABILIZATION OF PERIVASCULAR MAST CELLS BY ENDOTHELIAL CNP (C-TYPE NATRIURETIC PEPTIDE). *Arteriosclerosis, Thrombosis, and Vascular Biology*. **2020**.

Knopp T., Karbach S., Wenzel P.. MYELOID CELLS TO THE RESCUE: IMPROVING THROMBUS RESOLUTION. *Thrombosis and Haemostasis*, **2020**.

Wild J., Schüler R., **Knopp T.**, Molitor M., Kossmann S., Münzel T., Daiber A., Waisman A., Wenzel P., Karbach SH., TELMISARTAN LOWERS ELEVATED BLOOD PRESSURE IN PSORIATIC MICE WITHOUT ATTENUATING VASCULAR DYSFUNCTION AND INFLAMMATION. *International Journal of Molecular Sciences*, **2019**.

Schönfelder T., Brandt M., Kossmann S., **Knopp T.**, Münzel T., Walter U., Karbach SH., Wenzel P., LACK OF T-BET REDUCES MONOCYTIC INTERLEUKIN-12 FORMATION AND ACCELERATES THROMBUS RESOLUTION IN DEEP VEIN THROMBOSIS. *Scientific Reports*, **2018**.

Reviews

Lagrange J., Lecompte T., **Knopp T.**, Lacolley P., Regnault V. ALPHA-2-MACROGLOBULIN IN HEMOSTASIS AND THROMBOSIS: AN UNDERESTIMATED OLD DOUBLE EDGE SWORD, Journal of Thrombosis & Haemostasis, 2022

Vorträge

Knopp T., Lagrange J., Schüler R., Ridder F., Wild J., Rossmann H., Spronk H.M.H., Münzel T., Lämmle B., Ruf W., Wenzel P., Waisman A., Karbach S.
CHRONICALLY ELEVATED INTERLEUKIN-6 LEVELS LEAD TO A
DISTURBANCE IN THE COAGULATION SYSTEM IN MICE
64th Annual Meeting, Society of Thrombosis and Haemostasis Research
(GTH), **18.-21. Februar 2020, Bremen, Deutschland**

Knopp T., Schüler R., Lagrange L., Ridder F., Wild H., Roßmann H., Spronk
H. M., Münzel T., Ruf W., Lämmle B., Wenzel P., Waismann A., Karbach S.,
CONSTITUTIVE OVEREXPRESSING OF INTERLEUKIN-6 IN MYELOID
CELLS INDUCES A SEVERE BLEEDING PHENOTYPE IN MICE
85. Jahrestagung der DGK, Basic science: Immunmodulation und
kardiovaskuläre Erkrankungen, **24.-27. April 2019, Mannheim,
Deutschland**

Posterpräsentationen

Knopp T., Lagrange J., Jung R., Wild J., Rossmann H., Spronk HMH., Wunderlich T., Hoevelmeyer N., Münzel T., Lämmle B., Ruf W., Wenzel P., Waisman A., Karbach S., CHRONICALLY ELEVATED INTERLEUKIN-6 DISTURBS THE COAGULATION CASCADE IN MICE,
63rd American Society of Hematology (ASH) Annual Meeting, 11.-14. Dezember 2021, Atlanta, USA.

Hans-Jürgen-Bretschneider-Abstract-Preis:

Knopp T., Jung R., Efentakis P., Wild J., Molitor M., Garlapati V.S., Bochenek M., Lagrange J., Masri J., Randriamboavonjy V., Wunderlich T., Hövelmeyer N, Daiber A., Bosmann B., Schäfer K., Fleming I., Münzel T., Wenzel P., Waisman A., Karbach S., INTERLEUKIN-6 OVEREXPRESSION IN MYELOID CELLS DRIVES VASCULAR DYSFUNCTION, INFLAMMATION AND FIBROSIS
DGK Herztage 2021, Clinical Research in Cardiology, **30. September-2.Oktober 2021, Hybrid Kongress, Bonn, Deutschland**

Knopp T., Lagrange J., Schüler R., Ridder F., Wild J., Rossmann H., Spronk HMH., Münzel T., Lämmle B., Ruf W., Wenzel P., Waisman A., Karbach S. CHRONICALLY ELEVATED INTERLEUKIN-6 LEVELS IN MICE LEAD TO A DISTURBANCE IN THE COAGULATION SYSTEM.
Research and Practice in Thrombosis and Haemostasis. 2020; International Society on Thrombosis and Haemostasis (ISTH) **30. Oktober – 12. November 2020, virtuel congress**